

Fakultät Mathematik und Naturwissenschaften
Technische Universität Dresden



Extension of Generalized Modeling and Application to Problems from Cell Biology

Dissertation

zur Erlangung des akademischen Grades

Doctor rerum naturalium

(Dr. rer. nat.)

vorgelegt von

Martin Zumsande

Geboren am 14. September 1981 in Georgsmarienhütte

Max-Planck-Institut für
Physik komplexer Systeme

Eingereicht am 5. Juli 2011

Eingereicht am 5. Juli 2011

Verteidigt am 17. November 2011

1. Gutachter: Prof. Dr. Frank Jülicher
2. Gutachter: Prof. Dr. Stefan Siegmund

Abstract

Mathematical modeling is an important tool in improving the understanding of complex biological processes. However, mathematical models are often faced with challenges that arise due to the limited knowledge of the underlying biological processes and the high number of parameters for which exact values are unknown. The method of generalized modeling is an alternative modeling approach that aims to address these challenges by extracting information about stability and bifurcations of classes of models while making only minimal assumptions on the specific functional forms of the model. This is achieved by a direct parameterization of the Jacobian in the steady state, introducing a set of generalized parameters which have a biological interpretation.

In this thesis, the method of generalized modeling is extended and applied to different problems from cell biology. In the first part, we extend the method to include also the higher derivatives at the steady state. This allows an analysis of the normal form of bifurcations and thereby a more specific description of the nearby dynamics. In models of gene-regulatory networks, it is shown that the extended method can be applied to better characterize oscillatory systems and to detect bistable dynamics.

In the second part, we investigate mathematical models of bone remodeling, a process that renews the human skeleton constantly. We investigate the connection between structural properties of mathematical models and the stability of steady states in different models. We find that the dynamical system operates from a stable steady state that is situated in the vicinity of bifurcations where stability can be lost, potentially leading to diseases of bone.

In the third part of this thesis, models of the MAPK signal transduction pathway are analyzed. Since mathematical models for this system include a high number of parameters, statistical methods are employed to analyze stability and bifurcations. Thereby, the parameters with a strong influence on the stability of steady states are identified. By an analysis of the bifurcation structure of the MAPK cascade, it is found that a combination of multiple layers in a cascade-like way allows for additional types of dynamic behavior such as oscillations and chaos.

In summary, this thesis shows that generalized modeling is a fruitful alternative modeling approach for various types of systems in cell biology.

Zusammenfassung

Mathematische Modelle stellen ein wichtiges Hilfsmittel zur Verbesserung des Verständnisses komplexer biologischer Prozesse dar. Sie stehen jedoch vor Schwierigkeiten, wenn wenig über die zugrundeliegende biologischen Vorgänge bekannt ist und es eine große Anzahl von Parametern gibt, deren exakten Werte unbekannt sind. Die Methode des Verallgemeinerten Modellierens ist ein alternativer Modellierungsansatz mit dem Ziel, diese Schwierigkeiten dadurch anzugehen, dass dynamische Informationen über Stabilität und Bifurkationen aus Klassen von Modellen extrahiert werden, wobei nur minimale Annahmen über die spezifischen funktionalen Formen getätigt werden. Dies wird erreicht durch eine direkte Parametrisierung der Jacobi-matrix im Gleichgewichtszustand, bei der neue, verallgemeinerte Parameter eingeführt werden, die eine biologische Interpretation besitzen.

In dieser Arbeit wird die Methode des Verallgemeinerten Modellierens erweitert und auf verschiedene zellbiologische Probleme angewandt. Im ersten Teil wird eine Erweiterung der Methode vorgestellt, bei der die Analyse höherer Ableitungen im Gleichgewichtszustand integriert wird. Dies erlaubt die Bestimmung der Normalform von Bifurkationen und hierdurch eine spezifischere Beschreibung der Dynamik in deren Umgebung. In Modellen für genregulatorische Netzwerke wird gezeigt, dass die so erweiterte Methode zu einer besseren Charakterisierung oszillierender Systeme sowie zur Erkennung von Bistabilität verwendet werden kann.

Im zweiten Teil werden mathematische Modelle zur Knochenremodellierung untersucht, einem Prozess der das menschliche Skelett kontinuierlich erneuert. Wir untersuchen den Zusammenhang zwischen strukturellen Eigenschaften verschiedener Modelle und der Stabilität von Gleichgewichtszuständen. Wir finden, dass das dynamische System von einem stabilen Zustand operiert, in dessen Nähe Bifurkationen existieren, welche das System destabilisieren und so potentiell Knochenkrankheiten verursachen können.

Im dritten Teil werden Modelle für den MAPK Signaltransduktionsweg analysiert. Da mathematische Modelle für dieses System eine hohe Anzahl von Parametern beinhalten, werden statistische Methoden angewandt zur Analyse von Stabilität und Bifurkationen. Zunächst werden Parameter mit einem starken Einfluss auf die Stabilität von Gleichgewichtszuständen identifiziert. Durch eine Analyse der Bifurkationsstruktur wird gezeigt, dass eine kaskadenartige Kombination mehrerer Ebenen zu zusätzliche Typen von Dynamik wie Oszillationen und Chaos führt.

Zusammengefasst zeigt diese Arbeit, dass Verallgemeinertes Modellieren ein fruchtbarer alternativer Modellierungsansatz für verschiedene zellbiologische Probleme ist.

Contents

1	Introduction	1
2	Introduction to dynamical systems and generalized modeling	7
2.1	Dynamical systems and steady states	7
2.1.1	Bifurcations and their normal forms	8
2.1.2	Codimension-1 bifurcations	10
2.1.3	Codimension-2 bifurcations	13
2.2	Introduction to generalized modeling	14
2.2.1	General model of a transcription factor with autoinhibition . . .	14
2.2.2	Abstract description of the method	18
2.2.3	Limitations of generalized modeling	19
2.2.4	Bifurcations in general models	21
3	Normal-form analysis of bifurcations in gene-regulatory networks	23
3.1	Normal-form parameters of codimension-1 bifurcations	24
3.1.1	Normal form of Hopf bifurcations	24
3.1.2	Normal form of saddle-node bifurcations	25
3.1.3	Incorporating normal forms into generalized models	26
3.2	Negative-feedback oscillations in gene regulation	27
3.3	Normal-form analysis of Hopf bifurcations in the Goodwin model . . .	28
3.4	Normal-form analysis in a model of a circadian oscillator	35
3.5	Cusp bifurcations and bistability	41
3.6	Discussion	43
4	Stability and bifurcations in bone remodeling	47
4.1	Introduction	47
4.1.1	Previous mathematical models	49
4.1.2	Stability in models of bone remodeling	50
4.2	A two-variable model of osteoblasts and osteoclasts	51
4.2.1	Bifurcation analysis of the two-variable model	55

4.3	A three-variable model with responding osteoblasts	59
4.3.1	Bifurcation analysis of the three-variable model	62
4.4	Bifurcations and diseases of bone	67
4.5	Discussion	69
5	Bifurcations and chaos in the MAPK signaling cascade	71
5.1	Biology of the MAPK pathway	72
5.1.1	History of modeling in the MAPK pathway	73
5.2	Mathematical model of the MAPK cascade	74
5.2.1	Generalized modeling for metabolic networks and signaling networks	74
5.2.2	Implementation of three subsystems	75
5.2.3	Parameter ranges	80
5.3	Dynamics of the one-layer model	81
5.3.1	Generation of random samples	81
5.3.2	Stability analysis of the single-layer model	82
5.3.3	Mechanisms of instability	84
5.3.4	Relation to bistability	85
5.4	Dynamics of the two-layer and three-layer models	87
5.4.1	Correlations of parameters with stability	87
5.4.2	Bifurcation structure of the larger models	89
5.4.3	Codimension-2 bifurcations and complex nonlocal dynamics	90
5.5	Explicit Feedback	92
5.6	Discussion	96
6	Discussion and outlook	99
A	Three-layer model of the MAPK cascade	105
B	Parameters for bifurcation diagrams of the three-layered MAPK cascade	107
C	List of abbreviations	111
	Bibliography	113

Chapter 1

Introduction

In the post-genomic era of biology, vast amounts of data are being generated by high-throughput methods at rapidly increasing speed and decreasing costs. However, while the amount of molecular information has grown tremendously, the understanding of most complex processes in living cells has not grown at a comparable pace. The underlying reason for these difficulties is that the cell constitutes a large complex network of interacting entities with processes acting over a wide range of timescales. Essential functions of the cell, such as proliferation, cell division or apoptosis, are not caused by single genes but appear as emergent properties of a complex network of interacting genes and proteins [1–4].

Due to these fundamental difficulties, it is necessary that current cell biology does not follow exclusively the bottom-up strategy of understanding complex functions of the cell by understanding the interactions of their elementary subsystems first. Instead, these approaches should be combined with top-down approaches. Methods of the latter class aim to describe systems starting from a higher level of abstraction and at the same time ignore or approximate the underlying processes on lower levels of abstraction. For example, the dynamics of a network of interacting genes can be studied without taking the structural properties of the involved proteins into account.

On a more abstract level, it is sometimes argued that for fundamental reasons, complex systems in general cannot be understood solely by the reductionistic approach of explaining them by the interaction of their basic building blocks [5, 6], while others emphasize the importance of finding the right level of description [7]. Regardless of whether one can agree to these philosophical positions, it is apparent that in the near future most complex phenomena in the living cell are not likely to be understood based solely on the interaction of their elementary subsystems (i.e., genes and proteins). Therefore, there is an ongoing need to develop models for complex systems that consist of subsystems that are not completely understood.

Considering that many different disciplines have encountered similar problems, it is not surprising that the theory of complex systems has a strongly interdisciplinary character. It borrows its methods from different fields, but particularly from statistical physics, network/graph theory and the theory of dynamical systems.

This thesis contributes to the formulation and analysis of mathematical models for complex processes in cell biology, using mostly methods from the theory of dynamical systems. More precisely, we investigate models of ordinary differential equations (ODEs) that are aimed to improve the understanding of dynamic processes of living cells. The copy number of the modelled entities, whether they are mRNA molecules, proteins or cells, must be sufficiently large to make a description by continuous ODEs adequate, leading to models that describe the dynamics of ensembles instead of single copies of the entities. The specific internal properties of these entities, which may be poorly understood in some cases, enter the model in the form of external parameters and functional forms, describing how the modelled variables change in time.

A very common approach to mathematical modeling, which will in the following be called *conventional modeling*, can be summarized as a three-step process:

- First, a system of ordinary differential equations is constructed that aims to describe the biological process.
- Second, the parameters of the model are estimated, making use of experimental data if available. Depending on the degree of certainty, some model parameters may be varied while others may be fixed to constant values.
- Third, the dynamics of the model are explored. Sometimes this is done using analytical methods from the theory of dynamical systems, particularly in smaller models. Larger models are often only accessible by numerical simulation, i.e., numerical integration of the system of ODEs.

Constructing a model of ODEs in this way entails a number of difficult decisions: Which biological processes should be included in the model, and which processes are of secondary importance to the actual problem? Which functional forms should be used for an interaction that is considered to be essential for the model? Do the actual functional forms used in the model affect the results strongly or does one have relative liberty to choose between different reasonable alternatives without changing the results? Finally, what size of the parameter space should be explored, gaining more generality in the results at the cost of higher computational efforts and perhaps reduced interpretability?

The above-mentioned problems are serious challenges in conventional modeling. Experiments cannot always provide straightforward answers to them because, in many cases, they can establish only qualitative relations, such as assigning a repressing or

activating nature to an interaction without quantifying it. Moreover, since both temporal and financial resources for experimental studies are limited, it is one of the tasks of mathematical models to create predictions in a situation of incomplete information, which can then be validated in specific experiments.

In this thesis, an alternative approach to modeling is employed that addresses the problems of conventional modeling by taking a different point of view. The method of generalized modeling (GM) [8–10] aims to classify a large number of specific models based on the stability properties of their steady states. It achieves this by performing a local linear stability analysis that uses the information encoded in the spectrum of the Jacobian at the steady state. GM does not assume specific functional forms for unknown interactions but covers their influence on stability of the steady states by introducing a set of general parameters. Because GM avoids numerical integration of the ODEs, it requires considerably less computational resources than other methods, which allows for the investigation of a large portion of the parameter space.

General models are an useful alternative approach to conventional models in particular in two different situations:

- In problems for which several competing modeling approaches coexist without a consensus as to which one is best suited, GM can distinguish the dynamical key features of different model structures. We demonstrate this for the problem of *bone remodeling*, which is analyzed in chapter 4.
- In problems for which an accepted model structure exists, but for which the parameter space is high-dimensional, GM can efficiently detect the different qualitative forms of dynamics that are possible (e.g., bistability, oscillations, chaos) and relate them to the general parameters. We demonstrate this for the *MAPK signaling cascade* in chapter 5.

Only in problems for which both the structure of the mathematical model is known with a high degree of certainty and in which, additionally, reliable estimates for most of the parameters exist, it is not reasonable to apply GM. However, most of the important problems in cell biology do not fall into that class.

By restricting the analysis to local steady states, information on nonlocal properties is not directly available. Among the nonlocal phenomena that cannot be extracted directly from the general model are transient dynamics and global bifurcations. In this thesis, these constraints are mitigated by an extension of the method that allows the inclusion of normal-form analysis in the framework of general modeling, since normal forms of bifurcations can indirectly point to nonlocal types of dynamics in the neighborhood.

This thesis is structured as follows: In chapter 2, we first provide a brief introduction to the most important concepts of the theory of dynamical systems and, in particular, of bifurcation theory that will be used throughout the thesis. The emphasis of this discussion is not on mathematical rigidity but on interpretability and proximity to practical applications. We then proceed to introduce the method of generalized modeling in detail. A toy model for gene-regulatory autoinhibition, comprising a gene coding for a protein that inhibits the transcription of its own mRNA, serves as an example.

In chapter 3, we describe an extension of the method that includes the second and third derivatives at the steady state for an analysis of the normal forms of bifurcations. All previous studies with GM had performed an analysis of the linearization at the steady state that is given by the Jacobian matrix. With the extension, we are able to extract more detailed information about the bifurcation structure and the dynamical properties of models. The extension of the method is applied to two model architectures of oscillating gene-regulatory networks: We first use analytical tools to investigate the Hopf bifurcations of the Goodwin model, which is one of the most basic models for gene regulation with autoinhibition. We then investigate the bifurcation landscape in a larger model for a circadian oscillator, in which two different genes interact.

In chapter 4, we apply GM to mathematical models of bone remodeling. Bone remodeling is a process that is accomplished by the interplay of two cell types, the bone-building osteoblasts and the bone-resorbing osteoclasts. The populations of these cell types are regulated by various hormones and cytokines and also interact with each other by means of signaling molecules. Mathematical modeling is still in its early stages for bone remodeling and there is no consensus yet on the question of which model architecture is best suited to describe the process. Experimental data is scarce since the collective phenomenon of bone remodeling can only be observed *in vivo*, while *in vitro* studies on cell cultures of osteoblasts and osteoclasts have led to conflicting results. We use GM to compare a large class of models and point out their advantages and disadvantages. We suggest that the system of bone remodeling has evolved to operate at a steady state close to a bifurcation. While this facilitates strong adaptive responses to varying external conditions, it also leads to the risk of losing stability. This loss of stability can possibly be related to diseases of bone.

In chapter 5, we investigate the MAPK cascade, an important signaling pathway in eukaryotic cells that is involved in the regulation of multiple cellular functions. The basic biochemistry of this pathway is well established, and there have been numerous studies in which mathematical modeling was applied to the system. However, the dynamics of this pathway in connection with its function are not understood well. For the MAPK cascade, we use GM to explore the different types of dynamic behavior that

are possible in a fixed model structure with many unknown parameters. Specifically, we describe regions of oscillations and weak forms of chaos.

Finally, the results of the different subprojects are summarized and discussed in chapter 6.

In summary, this thesis shows that various different problems from cell biology can be studied fruitfully in the framework of generalized modeling. By an extension of the method that allows the analysis of normal form parameters of bifurcations, it is demonstrated that important properties of gene-regulatory networks such as oscillations and bistability can be investigated in general models. Further, it is shown for models of bone remodeling that the generality of the method, which allows to study stability and bifurcations in large classes of feasible models, can be used to compare existing modeling approaches, point out connections between the structure of models and the resulting dynamics and reveal connections between bifurcations and diseases. Finally, this thesis shows that due to its computational efficiency, the application of the method of GM can also lead to new insights in large models for which the functional forms are largely known such as the MAPK cascade. Using a combination of statistical sampling and bifurcation analysis, previously unidentified types of dynamics can be detected in the model and analyzed in a high-dimensional parameter space.

Chapter 2

Introduction to dynamical systems and generalized modeling

In this chapter, we first review the basic mathematical foundations of dynamical systems theory and introduce the concepts that are needed in the following chapters, in which they are applied to specific mathematical models. In doing so, we follow mostly the textbooks by Kuznetsov [11] and by Guckenheimer and Holmes [12]. In the second part of this chapter, the method of generalized modeling is introduced.

2.1 Dynamical systems and steady states

Dynamical systems are widely used throughout different scientific disciplines to describe and predict the behavior of systems that change in time. A dynamical system consists of a set of state variables and a set of rules that describes the evolution of the state variables in time [11]. There exist various different formalisms that are commonly used to formulate the rules of evolution, such as ordinary, partial or stochastic differential equations or discrete time maps.

This thesis focuses on studying dynamical systems that are described by ordinary differential equations (ODEs). An n -dimensional system of ODEs can be written as

$$\frac{d}{dt}\mathbf{X} = \mathbf{F}(\mathbf{X}) \tag{2.1}$$

where $\mathbf{X} = (X_1, \dots, X_n)$ is an n -dimensional vector of *variables* that changes in time and $\mathbf{F} = (F_1, \dots, F_n)$ is a vector-valued, possibly nonlinear function that describes the way in which the variables change. Additionally, the function \mathbf{F} can depend on external *parameters*.

A *steady state* \mathbf{X}^* of a dynamical system is defined as a special set of variables for which $\mathbf{F}(\mathbf{X}^*) = 0$. This implies that the variables of a system which is located exactly

at the steady state do not change in time. Steady states are also called *equilibria* in the literature of dynamical systems theory [11, 12], a term which has a different meaning in physics and chemistry. In this thesis, the term “equilibrium” is used synonymously with “steady state” unless explicitly stated otherwise.

In nature, dynamical systems are always subject to fluctuations and external influences that affect the values of the variables. Even if these effects are not explicitly included in the model, they necessitate considering the behavior of trajectories close to steady states. The local *stability* of a steady state describes the response of the dynamical system to infinitesimally small perturbations. It should be noted that different notions of stability are discussed in the different fields that the theory of dynamical systems is applied to, such as astronomy [13] or ecology [14]. In this thesis, we use the term “stability” synonymously with “local asymptotic stability”, which is a special form of Lyapunov stability [11].

The response to a perturbation of a dynamical system residing in a steady state is characterized by the linearization of the system, which is given by the *Jacobian matrix*. The Jacobian of an n -dimensional system of ODEs is a matrix of size $n \times n$ defined by

$$J_{ij} = \left. \frac{\partial F_i}{\partial X_j} \right|_{\mathbf{x}=\mathbf{x}^*} \quad i, j = 1 \dots n. \quad (2.2)$$

If all eigenvalues of the Jacobian have nonzero real parts, the steady state is *hyperbolic* and the dynamics close to the steady state are governed by the linearization of the system. For hyperbolic steady states, the eigenvalue of \mathbf{J} with the largest real part determines the stability of the steady state. If its real part is positive, infinitesimally small perturbations lead to trajectories that depart from the steady state exponentially. In this case, the steady state is *asymptotically unstable*. If the real part is negative and all eigenvalues have a negative real part, local trajectories return to the steady state as a response to a perturbation, and the steady state is *asymptotically stable*. If the Jacobian at the steady state has an eigenvalue with a real part that is exactly zero, the steady state is *nonhyperbolic*. In this case, the dynamics in the neighborhood of the equilibrium cannot be fully described by the Jacobian and higher terms become important. The properties of nonhyperbolic steady states are further investigated in the following section on bifurcations.

2.1.1 Bifurcations and their normal forms

Dynamical systems that describe a part of reality usually depend on a number of parameters. We can make the dependence on a vector of parameters \mathbf{p} explicit by writing Eq. (2.1) as

$$\frac{d}{dt}\mathbf{X} = \mathbf{F}(\mathbf{X}, \mathbf{p}). \quad (2.3)$$

A *bifurcation* can be defined as “the appearance of a topologically nonequivalent phase portrait under variation of parameters” [11]. In other words, bifurcations mark the transitions between regions of qualitatively different dynamic behavior resulting from a change of external parameters.

Bifurcations can be *local* or *global*. Local bifurcations can be detected by the properties of an infinitesimally small region around a bifurcation point, whereas global bifurcations can only be detected by investigating an extended region of the phase space.

Bifurcations can be broadly characterized by their *codimension*, which is determined by the difference between the dimension of the varied parameter space and the dimension of the corresponding bifurcation boundary [11]. More intuitively, it can be understood as “the smallest dimension of a parameter space which contains the bifurcation in a persistent way” [12]. For example, a codimension-2 bifurcation appears as a zero-dimensional point in a two-parameter bifurcation diagram, whereas it appears as a one-dimensional line in a three-parameter bifurcation diagram.

Dynamical systems theory has shown that for many types of bifurcations, *normal forms* can be defined. Normal forms are simplified descriptions of the system that are locally topologically equivalent to the bifurcation in arbitrary systems. With the help of normal forms, a catalog of codimension-1 and codimension-2 bifurcations has been established. Thereby, local bifurcations that occur in larger systems can be classified and information on the dynamics of their neighborhood can be retrieved based on the analysis of the respective normal forms.

The possibility of deriving normal forms relies on the *center manifold theorem for flows* [12], which states that it is possible to divide the flow close to a steady state into a stable manifold, an unstable manifold and a center manifold. The stable manifold corresponds to the directions in eigenspace that belong to the eigenvalues with a negative real part, whereas the unstable manifold corresponds to those with a positive real part. The center manifold, which is given by the eigenspace belonging to the eigenvalues with zero real part, contains the essential dynamical properties of the bifurcation.

Since trajectories in the unstable or stable directions either leave or approach the steady state exponentially, the more detailed dynamic behavior of the corresponding manifolds is not of primary interest. It is therefore useful to apply a transformation that reduces the system to a lower-dimensional system given by its center manifold, which describes the nontrivial dynamics. The simplified system can then be further transformed to the normal form of the bifurcation. It is a generic qualitative description of the dynamical behavior of a large class of systems that can all be reduced to the same normal form. The behavior of the system close to the bifurcation point can be related to the coefficients that appear in the normal form.

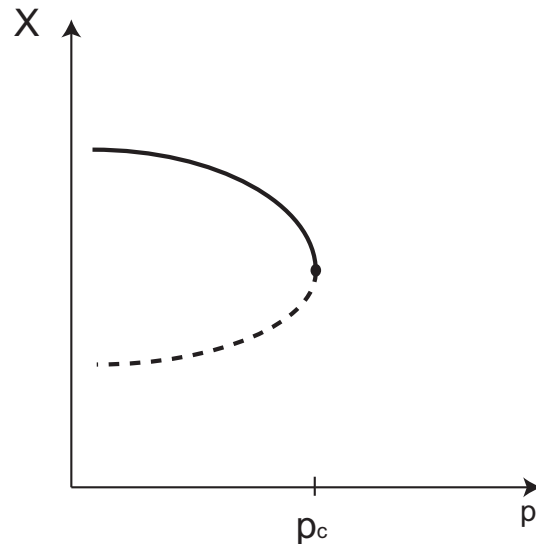


Figure 2.1: Bifurcation diagram of a saddle-node bifurcation. The steady-state value of a variable X is plotted against a parameter p . For $p < p_c$, an unstable steady state coexists with a stable one. For $p > p_c$, no steady state exists.

The mathematical theory of normal form analysis has thus provided powerful tools that can be applied to large classes of dynamical systems. In the following, we classify the most important local bifurcations of steady states with codimension 1 and 2.

2.1.2 Codimension-1 bifurcations

There are two generic types of local codimension-1 bifurcations that can be distinguished by the signature of the eigenvalues of the Jacobian.

A *saddle-node* bifurcation (SN bifurcation, *fold* bifurcation) is characterized by a zero eigenvalue. The generic type of a saddle-node bifurcation leads to the bifurcation diagram shown in Fig. 2.1. When a SN bifurcation is approached from one side by changing an external parameter, an unstable steady state collides with a stable one when the parameter approaches its critical value. For parameter values on the other side of the bifurcation, no steady state exists.

In biological systems, it is often undesirable to traverse an SN bifurcation because the change of the external parameter causes the system to depart from its previous operation point, potentially removing the functionality of the system. A situation in which SN bifurcations can be beneficial are *bistable* systems in which the loss of stability in a SN bifurcation is an important dynamical feature because it allows the system to switch to a second stable steady state which corresponds to a different functional operating point [15, 16].

Other codimension-1 bifurcations, such as *pitchfork* bifurcations or *transcritical*

bifurcations, are related to SN bifurcations. They are caused by an additional symmetry and lead to a different phase portrait. However, there always exists a perturbation to the model which destroys the symmetry and recovers the generic SN bifurcation [11]. In larger models without any apparent symmetries, one usually encounters generic SN bifurcations.

The second class of codimension-1 bifurcations are *Hopf* bifurcations (sometimes also called *Andronov-Hopf* bifurcations) [17]. This class of bifurcations is characterized by a Jacobian with a pair of conjugate complex eigenvalues with a zero real part. Hopf bifurcations are associated with the birth and decay of limit cycles. Therefore, many models with oscillatory dynamics feature Hopf bifurcations.

Depending on which side of the bifurcation a limit cycle exists, one can further distinguish between *supercritical* and *subcritical* Hopf bifurcations. A Hopf bifurcation is supercritical (Fig. 2.2A) when the transition from a stable steady state to an unstable one involves the appearance of a stable limit cycle. Supercritical Hopf bifurcations are associated with sustained oscillations and with a *soft loss of stability* because a system that approaches the limit cycle can remain close to the original steady state in phase space.

A Hopf bifurcation is subcritical (Fig. 2.2B) when an unstable limit cycle coexists with a stable equilibrium on one side of a bifurcation. The limit cycles vanishes when the equilibrium becomes unstable. Subcritical Hopf bifurcations can lead to a *catastrophic* loss of stability because trajectories are no longer confined to a region in phase space close to the equilibrium after stability is lost. The long-term behavior of trajectories that leave the region of the stable state cannot be analyzed by a local bifurcation analysis. However, subcritical Hopf bifurcations are often associated with large-amplitude oscillations. A typical scenario for this case is shown in Fig. 2.2C, in which the unstable limit cycle bends and gains stability in a global bifurcation.

Normal-form analysis allows to distinguish whether a Hopf bifurcation is supercritical or subcritical. The normal form parameter l_1 , called *first Lyapunov coefficient*, is a quantity that is positive at subcritical Hopf bifurcations and negative at supercritical Hopf bifurcations. In chapter 3, the calculation of l_1 is introduced in the context of generalized models.

There are also nonlocal bifurcations of codimension 1. An important example are *homoclinic bifurcations* of codimension 1 that occur when a saddle collides with a periodic orbit. The bifurcation point is characterized by a *homoclinic orbit*, i.e., a trajectory that approaches the saddle in both directions of time.

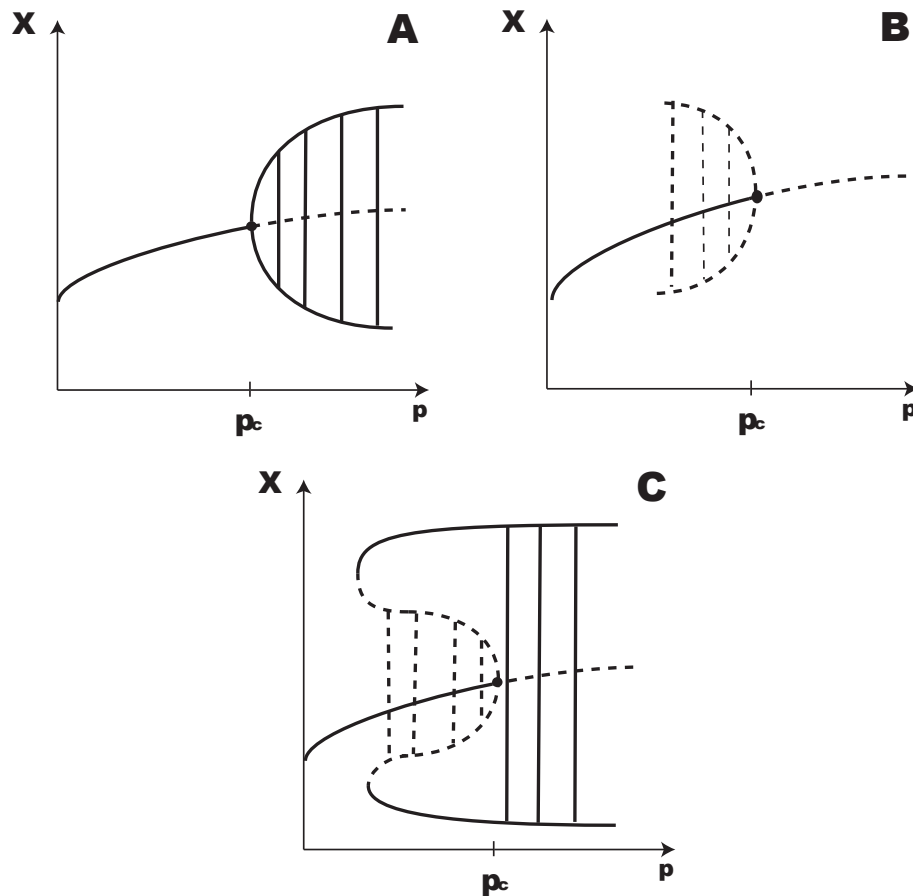


Figure 2.2: Supercritical and subcritical Hopf bifurcations. In panel A, a supercritical Hopf bifurcation is shown. A stable limit cycle emerges at the bifurcation point. In panel B, a subcritical Hopf bifurcation is shown. At one side of the bifurcation, a stable steady state coexists with an unstable limit cycle. In panel C, a possible but non-generic scenario is shown that motivates why subcritical Hopf bifurcations are often associated with large-amplitude oscillations.

2.1.3 Codimension-2 bifurcations

In bifurcations of codimension 2, two parameters must be tuned to critical values. This means that codimension-2 bifurcations appear as points in two-dimensional bifurcation diagrams, possibly forming the intersection of two codimension-1 bifurcations. Therefore, the variation of a single parameter usually does not lead to a bifurcation of codimension 2 and typically only codimension-1 bifurcations are directly crossed in nature. However, the detection of codimension-2 bifurcations in a model is not only of theoretical interest because these bifurcations can provide information on the dynamics of the surrounding parameter space, functioning for example as proxies for global properties such as bistability or chaos. Here, we give a short overview of the most common bifurcations of codimension 2.

- A *Takens-Bogdanov* (TB) bifurcation [18, 19] is characterized by two real zero eigenvalues in the Jacobian. In a TB bifurcation, a saddle-node bifurcation collides with a Hopf bifurcation. A limit cycle exists in the nearby parameter regime, which disappears in a homoclinic bifurcation. The detection of a local TB bifurcation therefore also provides information on nonlocal dynamical behavior.
- A *Gavrilov-Guckenheimer* (GG) bifurcation or *fold-Hopf* bifurcation [20, 21] is characterized by a zero eigenvalue and a complex conjugate pair of eigenvalues, leading to a three-dimensional center manifold. The bifurcation is found at the intersection of two codimension-1 bifurcations, a saddle-node bifurcation and a Hopf bifurcation.
- A *double Hopf* (DH) bifurcation or Hopf-Hopf bifurcation [22] is characterized by two conjugate pairs of purely imaginary eigenvalues, implying that for a system with a DH bifurcation, $n \geq 4$. Two Hopf bifurcations intersect in a DH bifurcation. Often, other bifurcations appear close to DH bifurcations, which can imply the birth of chaos, even though the chaotic manifold can be unstable in some systems. The search for DH bifurcations can thus be used by local methods as a means of detecting possible chaotic parameter regions.
- A *Bautin bifurcation* (BB) or *generalized Hopf* bifurcation [23, 24] is the transition between a supercritical and a subcritical Hopf bifurcation. It is characterized by a vanishing first Lyapunov coefficient. In contrast to the previously discussed codimension-2 bifurcations, a Bautin bifurcation cannot be detected by an analysis of the Jacobian but requires the knowledge of the local second and third derivatives.
- A *cusp bifurcation point* (CP) [25] is a special form of a SN bifurcation that

is characterized by a vanishing normal form parameter and thus, similar to the Bautin bifurcation, not detectable by the spectrum of the Jacobian alone. Close to cusp bifurcations, there is a regime with three coexisting steady states. Depending on the cubic normal form parameter, two of the steady states are stable and one is unstable, or vice versa [11]. Because of this property, cusp bifurcations can serve as cues in a search for bistable regions in parameter space.

2.2 Introduction to generalized modeling

In this section, the method of generalized modeling is introduced. In earlier studies, this method has been applied to models from various different disciplines such as ecological systems [26–29, 10, 30, 31], metabolic systems [9, 32, 33], gene-regulatory networks [34] and socio-economic systems [8].

The idea of GM is to describe a large class of models by their steady-state properties without having to determine explicit functional forms. Instead, the Jacobian is directly parametrized by a procedure that, in spite of its generality, maintains the biological interpretability of the parameters. Subsequently, the stability of the steady states and the bifurcations occurring in the model are determined. Since different classes of functional forms in conventional models lead to the same set of general parameters, a general model can describe the steady-state behavior of a large set of conventional models.

We introduce GM at the example of a simple toy model for gene-regulation with negative feedback. Subsequently, we discuss the method in a more abstract way and discuss its advantages and disadvantages. Finally, some important differences in the bifurcation analysis of conventional and generalized models are discussed. For a mathematically more rigorous introduction to generalized models we refer to Ref. [35].

2.2.1 General model of a transcription factor with autoinhibition

The method of GM is best introduced by applying it to a simple example. For that purpose, we choose a class of models describing a gene with autoinhibiting feedback. For an in-depth discussions of the biological processes and ways to model them, we refer to textbooks such as Refs. [36, 37]. The basic processes described by this model are transcription and translation. In the process of transcription, genes are read by the enzyme RNA-Polymerase and mRNA is generated as a result. This step is regulated by several enzymes that can enhance or inhibit the production rate of mRNA. In eukaryotic cells, transcription take place in the nucleus of the cell. The mRNA molecules then leave

the nucleus and are used as templates in the cytoplasm for the synthesis of proteins. This process takes place at the ribosomes and is called translation. We consider here the special case of a protein that acts as an inhibiting transcription factor, such that it represses the transcription of its own gene. This introduces a negative feedback loop, which can lead to oscillations in the concentrations of mRNA and protein.

As an intuitive first approach to a mathematical model, it is natural to capture the processes of transcription and translation by the two equations

$$\begin{aligned}\dot{X}_1 &= F(X_2) - G(X_1) \\ \dot{X}_2 &= H(X_1) - K(X_2)\end{aligned}\tag{2.4}$$

where X_1 denotes the concentration of the mRNA and X_2 the concentration of the protein. For both variables, there is a positive production term ($F(X_2)$ and $H(X_1)$) and a positive decay term ($G(X_1)$ and $K(X_2)$) which consist of undetermined, possibly nonlinear functions. While the decay terms of both variables depend only on the respective concentrations of the same variable, the production terms depend on the concentration of the respective other variable. In the case of $H(X_1)$ this reflects that X_1 serves as a template for translation, whereas in the case of $F(X_2)$ it reflects the negative feedback exerted by the transcription factor X_2 . At this point, no further assumptions are made on the functional forms $F(X_2)$, $G(X_1)$, $H(X_1)$ and $K(X_2)$ because general models aim to describe general aspects of the dynamics that are valid for different classes of possible functional forms.

We now *assume* that there exists a steady state in the model, which is characterized by concentrations $X_1^*, X_2^* > 0$. The steady-state values of the functions are denoted F^*, G^*, H^*, K^* . In Sec. 2.2.3 we discuss cases in which this assumption is not justified and to what extent it restricts the class of models that can be considered by the method of GM.

In the next step, the system of ODEs from Eq. (2.4) is normalized by defining

$$\begin{aligned}x_1 &= \frac{X_1}{X_1^*} \\ x_2 &= \frac{X_2}{X_2^*}.\end{aligned}\tag{2.5}$$

We also define normalized functions

$$\begin{aligned}f(x_2) &= \frac{F(x_2 X_2^*)}{F^*} & g(x_1) &= \frac{G(x_1 X_1^*)}{G^*} \\ h(x_1) &= \frac{H(x_1 X_1^*)}{H^*} & k(x_2) &= \frac{K(x_2 X_2^*)}{K^*}.\end{aligned}\tag{2.6}$$

In the new variables, the steady state is located at $x_1^* = x_2^* = 1$ and the system of

equations can be written as

$$\begin{aligned} \dot{x}_1 &= \alpha_1 (f(x_2) - g(x_1)) \\ \dot{x}_2 &= \alpha_2 (h(x_1) - k(x_2)). \end{aligned} \quad (2.7)$$

The terms

$$\alpha_1 = \frac{F^*}{X_1^*} = \frac{G^*}{X_1^*} \quad (2.8)$$

and

$$\alpha_2 = \frac{H^*}{X_2^*} = \frac{K^*}{X_2^*} \quad (2.9)$$

are constant *scaling parameters*. They are defined as the ratio of the steady-state values of a function and a variable or, in physical terms, a flux and a concentration. Therefore, the α_i are positive and have the dimension of an inverse time. They can be interpreted as timescales of the corresponding processes.

In the next step, we formally derive an expression for the Jacobian \mathbf{J} in the normalized coordinates. In \mathbf{J} , local derivatives of the normalized function with respect to the normalized variables appear that are defined as

$$f_2 = \left. \frac{\partial f}{\partial x_2} \right|_{x_2=1} \quad g_1 = \left. \frac{\partial g}{\partial x_1} \right|_{x_1=1} \quad h_1 = \left. \frac{\partial h}{\partial x_1} \right|_{x_1=1} \quad k_2 = \left. \frac{\partial k}{\partial x_2} \right|_{x_2=1}. \quad (2.10)$$

The local derivatives are logarithmic derivatives when expressed in the original variables, as can be seen at the example of f_2 :

$$f_2 = \left. \frac{\partial f}{\partial x_2} \right|_{x_2=1} = \left. \frac{X_2^*}{F^*} \frac{\partial F}{\partial X_2} \right|_{X_2=X_2^*} = \left. \frac{\partial (\ln F)}{\partial (\ln X_2)} \right|_{X_2=X_2^*} \quad (2.11)$$

In GM, the local derivatives are treated as model parameters. They are denoted as *elasticities* (a term from metabolic control analysis [38]) or *exponent parameters*.

In the case of a linear functional dependency, the corresponding elasticity is equal to 1. This relation is a special case of the more general power-law function $f(x) = ax^p$, where the elasticity is given by the power-law exponent p . In Table 2.1, we list the elasticities and their possible values for various functional forms that are frequently used in biological modeling.

With the introduced scale parameters and elasticities, the Jacobian of the generalized model defined by Eq. (2.7) is given by

$$\mathbf{J} = \begin{pmatrix} \alpha_1 \\ \alpha_2 \end{pmatrix} \begin{pmatrix} -g_1 & f_2 \\ h_1 & -k_2 \end{pmatrix}. \quad (2.12)$$

We next narrow down the values for the elasticities. Assuming that the decay of both mRNA and protein are not regulated by additional feedback mechanisms, it is sensible to assume that both decay terms are linear, leading to $g_1 = k_2 = 1$. Moreover,

Name	Function	Elasticity	Range
Linear	AX	1	-
Power law	AX^n	n	-
Michaelis-Menten	$\frac{AX}{K+X}$	$\frac{1}{1+(X^*/K)}$	$[0, 1]$
Hill function	$\frac{AX^n}{K^n+X^n}$	$n\frac{1}{1+(X^*/K)^n}$	$[0, n]$
Sigmoidal inhibition	$\frac{A}{K^n+X^n}$	$-n\frac{1}{1+(K/X^*)^n}$	$[-n, 0]$

Table 2.1: Elasticities corresponding to various functional forms that are frequently used in biological models. The rightmost column displays the range of values that the elasticity can assume. All functions depend on a variable X with a steady-state value X^* . The parameters $A, K, n > 0$ are positive constants.

we assume that the rate of protein production scales linearly with the concentration of mRNA, $h_1 = 1$. Because the transcriptional feedback is assumed to be inhibitory, $f_2 < 0$ is negative. In principle, we could now restrict f_2 to a range of biologically reasonable values. For example, the assumption of sigmoidal inhibition with $n = 1$ leads to $f_2 \in [-1, 0]$. In this case, however, it is not necessary to make any assumptions except $f_2 < 0$.

Under these assumptions, the Jacobian of steady states in all models with the mentioned structure can be written as

$$\mathbf{J} = \begin{pmatrix} \alpha_1 \\ \alpha_2 \end{pmatrix} \begin{pmatrix} -1 & f_2 \\ 1 & -1 \end{pmatrix}. \quad (2.13)$$

A necessary condition for a saddle-node bifurcation is $\det J = 0$, leading to a zero eigenvalue. However, since $\det J = \alpha_1 \alpha_2 (1 - f_2) > 0$ because of $f_2 < 0$, no saddle-node bifurcations occur in the model.

Since Hopf bifurcations are characterized by two purely imaginary conjugate eigenvalues, the trace of the Jacobian vanishes in a Hopf bifurcation of a two-dimensional system of ODEs. However, since $\text{tr}(J) = -\alpha_1 - \alpha_2 < 0$, no Hopf bifurcations can occur in the model, regardless of the functional form that is assumed for f_2 . Indeed, applying Bendixson's criterion [12] shows that no closed orbits are possible in this model. Therefore, the model structure at hand is not suitable for modeling genetic oscillations. For the present toy model, the impossibility of oscillations has been known for many years [39], so that more sophisticated models are needed to describe genetic oscillations. In chapter 3, some of these models are analyzed with the method of GM with the focus on the type of their Hopf bifurcations. We note that in larger and more complicated models, statements about the existence of certain bifurcation types as a function of the topology and the functional forms can lead to new insights both about appropriate

mathematical models and about the processes in nature that are modeled.

2.2.2 Abstract description of the method

The GM approach to a problem can be summarized by the following steps: In the first step, a system of ODEs is constructed in a general way. This includes the choice of n positive variables X_i , $i = 1 \dots n$ that could, for example, correspond to concentrations of proteins, mRNA molecules or cells. It also includes the choice of processes that increase or decrease these variables, which are grouped into gain terms and loss terms. However, no explicit functional forms are chosen for these processes. Instead, we only stipulate for each process on which variables its function can depend and assume that the functional forms are continuously differentiable. Furthermore, it is assumed that the system has at least one steady state \mathbf{X}^* in which all variables have positive, nonzero values. Below, we will argue that this assumption, which is fundamental to the method of GM, does not strongly limit the range of systems that can be analyzed.

The second step of GM consists of an entirely formal normalization of the system of ODEs with respect to the steady state. The normalization solves the problem that even though the existence of a steady state is assumed, it is unknown for which values of the variables the steady state exists. The normalization which consists of a division of both sides of each equation by the respective steady state concentration X_i^* leads to a system for which the steady state is known, because

$$x_i^* = X_i/X_i^*|_{\mathbf{x}=\mathbf{x}^*} = 1 \quad \forall i. \quad (2.14)$$

This gain of knowledge about the steady state in the normalized system is achieved at the cost of introducing unknown steady-state concentrations X^* on the right hand side of the system of equations. We can, however, combine these constants to a new set of parameters. These *scale parameters* have the dimension of an inverse time and can be interpreted as the timescales of the respective processes. In many cases, the scale parameters can be estimated by experimental data.

For the normalized system, the Jacobian matrix at the steady state $\mathbf{x}^* = \mathbf{1}$ is formally derived. For this purpose, the derivatives of the (normalized) functions with respect to the (normalized) variables are formed. These quantities can also be interpreted as the logarithmic derivatives of the functions in the original system of ODEs. These quantities are called elasticities, and together with the time scale parameters they form the set of general parameters. It might seem that in order to know the exact values of the derivatives, knowledge of both the functional form and the steady-state values of the variables would be required. However, the elasticities also have an independent interpretation as the local degree of saturation of the function with respect to

the normalized variables, which can be used to determine them or restrict them to a range of feasible values [9, 32].

In the last step, values are assigned to the general parameters in the Jacobian. Depending on the degree of certainty given by the specific properties of the problem, some of the parameters are fixed while other parameters are restricted to ranges of feasible values. Instead of parameterizing the specific rate functions in a conventional model, we thereby directly parametrize the Jacobian matrix, governing the dynamics close to all possible steady states in all models that are consistent with the observed interaction network. Only subsequently, the class of models under consideration is narrowed down by fixing some of the parameters of the generalized model.

2.2.3 Limitations of generalized modeling

In this section, we discuss different arguments that can be brought up against the method of GM and its generality. A possible objection is that the requirement that the model has a steady state restricts the class of models that can be analyzed with GM. While it is accurate that models without a steady state cannot be approached with GM, the method aims at biologically relevant systems describing processes that occur in nature. When the dynamics of a typical biological system is observed over an extended duration, there are not many realistic possibilities of dynamical behavior which do not involve either stationary dynamics from a stable steady state, or nonstationary dynamics such as limit cycles, that involve the existence of nearby unstable steady states when they arise via Hopf bifurcations. In particular, unbounded growth or decay is not a realistic type of dynamics for the problems that we investigate.

Another possible objection is that the steady-state concentrations are assumed to be positive. The assumption of excluding steady states with zero concentrations, for which the normalization process fails, restricts the set of steady states that we can analyze, since many models have steady states in which at least one of the variables is zero. We note that the existence of such a trivial steady state does not prevent us from analyzing other nontrivial steady states that possibly exist in the same model. Moreover, these singular steady states are usually not biologically relevant, because the fact that a certain concentration is represented in the form of a dynamic variable to our model usually implies that it is expected to be larger than zero in all meaningful circumstances.

A third possible objection is that active systems of living matter do not operate from a steady state but are subject to continuous change. However, this objection is based on a misunderstanding of the level of abstraction of the models we want to investigate. While active processes in the cell do operate far from equilibrium in the sense of a

physical system property, the mathematical concept of a steady state or equilibrium from dynamical systems theory is different: The steady states that are investigated by GM are properties of specific mathematical models and thus depend on the choice of the variables. For example, the transcription of a gene is a process operating far from equilibrium from a biophysical point of view. But for many purposes, only the effects of this process, i.e., the changes in the concentration of mRNA molecules, are important, whereas the mechanistic details of the process of transcription are neglected. This leads to a set of variables that is well-described by a steady state. Biological models that are formulated in the framework of ODEs exhibit particularly often stationary dynamics since the continuous nature of the dynamical variables often requires them to be quantities that are averaged over an extended region. The sum of the contributions of the constantly changing subsystems that is formed in the average often leads to a stationary dynamics of the model variable.

We next discuss the inability of investigating nonlocal aspects of dynamical systems in general models. The impossibility of detecting global bifurcations is a limitation of the method, which is local by design. However, as shown in section 2.1.3, there are connections between global and local bifurcations, so that local properties can in some cases imply the existence of certain nonlocal dynamics. Examples for this include codimension-2 bifurcations that are associated with chaotic (double Hopf bifurcation) or bistable (cusp bifurcation) dynamics or that involve homoclinic bifurcations (Takens-Bogdanov bifurcation). Therefore, the local analysis can point towards the existence of global properties, especially when codimension-2 bifurcations are involved.

In a strict sense, the general results for local bifurcations describe the dynamics only in an infinitesimally small region at the bifurcation manifold. This also applies to bifurcation diagrams that characterize different types of bifurcations. In most practical examples, however, properties of the infinitesimal environment of a bifurcation extend to a significantly larger region of parameter space. For example, a supercritical Hopf bifurcation involves an extended parameter regime of sustained oscillations in most practical applications. The main focus of this thesis is thus not on mathematically rigorous results of ideal systems but on the characterization the dynamic properties of models for practical biological problems. To that end, we will often make use of heuristic arguments and use local information in order to spot *possible* dynamic behavior of a larger region in parameter space. When there is a need for strict statements with respect to nonlocal properties of models, GM must be supplemented by nonlocal methods in specific conventional models.

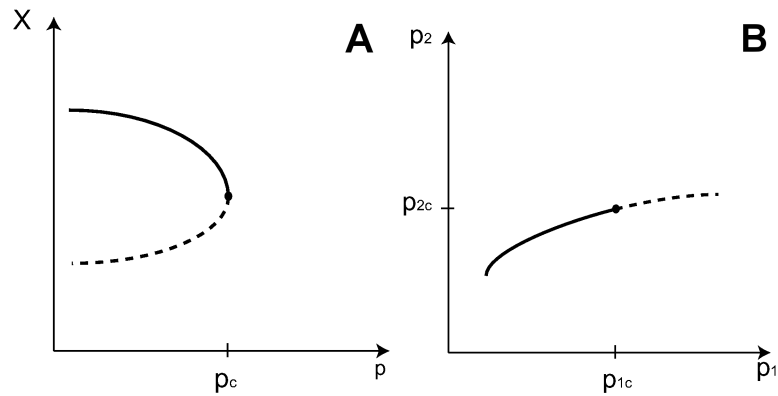


Figure 2.3: Bifurcation diagram of a generic saddle-node bifurcation in a conventional model (left) and a general model (right). In contrast to conventional models, a steady state exists for each parameter value in the general model. Its stability changes at (p_{1c}, p_{2c})

2.2.4 Bifurcations in general models

Bifurcation analysis of generalized models differs in various aspects from the bifurcation analysis of conventional models. This is mostly due to the difference between conventional and general parameters. While these sometimes subtle differences have been discussed in more detail in earlier studies [40, 35], we summarize in this section the most important aspects in which bifurcation diagrams of general parameters differ from those in conventional models.

The normalization which is performed in general models constructs the general parameters such that it is automatically ensured that for all admissible parameter values, the normalized system describes a steady state. In this steady state, all variables are equal to 1 by definition. Regions in parameter space without a steady state are thus not described by GM because they do not correspond to any set of general parameters.

For these reasons, saddle-node bifurcations have a different shape in bifurcation diagrams of general parameters. Since the normalized variables are fixed to 1, bifurcation diagrams that are equivalent to Fig. 2.3A cannot be shown, so that only bifurcation diagrams depending on two generalized parameters are meaningful. Moreover, the part of the bifurcation diagram in Fig. 2.3A in which no steady state exists does not correspond to any set of general parameters. The shape of a SN bifurcation in a bifurcation diagram of generalized parameters is shown in Fig. 2.3B. Note that while stability changes, an equilibrium exists for all values of the general parameter. The transformation to general variables means effectively that the parabola appearing in Fig. 2.1 a) is directly parametrized by the general parameter. A similar situation is encountered for cusp bifurcation of codimension 2, which are SN bifurcations in which the normal

coefficient of second order vanishes. The typical cusp-like structure which has given the bifurcation its name is not preserved by the transition to the general model.

In Hopf bifurcations, the shape of bifurcation diagrams does not differ qualitatively. However, it is necessary to keep in mind that also for Hopf bifurcations, there is a difference between bifurcation diagrams depending on conventional and general parameters. The former describe the behavior of a single model realization in which only the varied parameters change, while the latter describe classes of models, so that different sets of general parameters can correspond to different steady states in different conventional models.

Chapter 3

Normal-form analysis of bifurcations in gene-regulatory networks

In this chapter, we describe an extension of the method of generalized modeling that consists of the integration of higher derivatives into the bifurcation analysis. Previous studies in which generalized modeling is applied are exclusively based on an analysis of the information encoded in the Jacobian at steady states. While this information is sufficient to determine the stability of the steady states and many properties of the bifurcation landscape, there are cases in which the additional information encoded in the higher derivatives at the steady state reveals biologically relevant properties of the dynamics that cannot be detected by analyzing only the Jacobian. We center our investigation on Hopf bifurcations in gene-regulatory networks with negative feedback, where it has direct consequences of practical importance on the dynamics whether the Hopf bifurcation is supercritical or subcritical. This property is determined by the first Lyapunov coefficient, a parameter of the Hopf normal form that depends on the second and third derivatives computed in the steady state. Higher-order terms also specify important properties of codimension-2 bifurcations. As an example of this class, the detection of cusp bifurcations is demonstrated as a tool to determine the existence and the onset of a parameter regime with bistable dynamics.

We introduce the extension of the method of generalized modeling in Sec. 3.1. After giving a brief overview over oscillatory gene-regulatory networks in Sec. 3.2, we investigate in Sec. 3.3 the type of Hopf bifurcations in the Goodwin model, a simple model which describes a protein that inhibits the transcription of its own gene into mRNA. Subsequently, a larger model of a circadian oscillator that contains instances of both positive and negative feedback is analyzed in Sec. 3.4. We then modify this model

to demonstrate the possibility of detecting bistable dynamics via cusp bifurcations in Sec. 3.5, and conclude with a discussion of the results of this chapter in Sec. 3.6.

3.1 Normal-form parameters of codimension-1 bifurcations

In this section, we review the normal forms of generic Hopf and saddle-node bifurcations and show how to implement the normal form analysis into the framework of GM.

3.1.1 Normal form of Hopf bifurcations

The normal form of a Hopf bifurcation [11] can be written as the two-dimensional system of ODEs

$$\mathbf{f}(\mathbf{x}, \alpha) = \begin{pmatrix} \dot{x}_1 \\ \dot{x}_2 \end{pmatrix} = \begin{pmatrix} \alpha & -1 \\ 1 & \alpha \end{pmatrix} \begin{pmatrix} x_1 \\ x_2 \end{pmatrix} \pm (x_1^2 + x_2^2) \begin{pmatrix} x_1 \\ x_2 \end{pmatrix} + O(|x|^4). \quad (3.1)$$

This system has a steady state at $x_1 = x_2 = 0$ which changes stability in a Hopf bifurcation at a parameter value $\alpha = 0$. The Hopf bifurcation is subcritical for a positive sign of the nonlinear term and supercritical for a negative sign.

The center manifold theorem states that bifurcations in higher-dimensional systems can be reduced to their normal form [12]. For many purposes, the existence of this reduction is sufficient. However, in order to determine the type of a Hopf bifurcation in an particular higher-dimensional model, it is necessary to actually determine the center manifold and to calculate its relevant normal form parameters.

For a Hopf bifurcation, the first Lyapunov coefficient l_1 determines whether the bifurcation is supercritical or subcritical. This coefficient is calculated most conveniently by a procedure proposed in Ref. [11]. Here we provide a brief outline of this procedure, which requires the Jacobian, and the second and third derivatives of the functions at the steady state as input.

We denote the Jacobian matrix of an n -dimensional system of ODEs $\mathbf{f}(\mathbf{x})$ with \mathbf{J} . At a Hopf bifurcation, the spectrum of \mathbf{J} contains two complex conjugate eigenvalues with zero real part. We denote the absolute value of the complex conjugate pair of eigenvalues with ω . In the first step, two vectors \mathbf{q} and \mathbf{p} are determined that fulfill the relations

$$\begin{aligned} \mathbf{J}\mathbf{q} &= i\omega\mathbf{q} \\ \mathbf{J}^T\mathbf{p} &= -i\omega\mathbf{p}. \end{aligned} \quad (3.2)$$

The vectors \mathbf{q} and \mathbf{p} are subsequently normalized so that they fulfill

$$\langle \mathbf{p}, \mathbf{q} \rangle = 1 \quad (3.3)$$

with the standard scalar product $\langle \dots \rangle$.

In the next step, multilinear functions $\mathbf{B}(\mathbf{x}, \mathbf{y})$ and $\mathbf{C}(\mathbf{x}, \mathbf{y}, \mathbf{z})$ are introduced that include the second and third partial derivatives of \mathbf{f} evaluated at the steady state \mathbf{x}^* :

$$\begin{aligned} B_i(\mathbf{x}, \mathbf{y}) &= \sum_{j,k=1}^n \left. \frac{\partial^2 f_i(\boldsymbol{\xi})}{\partial \xi_j \partial \xi_k} \right|_{\boldsymbol{\xi}=\mathbf{x}^*} x_j y_k \quad i = 1, 2, \dots, n \\ C_i(\mathbf{x}, \mathbf{y}, \mathbf{z}) &= \sum_{j,k,l=1}^n \left. \frac{\partial^3 f_i(\boldsymbol{\xi})}{\partial \xi_j \partial \xi_k \partial \xi_l} \right|_{\boldsymbol{\xi}=\mathbf{x}^*} x_j y_k z_l, \quad i = 1, 2, \dots, n \end{aligned} \quad (3.4)$$

When the functional forms of the model are known, the derivatives appearing in $\mathbf{B}(\mathbf{x}, \mathbf{y})$ and $\mathbf{C}(\mathbf{x}, \mathbf{y}, \mathbf{z})$ can be computed either from analytic expressions or numerically, using finite differences. In generalized models where the functional forms are not explicated, they can be represented by parameters, as will be explained below.

Using these definitions, the formula for the first Lyapunov coefficient is

$$\begin{aligned} l_1 &= \frac{1}{\omega} \Re \left(\langle \mathbf{p}, \mathbf{C}(\mathbf{q}, \mathbf{q}, \bar{\mathbf{q}}) \rangle - 2 \langle \mathbf{p}, \mathbf{B}(\mathbf{q}, \mathbf{J}^{-1} \mathbf{B}(\mathbf{q}, \bar{\mathbf{q}})) \rangle \right. \\ &\quad \left. + \langle \mathbf{p}, \mathbf{B}(\bar{\mathbf{q}}, (2i\omega \mathbf{I}_n - \mathbf{J})^{-1} \mathbf{B}(\mathbf{q}, \mathbf{q})) \rangle \right) \end{aligned} \quad (3.5)$$

where \mathbf{I}_n is the unit matrix of size n . The derivation of this expression, shown in [11], is based on a Taylor expansion of $\mathbf{f}(\mathbf{x})$ at a Hopf bifurcation up to terms of third order. For a more convenient computational implementation, an algorithm outlined in [11] can be applied which reduces the number of higher derivatives that need to be calculated. In addition, this algorithm allows to calculate l_1 using only real-valued arithmetics.

3.1.2 Normal form of saddle-node bifurcations

The normal form of a generic saddle-node bifurcation is given by the one-dimensional system

$$\dot{x} = \alpha + \sigma x^2 + O(x^3). \quad (3.6)$$

with a parameter α and $\sigma = \pm 1$. For $\alpha = 0$ the system exhibits a nonhyperbolic steady state at $x = 0$. The quadratic normal form parameter which specifies the type of the saddle-node bifurcations is

$$a = \frac{1}{2} \frac{\partial^2 f}{\partial x^2}. \quad (3.7)$$

It is related to σ via

$$\sigma = \text{sgn}(a) \quad (3.8)$$

Unlike the sign of the Lyapunov coefficient of a Hopf bifurcation, the sign of a does not contain information of direct importance for practical applications. However, cusp bifurcations are characterized by $a = 0$. Since the existence of a cusp bifurcation points to a regime of bistability in parameter space, it can be useful to calculate a along a manifold of saddle-node bifurcations with the aim of finding the origin of a bistable parameter regime in a cusp bifurcation.

Similar to the procedure for a Hopf bifurcation outlined above, the normal form parameter a can be determined for n -dimensional systems using the center manifold theorem. From the Jacobian, normalized eigenvectors \mathbf{p} and \mathbf{q} are determined that fulfill the relations

$$\mathbf{J}\mathbf{q} = 0, \quad \mathbf{J}^T\mathbf{p} = 0 \quad (3.9)$$

Following Ref. [11], a is given by

$$a = \frac{1}{2}\langle \mathbf{p}, \mathbf{B}(\mathbf{q}, \mathbf{q}) \rangle \quad (3.10)$$

where the term $\mathbf{B}(\mathbf{q}, \mathbf{q})$, as defined in Eq. (3.4), contains only the second derivatives, so that in contrast to Eq. (3.5), third derivatives are not required.

3.1.3 Incorporating normal forms into generalized models

With the procedures outlined above, it is possible to calculate the numerical values of normal form parameters in a given conventional model. In fact, the automatic calculation of the first Lyapunov coefficient has been integrated into the newest generation of bifurcation software such as MATCONT [41]. However, it is less straightforward to integrate the calculation of Lyapunov coefficients into the framework of generalized modeling. The reason for this is that l_1 depends on the second and third derivatives at the steady state, which can be determined directly only in conventional models where the functional forms are specified. In generalized models, where the Jacobian is directly parametrized without the assumption of specific functional forms, the higher derivatives are unknown quantities. We apply two alternative strategies to solve this problem:

In the first strategy, the higher derivatives of the functions are incorporated into the model as additional parameters. The advantage of this approach is its high degree of generality. For example, it allows to reveal signatures in the higher derivatives of the functions under which a Hopf bifurcation is always supercritical. The most important disadvantage of this strategy is that the number of parameters can increase strongly, especially when the model under investigation includes multiple unknown nonlinear functions.

The alternative strategy is to restrict the functional forms to classes of functions. For example, certain processes may be well-described by a Hill function $F(X) = a \frac{X^n}{K+X^n}$ with positive parameters a , K and n . The assumption that the functional form under consideration obeys a Hill function leads to relations between the first derivative and higher derivatives of the normalized function and thus to a reduction in the number of parameters. Even though the second strategy has a lower degree of generality than the first strategy and thus more similarity to approaches in conventional models, it still retains several of the benefits of GM. Most importantly, due to the normalization, all steady states that exist in the model can be analyzed directly, without having to locate the steady states by numerical methods first. Therefore, this strategy still represents an efficient and general way to investigate the types of bifurcations that exist in a possibly large parameter space. Note that the two strategies can be combined by determining certain functional forms and leaving others undetermined by introducing additional parameters.

3.2 Negative-feedback oscillations in gene regulation

Before applying the extension of generalized modeling to Hopf bifurcations in specific models of oscillating gene-regulatory networks, we give a brief overview of the biological systems in which oscillations occur.

Various gene-regulatory networks are known in which oscillations play a functional role. The most famous example are circadian rhythms [42, 43] that are widespread among species, existing in animals, plants and even bacteria. Other notable examples of genetic oscillators include the cell cycle [44], the segmentation clock of vertebrates [45] and the p53 tumor suppressor protein [46]. The core mechanism that causes the oscillations in all of these examples is negative feedback, which is exerted by a transcription factor inhibiting the production of its own mRNA either directly by binding to its own promoter or indirectly, involving intermediate proteins.

The genetic oscillators that have evolved in nature need to fulfill additional requirements such as synchronization to oscillators in adjacent cells or robustness to noise. For that reason, they are not simple oscillators that rely on a single gene with autoinhibition. Instead, the inhibitory feedback loop is embedded in a larger network of interacting genes. Simple examples of genetic oscillators have been realized synthetically. The most prominent example is the *repressilator* [47] which is based on cyclic inhibition of three genes.

The basic mechanism of negative-feedback oscillations can be described qualita-

tively as follows: When the abundance of the protein is small, the inhibitional feedback on transcription is weak and the concentration of mRNA can increase. With a temporal delay, the concentration of the protein will also increase and at some point the inhibition will be so strong that mRNA levels decays again. Again, protein numbers follow the change in mRNA with a delay and the cycle repeats.

In Sec. 2.2, we have introduced the method of GM with the help of a toy model for this process. However, it was found that sustained oscillations were not possible in this model. The reason for the absence of oscillations is that the negative feedback from protein to mRNA acts too abruptly. There is not enough time for the system to generate a sufficient amount of mRNA before the negative feedback from the protein inhibits its own gene. In the cell, a protein cannot repress transcription immediately after its synthesis in the cytoplasm because it has to reach the nucleus first.

This inadequacy of the model can be overcome by different modifications. The most straightforward modification consists of implementing an explicit time delay in the model which can be discrete or follow a continuous distribution. In this case, the model becomes a system of delay differential equations (DDEs). It has been shown that in a realization of the toy model of Sec. 2.2 with explicit time delays, oscillations are indeed possible [48]. However, a disadvantage of this strategy is that DDEs are harder to analyze both numerically and analytically, since they are equivalent to an infinite-dimensional system of ODEs. Even though the analysis becomes more complicated, it is possible to approach systems of DDEs with the method of GM as well [49].

In this study, we choose a different modification of the toy model from Sec. 2.2, leading to the Goodwin model, which is analyzed in the subsequent section. Instead of introducing artificial time delays, an additional intermediate variable is added to the model in order to distinguish the protein concentrations in different parts of the cell such as the cytoplasm or nucleus by different dynamic variables. Thereby, a delay is introduced indirectly into the model without leaving the framework of ODEs.

3.3 Normal-form analysis of Hopf bifurcations in the Goodwin model

The Goodwin model, which has been proposed in 1965 by Brian C. Goodwin [39], is one of the earliest models for gene regulation with negative transcriptional feedback. In its original form, the model consists of three ODEs

$$\begin{aligned}\dot{X}_1 &= a_1 F(X_3) - a_2 X_1 \\ \dot{X}_2 &= a_3 X_1 - a_4 X_2 \\ \dot{X}_3 &= a_5 X_2 - a_6 X_3\end{aligned}\tag{3.11}$$

where X_1 denotes the concentration of mRNA that is translated into a protein, X_2 is the protein concentration in the cytoplasm, and X_3 is the concentration of the protein in the nucleus, where it acts repressively on the transcription of its own mRNA. The parameters a_i are rate constants. The function $F(X_3)$ describes the nonlinear negative feedback exerted by the protein on the process of transcription. Goodwin assumed the functional form

$$F_{orig}(X_3) = \frac{1}{1 + kX_3} \quad (3.12)$$

for the negative feedback term and erroneously detected a region in parameter space with sustained oscillations in his original computational analysis [39]. In 1968, Griffith [50] pointed out an error in the numerical simulations of Goodwin and showed analytically that for a general form of an inhibiting Hill function

$$F(X_3) = \frac{1}{1 + (kX_3)^n} \quad (3.13)$$

with a Hill coefficient n , Hopf bifurcations and sustained oscillations are only possible if $n \geq 8$. In the following decades, the existence of oscillations was studied for various generalizations of the Goodwin model, see e.g. [51, 52].

We study the Hopf bifurcations in the Goodwin model in the framework of generalized modeling. The first step in the transition to the general model is the normalization with respect to the steady state concentrations X_i^* . The normalized system is given by

$$\begin{aligned} \dot{x}_1 &= \alpha_1 (f(x_3) - x_1) \\ \dot{x}_2 &= \alpha_2 (x_1 - x_2) \\ \dot{x}_3 &= \alpha_3 (x_2 - x_3), \end{aligned} \quad (3.14)$$

where normalized variables $x_i = \frac{X_i}{X_i^*}$ and functions $f(x_3) = \frac{F(X_3)}{F(X_3^*)}$ are introduced. The parameters $\alpha_1 = a_2$, $\alpha_2 = a_4$, $\alpha_3 = a_6$ are positive and describe the time scales of the turnover of mRNA and protein in the cytoplasm and nucleus.

In the general model, there is only one nonlinear function, $f(x_3)$, so that the elasticities corresponding to the remaining functions are trivially equal to zero or, in case of linear functions, one. For this reason, the Goodwin model is conceptually simple. The conditions under which a Hopf bifurcation can occur in the Goodwin model and similar models are known, and we show that they can be directly transferred to the general model. However, the normal form of Hopf bifurcations in the Goodwin model has not been studied before, so that the emphasis of our investigation is placed on the effect of the functional forms used for $f(x_3)$ on the type of the Hopf bifurcation in the system.

In the steady state, the Jacobian of Eq. (3.14) is

$$J = \begin{pmatrix} \alpha_1 & 0 & 0 \\ 0 & \alpha_2 & 0 \\ 0 & 0 & \alpha_3 \end{pmatrix} \begin{pmatrix} -1 & 0 & f^{(1)} \\ 1 & -1 & 0 \\ 0 & 1 & -1 \end{pmatrix} \quad (3.15)$$

where

$$f^{(1)} = \left. \frac{df(x_3)}{dx_3} \right|_{x_3=1}. \quad (3.16)$$

Below, we will use the analogous notation for

$$f^{(2)} = \left. \frac{d^2f(x_3)}{dx_3^2} \right|_{x_3=1}, \quad f^{(3)} = \left. \frac{d^3f(x_3)}{dx_3^3} \right|_{x_3=1}. \quad (3.17)$$

In the following, we determine the Hopf bifurcation and its normal form in the model without restricting $f(x_3)$ to a specific functional form. The characteristic polynomial for J with an eigenvalue λ is

$$\lambda^3 + c_2\lambda^2 + c_1\lambda + c_0 \quad (3.18)$$

with

$$\begin{aligned} c_2 &= \alpha_1 + \alpha_2 + \alpha_3 \\ c_1 &= \alpha_1\alpha_2 + \alpha_1\alpha_3 + \alpha_2\alpha_3 \\ c_0 &= \alpha_1\alpha_2\alpha_3(1 - f^{(1)}) \end{aligned} \quad (3.19)$$

According to the method of resultants [53], the condition for a Hopf bifurcation in the three-dimensional case is

$$c_2c_1 - c_0 = 0. \quad (3.20)$$

In the following, we use the notation

$$\begin{aligned} \beta &= \alpha_1 + \alpha_2 + \alpha_3 \\ \omega^2 &= \alpha_1\alpha_2 + \alpha_1\alpha_3 + \alpha_2\alpha_3 \\ \gamma &= \alpha_1\alpha_2\alpha_3 \end{aligned} \quad (3.21)$$

where $\beta, \omega^2, \gamma > 0$ because all α_i are positive. In terms of these parameters, the condition Eq. (3.20) for a Hopf bifurcation is

$$f^{(1)} = 1 - \frac{\beta\omega^2}{\gamma} \quad (3.22)$$

Following Griffith's argument [50], β , ω and γ from Eq. (3.21) satisfy the algebraic inequality

$$\frac{1}{3}\beta \geq \left(\frac{1}{3}\omega^2\right)^{1/2} \geq \gamma^{1/3} \quad (3.23)$$

which is valid for all positive $\alpha_1, \alpha_2, \alpha_3$. Multiplication with $3\omega^2$ and use of the inequality yields

$$\beta\omega^2 \geq \sqrt{3}\omega^3 \geq \left(\frac{1}{3}\omega^2\right) 9\gamma^{1/3} \geq 9\gamma. \quad (3.24)$$

Therefore, the condition Eq. (3.22) can only be satisfied for

$$f^{(1)} \leq -8 \quad (3.25)$$

Griffith's results, that were derived for the special functional form Eq. (3.13), can thus be directly transferred into the framework of GM. Because $f^{(1)} \in [-n, 0]$ for a repressing Hill function according to Tab. 2.1, it follows that condition (3.22) is only fulfilled for $n > 8$ in this particular functional form.

If the Hopf condition of Eq. (3.22) is fulfilled, the eigenvalues of the Jacobian at the bifurcation are

$$\lambda_1 = -\beta, \lambda_2 = i\omega \quad \lambda_3 = -i\omega. \quad (3.26)$$

In the next step, we derive an expression for the first Lyapunov coefficient at the Hopf bifurcation. From \mathbf{J} and its transpose \mathbf{J}^T , eigenvectors \mathbf{p} and \mathbf{q} according to Eq. (3.2) are calculated. Prior to normalization, their expressions are

$$\mathbf{q} = \left(\frac{\alpha_1 f^{(1)}}{\alpha_1 + i\omega}, \frac{\alpha_3 + i\omega}{\alpha_3}, 1 \right), \quad \tilde{\mathbf{p}} = \left(\frac{\alpha_3 - i\omega}{\alpha_1 f^{(1)}}, \frac{\alpha_3}{\alpha_2 - i\omega}, 1 \right). \quad (3.27)$$

The normalization condition, $\langle \mathbf{p}, \mathbf{q} \rangle = 1$, leads to

$$\mathbf{p} = \overline{\langle \tilde{\mathbf{p}}, \mathbf{q} \rangle}^{-1} \tilde{\mathbf{p}} = \left(1 + \frac{\alpha_3 - i\omega}{\alpha_2 - i\omega} + \frac{\alpha_3 - i\omega}{\alpha_1 - i\omega} \right)^{-1} \tilde{\mathbf{p}}. \quad (3.28)$$

Since $f(x_3)$ is the only nonlinear function in the model

$$\mathbf{B}(\mathbf{x}, \mathbf{y}) = (\alpha_1 f^{(2)} x_3 y_3, 0, 0) \quad \mathbf{C}(\mathbf{x}, \mathbf{y}, \mathbf{z}) = (a_1 f^{(3)} x_3 y_3 z_3, 0, 0). \quad (3.29)$$

Evaluating Eq. (3.5),

$$l_1 = \frac{1}{\omega} \Re [\langle \mathbf{p}, \mathbf{C}(\mathbf{q}, \mathbf{q}, \bar{\mathbf{q}}) \rangle - 2\langle \mathbf{p}, \mathbf{B}(\mathbf{q}, \mathbf{J}^{-1} \mathbf{B}(\mathbf{q}, \bar{\mathbf{q}})) \rangle + \langle \mathbf{p}, \mathbf{B}(\bar{\mathbf{q}}, (2i\omega \mathbf{I}_n - \mathbf{J})^{-1} \mathbf{B}(\mathbf{q}, \mathbf{q})) \rangle]$$

for the Goodwin model therefore leads to

$$l_1 = \Re(\bar{p}_1 q_1 \bar{q}_1 (f^{(3)} + \alpha_1 f^{(2)} f^{(2)} (2\chi_1 + \chi_2))) \quad (3.30)$$

with

$$\begin{aligned} \chi_1 &= \mathbf{J}^{-1}_{1,3} = \frac{1}{\alpha_1 (f^{(1)} - 1)} \\ \chi_2 &= (2i\omega \mathbf{I}_n - \mathbf{J})^{-1}_{1,3} = -\frac{\alpha_2 \alpha_3}{3\omega^2 (\beta + 2i\omega)}. \end{aligned} \quad (3.31)$$

Next, the real part of Eq. (3.30) is evaluated and after several simplifications, the expression for l_1 is reduced to

$$l_1 = -f^{(3)} - \frac{1}{1 - f^{(1)}} \frac{\beta^2 + 8\omega^2}{\beta^2 + 4\omega^2} f^{(2)} f^{(2)}. \quad (3.32)$$

Positive prefactors were dropped in Eq. (3.32) because only the sign of l_1 determines the type of the Hopf bifurcation. The above calculation therefore leads to a general expression for l_1 which depends on the time scale parameters and the local derivatives of the nonlinear feedback functions.

We proceed by investigating l_1 for the case of Griffith's function, $F(X_3) = \frac{1}{1+(kX_3)^n}$. Normalization of $F(X_3)$ yields

$$f(x) = \frac{F(X_3)}{F(X_3^*)} = \frac{1 + \tilde{X}^n}{1 + (x_3 \tilde{X})^n}, \quad \tilde{X} = kX_3^*. \quad (3.33)$$

Evaluating the derivatives at the steady state and expressing the higher derivatives as functions of the Hill coefficient n and the first derivative leads to

$$\begin{aligned} f^{(1)} &= \left. \frac{df(x_3)}{dx_3} \right|_{x_3=1} = -n \frac{\tilde{X}^n}{1 + \tilde{X}^n} =: -n\theta \\ f^{(2)} &= \left. \frac{d^2f(x_3)}{dx_3^2} \right|_{x_3=1} = -n\theta (n - 1 - 2n\theta) = f^{(1)} (n - 1 + 2f^{(1)}) \\ f^{(3)} &= \left. \frac{d^3f(x_3)}{dx_3^3} \right|_{x_3=1} = f^{(1)} \left[(n - 1 + 2f^{(1)})^2 + 2f^{(1)}f^{(1)} + (2f^{(1)} - 1)(n - 1) \right]. \end{aligned} \quad (3.34)$$

In combination with Eq. (3.32), the first Lyapunov coefficient can therefore be expressed as a function of α_1 , α_2 , α_3 (determining $f^{(1)}$ via the Hopf condition Eq. (3.22)) and n . We fix $\alpha_3 = 1$, which implies no loss of generality because time can be measured in units of α_3 without affecting the bifurcations in the model. In Fig. 3.1, it is shown that $l_1 < 0$, for all values of the remaining parameters. Therefore, Hopf bifurcations are always supercritical in the Goodwin model with Griffith's feedback function $F(X_3)$, regardless of the specific parameters.

Next, we investigate the effect of small changes in the nonlinear feedback functions. For this we also fix the remaining time scales $\alpha_2 = 1$, $\alpha_1 = 0.8$, leading to $f^{(1)} = -8.1$ because of Eq. (3.22). We chose this set of parameters because it leads to a Hopf bifurcation close to the threshold $f^{(1)} = -8$ and avoids possible artifacts of parameter sets exactly at the threshold. Bifurcations described by this parameter set can be realized by Hill functions with integer exponents $n \geq 9$ or with fractional exponents $n \geq 8.1$. In Fig. 3.2, the curve of $l_1 = 0$ is drawn in the plane of $f^{(2)}$ and $f^{(3)}$. This curve marks a Bautin bifurcation, dividing the plane into a domain in which the Hopf bifurcation is supercritical and another domain in which it is subcritical. In Fig. 3.2, the

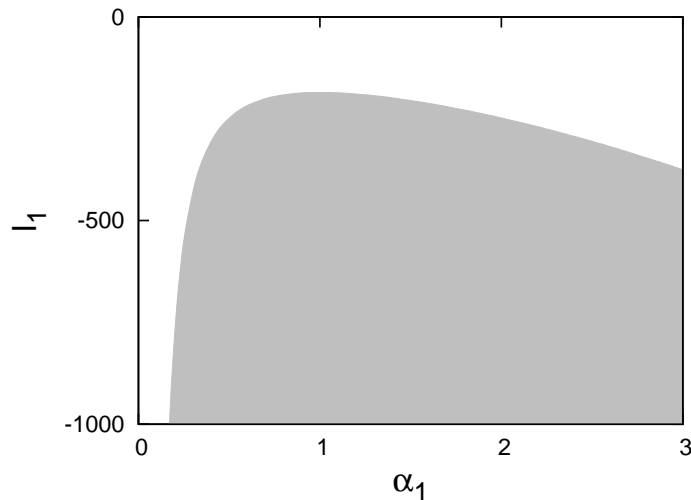


Figure 3.1: Possible values of l_1 for Hopf bifurcations in the Goodwin model with Griffith's function $F(X_3) = \frac{1}{1+(kX_3)^n}$. The shaded area visualizes the domain of possible values for $l_1(\alpha_1, \alpha_2, n)$, plotted as a function of α_1 . It continues to more negative values of l_1 outside the plotted region. The parameters α_1, α_2 were varied in the range $[0.01 : 10]$, n was varied in $[n_{min}, 100]$ where $n_{min} = -f^{(1)}$. For all parameter combinations, l_1 is negative and the Hopf bifurcation is supercritical. The maximum of l_1 corresponds to $\alpha_1 = \alpha_2 = \alpha_3 = 1$ and $n = 8$.

higher derivatives for the choice of Griffith's function $F(X_3) = \frac{1}{1+(kX_3)^n}$ are also shown. The exponent $n > 8.1$ is varied continuously while k is determined by the condition $f^{(1)} = -8.1$. In agreement with the more general results above, this curve does not leave the region of supercritical Hopf bifurcations, resulting in no intersection with the Bautin bifurcation curve.

We then vary $F(X_3)$ slightly and use a different function

$$G(X_3) = \frac{1}{1 + (kX_3)^n + (k_2X_3)^m},$$

thus adding a second term with another Hill coefficient to the denominator. Note that the shape of $F(X_3)$ and $G(X_3)$ does not differ strongly qualitatively (Fig. 3.2 bottom). However, in contrast to $F(X_3)$, the function $G(X_3)$ can lead to a subcritical Hopf bifurcation in the Goodwin model. Figure 3.2 (top) shows an intersection of the higher derivatives corresponding to $G(X_3)$ with the Bautin curve of $l_1 = 0$. However, this intersection occurs at a high Hill coefficient $n = 30.6$.

In conclusion, it is shown the Goodwin model belongs to a class of models in which the supercriticality of the Hopf bifurcation is robust with respect to changes in the parameters. If a sigmoidal inhibition function is used to model the feedback, the Hopf bifurcation is supercritical for arbitrary values of the Hill coefficient. While it

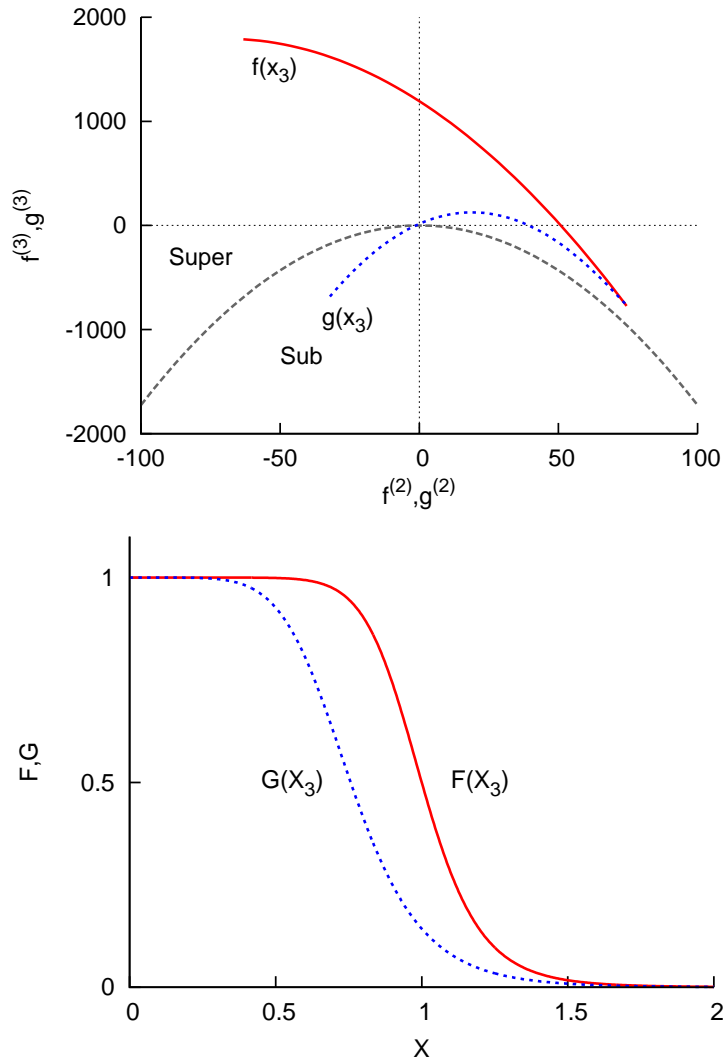


Figure 3.2: Top: Types of Hopf bifurcations in the Goodwin model: In the plane spanned by the second and third derivative of the feedback function, the dashed Bautin curve (gray) separates two domains of supercritical and subcritical Hopf bifurcations. The solid red curve depicts the higher derivatives of a sigmoidal inhibition function $F(X_3)$ with a varied Hill coefficient n , while the dotted blue curve depicts the higher derivatives of the slightly changed function $G(x_3)$ (with $m = 6$, $k_2 = 5k$ and n varied). Bottom: The functions $F(X_3)$, $G(X_3)$ with the same parameters and $n = 10$.

is easy to construct artificial feedback functions with higher derivatives that lead to a subcritical Hopf bifurcation, the biological meaningfulness for most of these functions is questionable. For the example function $G(X_3)$, which is qualitatively similar to $F(X_3)$, subcriticality is possible but occurs only at very large Hill coefficients.

We note that the extension of the method can be used to predict the bifurcation behavior for arbitrary functions. If the specific properties of a particular gene-regulatory network justify a differential functional form, the combination of general modeling with normal form analysis determines the type of Hopf bifurcation and thus whether the loss of stability is soft or catastrophic.

3.4 Normal-form analysis in a model of a circadian oscillator

In this section we proceed to investigate the normal form of Hopf bifurcations in a gene-regulatory network that is more complicated than the Goodwin model. For this purpose, we chose a model of the mammalian circadian oscillator that was developed in Ref. [54]. The model includes both negative and positive transcriptional feedbacks, a feature that is specific to mammalian circadian oscillators. Since there exist various larger and more detailed mechanistic models of circadian oscillators, such as those formulated in Refs. [44,55], the model under consideration model is of medium complexity.

At the basis of the mammalian circadian clock are the genes *per2* (Period) and *cry* (Cryptochrome) that are activated by the heterodimer BMAL1/CLOCK. By suppressing this activation of the BMAL1/CLOCK dimer, the proteins PER2 and CRY exert a negative feedback on the transcription of their own mRNA. Moreover, PER2 and CRY indirectly activate the transcription of the *Bmal1* gene by a double negative feedback, inhibiting the transcription of the gene *Rev-erba* (not explicitly included in the model), which in turn encodes for a protein that inhibits *Bmal1* transcription.

These interactions have been captured by a model [54], which is schematically depicted in Fig. 3.3. It includes seven variables that represent mRNA and protein concentrations of two genes, *per2/cry* and *bmal1*. Even though *per2* and *cry* are separate genes, they are assumed to have identical functional properties at the level of mRNA and are thus reduced to a single variable. Because the proteins PER2 and CRY form a complex, a single variable is used to describe the concentrations of the proteins as well. Three dynamic variables are associated with the *per2/cry* gene: the concentration of *per2/cry* mRNA (X_1), the concentration of the PER2/CRY complex in the cytoplasm (X_2) and in the nucleus (X_3). The *bmal1* gene is described by four variables, representing the concentrations of *bmal1* mRNA (X_4), BMAL1 protein in cytoplasm

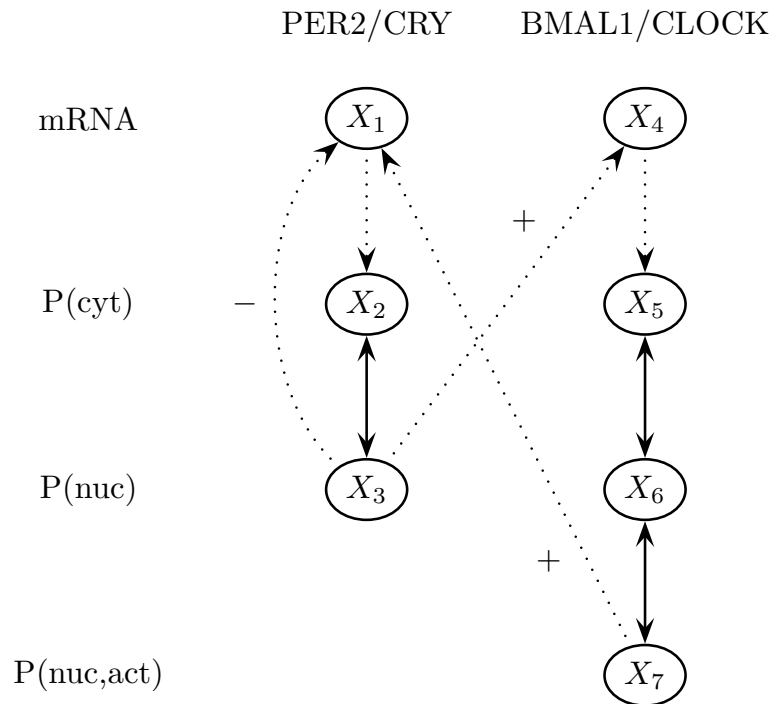


Figure 3.3: Schematic overview over the model of the mammalian circadian oscillator. The two genes that form the basis of the circadian oscillator, PER2/CRY and BMAL1/CLOCK, are represented by the concentration of mRNA and the concentrations of protein in cytoplasm and nucleus. For BMAL1/CLOCK, an additional variable describes the transcriptionally active form of the gene. Solid lines denote the (reversible) flow of biomass while dashed lines denote activating or inhibiting feedback without a flow of biomass.

(X_5), in the nucleus (X_6) and in its phosphorylated transcriptionally active form in the nucleus (X_7). There are three instances of nonlinear feedback in the model. The negative feedback by autoinhibition which forms the basis of the genetic oscillator is exerted by the PER2/CRY complex X_3 on its own mRNA X_1 . It is supplemented by two positive feedbacks: The PER2/CRY complex X_3 exerts a second type of feedback by promoting the transcription of the *bmal1* gene X_4 . Moreover, BMAL1 promotes the transcription of the *per2/cry* gene, so that there is another positive feedback link from X_7 to X_1 . For a more detailed discussion of the structure of the model we refer to the original publication [54].

From a structural point of view, the model under consideration can be seen as an extension of the simple Goodwin model that has been analyzed in the previous section. Here, the gene with negative autoinhibition is interconnected with another gene via positive-feedback transcriptional regulation.

The system of ODEs for the model in [54] is

$$\begin{aligned}
\frac{dX_1}{dt} &= f(X_3, X_7) - k_1 X_1 \\
\frac{dX_2}{dt} &= q(X_1) - k_2 X_2 + k_3 X_3 - k_4 X_2 \\
\frac{dX_3}{dt} &= k_2 X_2 - k_3 X_3 - k_5 X_3 \\
\frac{dX_4}{dt} &= g(X_3) - k_6 X_4 \\
\frac{dX_5}{dt} &= k_7 X_4 - k_8 X_5 + k_9 X_6 - k_{10} X_5 \\
\frac{dX_6}{dt} &= k_8 X_5 - k_9 X_6 - k_{11} X_6 + k_{12} X_7 - k_{13} X_6 \\
\frac{dX_7}{dt} &= k_{11} X_6 - k_{12} X_7 - k_{14} X_7
\end{aligned} \tag{3.35}$$

where all k_i are rate constants.

The nonlinear functions that were used in the original model are

$$\begin{aligned}
f(X_3, X_7) &= \frac{v_{1b}(X_7 + c)}{k_{1b}(1 + (X_3/k_{1i})^p) + (X_7 + c)} \\
g(X_3) &= \frac{v_{4b} X_3^r}{k_{4b}^r + X_3^r} \\
q(X_1) &= k_q X_1^q
\end{aligned} \tag{3.36}$$

where $n, p, q, r, v_{1b}, k_{1b}, k_{1i}, v_{1b}, c, k_q$ are further parameters, leading to a total number of 24 parameters.

When we implement the system of ODEs given by Eq. (3.35) into the framework of generalized modeling, we adopt the linearity of the functions that are not affected by any feedback mechanism from the original conventional model. The corresponding

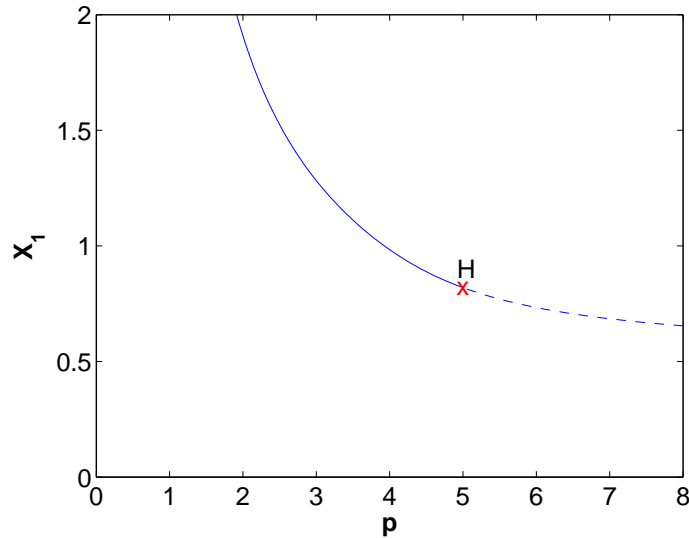


Figure 3.4: Bifurcation diagram of the conventional from Ref. [54]. If p is lowered from $p = 8$ to $p = 4.916$, the unstable steady state becomes stable in a supercritical Hopf bifurcation.

elasticities in the general model are accordingly fixed to 1. Because the PER2/CRY complex described by the variable X_2 is a dimer, the function $q(X_1)$ is assumed to be quadratic and the corresponding elasticity is fixed to the value 2. However, the nonlinear feedback functions $f(X_3, X_7)$ and $g(X_3)$ are not restricted to the functional forms of Eq. (3.36). Instead, the derivatives of these nonlinear functions are represented by parameters of the general model.

As a starting point for the analysis of Hopf bifurcations, the conventional model with the parameters of Table 1 in Ref. [54] is chosen. For this parameter set, sustained oscillations with a period of $T = 23.8h$ were observed [54]. Using the standard bifurcation software MATCONT [41], we detect an unstable steady state in the conventional model for this parameter set. Staying in the conventional model, we then proceed to search for a Hopf bifurcation by variation of the Hill coefficient p . Figure 3.4 shows that the unstable steady state becomes stable in a Hopf bifurcation when the Hill coefficient p of the function $f(X_3, X_7)$ is lowered from its original value $p = 8$ to $p = 4.916$. This Hopf bifurcation is supercritical.

We want to investigate to what extent the supercriticality of Hopf bifurcations is a robust property of the model structure and to what extent it is a mere property of this particular set of parameters. For this purpose, it is explored in the corresponding general model whether it is possible to continue the Hopf bifurcation in parameter space so that it becomes subcritical. We first construct the set of general parameters corresponding to the Hopf bifurcation of the conventional model. Subsequently, the

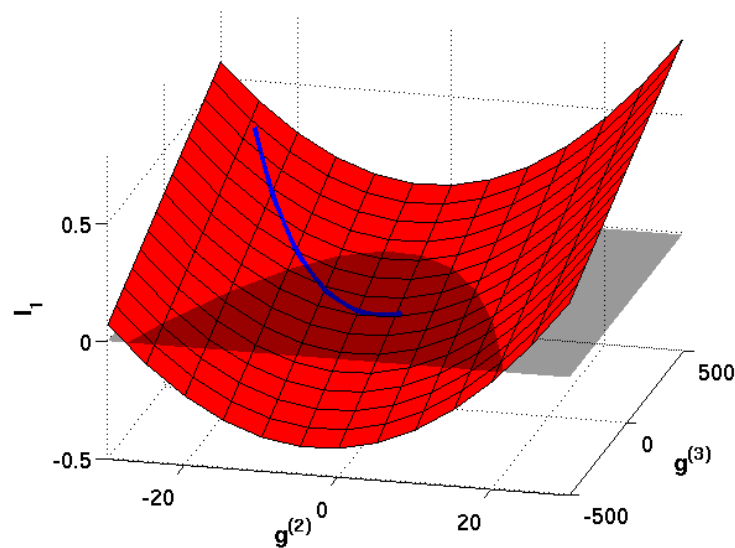


Figure 3.5: Plot of the first Lyapunov coefficient l_1 as a function of the higher derivatives $g^{(2)}$ and $g^{(3)}$ of $G(X_3)$ (red surface) at a Hopf bifurcation point. The intersection with $l_1 = 0$ (gray surface) marks the Bautin bifurcation. The red curve, embedded in the red surface, shows the subset of higher derivatives that results from the restriction of $G(X_3)$ to a Hill function with an arbitrary exponent.

time scale parameters and exponent parameters of the general model are fixed, however without restricting the functional form of $g(X_3)$. This has the consequence that the second and third derivatives of this function can be represented by parameters. Note that the first derivative $g^{(1)}$, which is one of the exponent parameters, is still fixed.

In Fig. 3.5, the first Lyapunov coefficient l_1 is plotted as a function of the higher derivatives of $g(X_3)$. For large values of $g^{(2)}$ and $g^{(3)}$, the Hopf bifurcation undergoes a Bautin bifurcation and its type changes from supercritical to subcritical. The figure also displays the cut through the bifurcation manifold that describes those pairs of second and third derivatives that are realized by the assumption of a Hill-type function with a varied Hill coefficient. The resulting set of points is one-dimensional because one of the two parameters of the function is determined by the constraint of a fixed first derivative. The region in which the curve is supercritical corresponds to small Hill coefficients r , whereas for large r , the Hopf bifurcation can become subcritical. Therefore, larger higher derivatives (associated with high Hill coefficients) of g can cause the Hopf bifurcation to become subcritical. In the current example, a Hill coefficient of $r = 19$ is necessary to cross the Bautin bifurcation, whereas $r = 3$ was assumed in Ref. [54]. An unusually high degree of cooperativity in the activation of Bmal1 transcription would be required to justify the assumption of such large parameter values.

In order to determine whether the model also exhibits subcritical Hopf bifurcations that do not require Hill functions with large exponents r , we extend our search to a larger portion of the parameter space. To this end, we use a random sampling algorithm that can be described as follows: In the first step, random values from ranges of feasible values are repeatedly assigned to the general parameters, leading to different steady states for which the spectrum of the Jacobian is calculated. From the steady states that this procedure yields we select those unstable samples that are close to a Hopf bifurcation because they are characterized by a conjugate pair of leading eigenvalues with a small but positive real part. We subsequently apply a Newton method [56] to optimize the general parameters until a point on the Hopf bifurcation is reached. The test function of the eigenvalues λ_i of the Jacobian that the Newton method minimizes was chosen as the absolute value of the real part of the complex pair of eigenvalues that is closest to the imaginary axis. After having detected a random Hopf bifurcation point, l_1 is calculated.

In order to reduce the number of free parameters, we restrict the functional forms to Hill-type functions. As a simplification of the model by Becker-Weimann *et al.* [54],

$$F(X_3, X_7) = F_3(X_3)F_7(X_7) = v \frac{1}{1 + (X_3/k_p)^p} \frac{1}{1 + (k_s/X_7)^s} \quad (3.37)$$

is assumed to be a product of a repressing and an activating sigmoidal function. This assumption leads to one additional parameter per function in the general model, which determines the second and third derivatives, provided that the elasticity (first derivative) is fixed. The additional parameters are chosen to be the Hill coefficients p for $F_3(X_3)$, r for $G(X_7)$ and s for $F_7(X_7)$. All three Hill coefficients are restricted to the range $[1 : 10]$.

The random sampling analysis yields that in the majority of samples, Hopf bifurcations are supercritical in the model. Only a small fraction of 1.5% of the sampled bifurcations are subcritical, showing that both types of Hopf bifurcations are possible in the model also for smaller Hill coefficients.

By a continuation of subcritical Hopf bifurcations, we construct bifurcation diagrams for various samples in which a subcritical Hopf bifurcation with low Hill coefficient is found. The bifurcation diagram for one of these samples is shown in Fig. 3.6. For other samples these bifurcation diagrams have a qualitatively similar shape.

Fig. 3.6 confirms again the above results showing that for large values of r , the Hopf bifurcation enters a subcritical regime. However, there is also an additional subcritical regime at much lower Hill coefficients. This shows that subcritical bifurcations are also possible at more realistic Hill coefficients in this model structure.

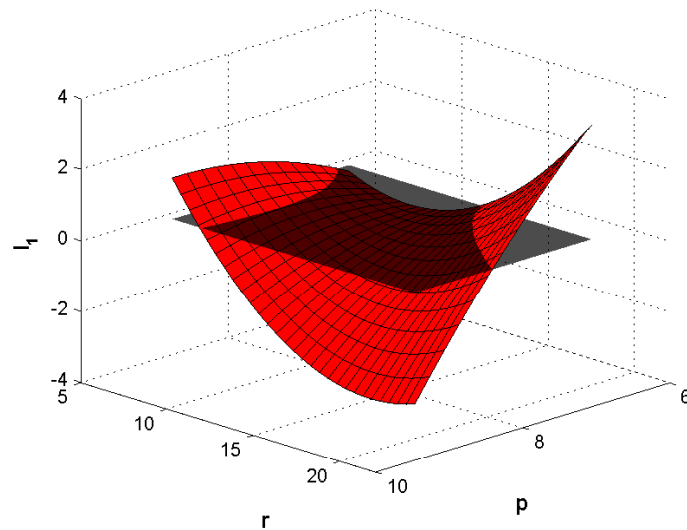


Figure 3.6: First Lyapunov coefficient depending on the Hill coefficients p and r of the functions $f(X_3)$ and $g(X_7)$. The Hopf bifurcation (red) is subcritical in the areas above the gray plane of $l_1 = 0$ and supercritical below.

3.5 Cusp bifurcations and bistability

Because of their connection to bistability, *cusp bifurcations* are a second bifurcation type in which normal form analysis reveals information of direct practical importance. In this section, we show that a search for cusp bifurcations in general models can be used to detect the existence of bistable parameter regimes. We apply the new approach to different abstract types of gene-regulatory networks that are based on the model of the circadian oscillator in Sec. 3.4 but do not correspond to real-world gene-regulatory networks. Future studies are needed for an application to models describing bistable systems in nature.

The models that we investigate in this section are based on the model of the circadian oscillator corresponding to Fig 3.3. There are three instances of feedback in the model that are represented by the functions $F(X_3, X_7)$ and $G(X_3)$. We assume that $F(X_3, X_7) = F(X_3)F(X_7)$ can be written as a product. In contrast to the previous section, we consider both positive and negative feedback for all three feedback functions. Instances of positive feedback are described by Hill functions of the form $F_+(X) = \frac{v(X/K)^n}{1+(X/K)^n}$, whereas instances of negative feedback are described by sigmoidal inhibition functions $F_-(X) = \frac{v}{1+(X/K)^n}$ with positive parameters v, n, K .

For each of the 2^3 combinations of positive and negative feedback, we search whether there exist cusp bifurcations in parameter space. Because of the large parameter space, we follow a similar approach as in Sec. 3.4, which is based on the calculation of normal form parameters in multiple random samples. In each sample, all parameters are as-

signed random values from uniform ranges. The Hill coefficients of the three feedback functions were restricted to values between 1 and 10.

In contrast to the previous section on Hopf bifurcations, random steady states are sampled in the vicinity of saddle-node bifurcations. With a Newton method, the general parameters are then optimized to the nearby bifurcation surface and the normal-form parameter b is calculated. If it is found that for a given combination of feedback, there exist both samples with $b > 0$ and samples with $b < 0$, bifurcation diagrams are constructed in order to find transitions corresponding to $b = 0$ and thus to cusp bifurcations.

Table 3.1: Existence of cusp bifurcations for different combinations of positive and negative feedback in gene-regulatory networks based on the model of the circadian oscillator [54].

$F(X_3)$	$G(X_3)$	$F(X_7)$	Cusp bifurcations
+	+	+	No
+	+	-	No
+	-	+	No
+	-	-	Yes
-	+	+	No
-	+	-	No
-	-	+	No
-	-	-	Yes

Table 3.1 shows for all eight possible combinations of positive and negative feedback whether bistability was found close to cusp bifurcation. Note that no cusp bifurcations are found for the combination $-/+ /+$ that corresponds to the circadian oscillator analyzed in the previous section. Even though in this model, saddle-node bifurcations are detected in addition to the Hopf bifurcations discussed above, all of these bifurcations are characterized by a normal form parameter $b < 0$. Since the model has been developed to describe oscillatory instead of bistable dynamics, the absence of cusp bifurcations is not unexpected.

However, for two combinations of feedbacks ($-/- /-$ and $+/- /-$), the resulting model includes saddle-node bifurcations with both positive and negative normal form coefficients b and cusp bifurcations. In Fig. 3.7A, a bifurcation diagram depending on two generalized parameters and the normal form parameter b is shown for the model in which all three types of feedback are inhibiting ($-/- /-$). The point at which b changes its sign corresponds to the cusp bifurcation. Note that the characteristic cusp shape is not detected in bifurcation diagrams of generalized parameters. However, if the system

is mapped back to a conventional model, a bifurcation analysis with MATCONT [41] shows that the typical cusp shape is recovered (Fig. 3.7B). Finally, it is verified by numerical integration in the conventional model that in the region inside the cusp, two stable steady states coexist.

The presented method based on a local analysis can thus be used to detect the nonlocal property of bistability by an analysis the normal form of saddle-node bifurcations. However, we note that bistability does not necessarily involve the existence of cusp bifurcations. In order to evaluate the practical benefit of normal-form analysis of saddle-node bifurcations to detect bistability in a general class of models, future studies are necessary in models for systems in which bistable dynamics plays a functional role.

3.6 Discussion

In this chapter, we have proposed an extension of the method of generalized modeling that includes the analysis of higher derivatives, thus allowing to analyze the normal forms of bifurcations. This extension has been applied to two models of gene-regulatory networks, the Goodwin model and a model of a circadian oscillator.

For Hopf bifurcations, the dynamics of the surrounding parameter space depends on whether the bifurcation is subcritical or supercritical, leading typically either to a sharp transition to large-amplitude oscillations or to a soft, reversible transition to low-amplitude oscillations. We have analyzed Hopf bifurcations in one of the earliest and simplest models for a gene with a negative-feedback auto-regulation, the Goodwin model. For this model, an analytic expression for the first Lyapunov coefficient of the Hopf bifurcation was obtained, depending on the higher derivatives of the nonlinear feedback function of the model. It was found that for the choice of a Hill function, the bifurcation in the model is supercritical for arbitrary Hill coefficients. We further showed that subcritical Hopf bifurcations can appear when functional forms are used that deviate only slightly from the Hill function.

In the larger model of a mammalian circadian oscillator, in which the self-inhibiting gene is part of a gene-regulatory network of two interacting genes, it was detected that the Hopf bifurcation in the vicinity of parameter sets used in the literature is supercritical. Only for strong changes to the model parameters, it can become subcritical in a Bautin bifurcation. Using a statistical sampling method, we then proceeded to show that the model exhibits a different region in parameter space where transitions between supercritical and subcritical regimes occur for parameter values that correspond to low Hill coefficients.

A second bifurcation type for which the knowledge of normal-form parameters reveals biologically relevant information are cusp bifurcations. They mark the onset of

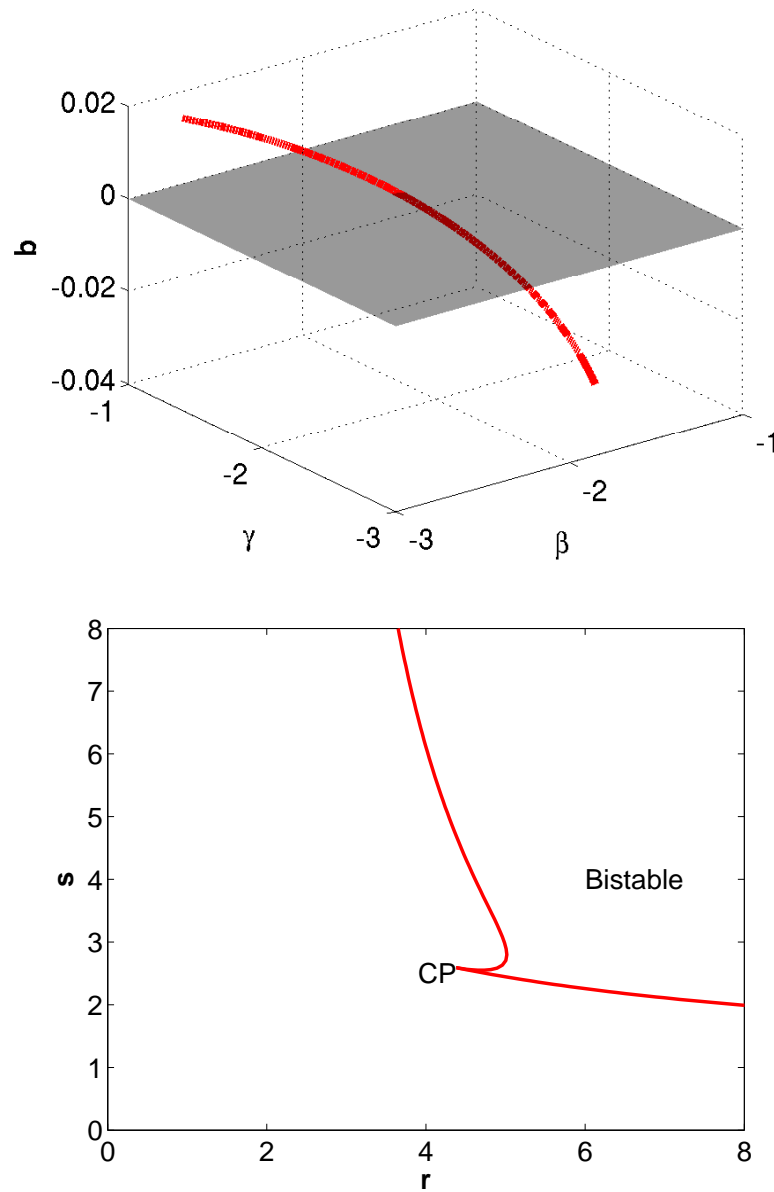


Figure 3.7: Cusp bifurcations in the general and the conventional model with three negative feedback loops. Top: The normal-form parameter b of a saddle-node bifurcation is plotted against β , the elasticity corresponding to $f(X_3)$ and γ , the elasticity corresponding to $g(X_7)$. Bottom: The bifurcation diagram in the vicinity of the cusp point in a corresponding conventional model is shown, depending on the Hill coefficients r and s .

a parameter regime in which two stable steady states coexist, so that the existence of a bistability in a given model structure can be confirmed by detecting a cusp point in parameter space. This is potentially useful for many applications in systems biology. We showed that cusp bifurcations indeed exist in a modified version of the circadian oscillator model, in which the instances of positive feedback were exchanged by negative feedback. In this hypothetical example of a gene-regulatory network, we then performed a mapping of the general parameter set corresponding to the cusp bifurcation to a conventional model and verified that the bifurcations indeed mark the onset of a bistable region.

While the existence of bistability in a model can be shown in the way outlined above, the absence of cusp bifurcations does not strictly imply that no bistability exist in the model. However, we expect that if a model exhibits a regime of bistability, it is very likely that a cusp bifurcation exists at its edge in a general model with multiple parameters. Since cusp bifurcations are of codimension two and thus typically only encountered in bifurcation diagrams of dimension two or larger, the absence of cusp bifurcations in some investigations of bistable models can be explained by the way in which the bifurcation analysis is performed. Although various prominent examples of bistable systems, among them the lac operon [57] and the cell cycle [58], exhibit cusp bifurcations, further studies are needed to investigate this point.

The combination of generalized modeling and normal form analysis introduced in this chapter constitutes an efficient way to extract not only the bifurcation landscape of models but also to draw conclusions about nonlocal dynamics. One of the potential applications of the method is to use it as a pre-screening tool in the initial stage of model development, where choices have to be made between different alternative model formulations. Here, generalized models can provide a list of dynamical features of steady states in different model candidates without necessitating time-consuming numerical integration. The extension of the method presented in this section is particularly useful in applications where the model is expected to incorporate non-stationary behavior such as oscillations or bistability as a functional property.

Chapter 4

Stability and bifurcations in bone remodeling

In this chapter, we analyze mathematical models for the process of bone remodeling with the method of generalized modeling. After giving an introduction to the biology of bone remodeling in Sec. 4.1, we investigate in Sec. 4.2 and Sec. 4.3 the dynamics of two different model structures on which most of the earlier modeling attempts are based. For both model structures, we estimate the parameter regime that is most likely realized in nature and then calculate the stability properties and the bifurcation landscape in this regime. In Sec. 4.4, we suggest a possible link between bifurcations in the mathematical model and Paget's diseases of bone. The results presented in this chapter have been published in Ref. [59].

4.1 Introduction

Bone is an active tissue that forms the skeleton of vertebrates [60–62]. The functions of bone are not limited to providing mechanical support to the skeleton, but also include the storage of minerals and the generation of blood cells in the bone marrow that resides in the hollow inside of bones.

During development and growth, the skeleton of vertebrates is formed in the process of *bone modeling* [63]. However, also the fully developed skeleton is actively reshaped and rebuilt throughout the life of an adult. This process, which is achieved by a separate mechanism than bone modeling, is known as *bone remodeling* or *bone turnover* [64]. It leads to the renewal of the complete human skeleton in a time span of approximately 10 years. Although the purpose of bone remodeling has not been elucidated ultimately, it is believed that bone remodeling helps to repair the skeleton from fatigue damage induced by stress or mechanical loading. Another important function of bone remodeling is to

prevent the accumulation of old bone tissue by constant replacement.

In contrast to bone modeling, in which tissue is either formed or removed at a particular site in bone, bone remodeling consists of two interconnected subprocesses: the resorption of old bone and the subsequent formation of new bone at the same site. In the past decades, it has become clear that, at the cellular level, bone remodeling depends on the interplay between two different cell types, osteoclasts and osteoblasts. The former are cells that resorb bone by acidification, while the latter have the ability to fill the gaps left by osteoclasts with newly formed bone tissue [62]. Although both osteoclasts and osteoblasts originate in the bone marrow, they derive from different types of stem cells. Osteoclasts are multinuclear cells of hematopoietic origin that arise by fusion of multiple progenitor cells, whereas osteoblasts are mononuclear and derive from mesenchymal stem cells [64].

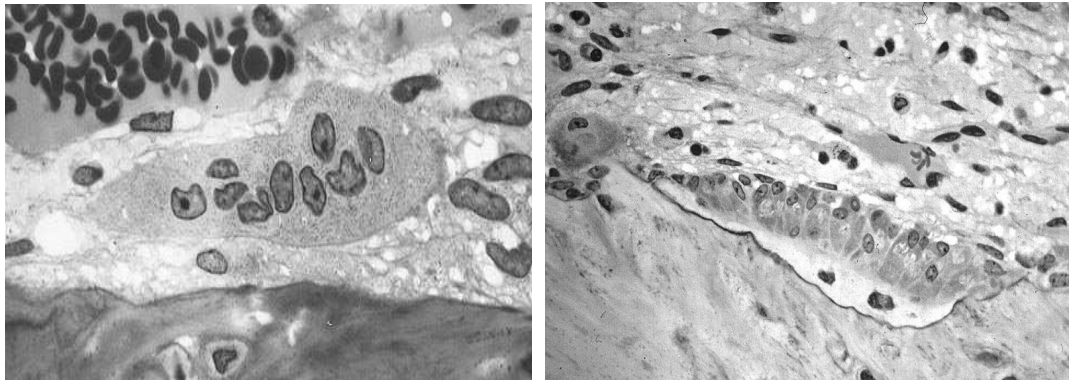


Figure 4.1: Micrographs of osteoclasts and osteoblasts. Left: A single osteoclast with multiple nuclei. Right: Active osteoblasts in the process of osteoid formation.

by Robert M. Hunt. License: pd (left), cc-by-sa-3.0 (right)

At a particular site in bone, osteoblasts and osteoclasts move collectively in discrete groups, remodeling tissue on their way. Such a collection of cells is called *basic multicellular unit* (BMU) since the work of Frost [65]. A single BMU has a cone-like structure and consists of 10 – 20 osteoclasts at the front, followed by 1000 – 2000 osteoblasts. At each moment, there are approximately 1 million BMUs present in the human skeleton [64].

In humans, bone remodeling is regulated by various factors that can be autocrine (acting on cells of the same type that releases them) or paracrine (acting on different cell types). In particular, a signaling pathway involving the Receptor Activator of NF- κ B (RANK), its ligand RANKL, and the cytokine receptor osteoprotegerin (OPG) plays an important role in the regulation of bone remodeling [66,63]. For osteoclasts to mature, it is necessary that RANKL, expressed by cells of osteoblastic lineage, attaches to RANK, which is expressed on cells of osteoclastic lineage. This process is antagonized

by the decoy receptor OPG, which is, like RANKL, expressed by cells of osteoblastic lineage. OPG inhibits the differentiation of osteoclasts by binding to RANKL and thus sequestering it. By adjusting the ratio of RANKL and OPG expression, osteoblasts can therefore control their feedback on osteoclastogenesis.

The cytokine $\text{TGF}\beta$ is another important regulator that is known to influence both osteoclasts and osteoblasts [67]. Over- or underexpression of $\text{TGF}\beta$ and the members of the RANKL pathway is related to several diseases of bone, such as osteoporosis and Paget's disease of bone [68–71]. There exist many other cytokines, hormones and vitamins for which an influence on bone remodeling has been shown, making them possible candidates for an inclusion in mathematical models. However, for the dynamics of bone remodeling it is most important to include those regulators that affect both osteoclasts and osteoblasts. For this reason, most earlier studies concentrate on the effects of the RANKL and $\text{TGF}\beta$ pathways.

4.1.1 Previous mathematical models

Mathematical models describing the process of bone remodeling have been proposed in a number of earlier studies. An overview of the literature is given in Ref. [72]. Some of the previous models aim to describe the dynamics of single BMUs. In this case, spatial aspects of the dynamics play an important role. Additionally, the small number of osteoclasts in a single BMU makes a description with continuous variables difficult. Nevertheless, a detailed spatio-temporal model has been proposed recently [73] which is based on the two-variable model structure analyzed later in this work.

The majority of the previous mathematical models are based on systems of ODEs. This approximation can be justified by the argument that spatial effects can be neglected when an average over an extended region with a high number of BMUs is taken. Averaging over many BMUs has the additional advantage that it allows to take into account systemic properties of bone remodeling, such as the response to global over- or under expression of different enzymes or hormones. Understanding these properties is of a higher practical significance than the dynamics of single BMUs because of the direct implications to various wide-spread diseases of bone.

The first mathematical model for bone remodeling was published in 2003 by Komarova *et al.* [74]. In this model, the dynamics of two variables, the number of osteoblasts and osteoclasts was studied, while the regulatory interactions were described by power laws. Thereby, the effects of different paracrine and autocrine factors were condensed into power law exponents. The model by Komarova *et al.* was subsequently extended in various later publications [75, 73, 76].

A different model structure, based on three dynamic variables, was proposed by

Lemaire *et al.* in 2004 [77] and also extended in subsequent studies [78, 79]. In these models, emphasis was placed on a biochemically motivated derivation of the functional forms, using nonlinear functions from enzyme kinetics instead of the power law formalism.

In most of the earlier studies, it was found that the system approaches a stable steady state in which the numbers of osteoclasts and osteoblasts remain constant in time. Starting from a particular stable steady state, it was then studied how the concentrations of osteoblasts and osteoclasts are influenced by changes in various external parameters such as production or decay rates of osteoclasts and osteoblasts. The response of the system was then linked to various diseases of bone. However, most of the earlier studies did not attempt to systematically explore the parameter space to prove that a stable steady state exists under all reasonable parameter choices. Moreover, many decisions for parameter values were not explicitly justified by biological reasoning.

4.1.2 Stability in models of bone remodeling

From a biological point of view, it is evident that under normal physiological conditions, the number of both osteoclasts and osteoblasts should remain constant in time. Otherwise, either the resorption of old bone or the formation of new bone would predominate, leading to an undesirable decrease or increase of bone volume. Mathematical models of bone remodeling that describe the dynamics of osteoclasts and osteoblasts should therefore operate from a stable steady state.

In order to maintain the balance between osteoblasts and osteoclasts, the system should be driven back to the steady state in response to random external fluctuations. At the same time, it is desirable that the stationary densities of osteoblasts and osteoclasts react sensitively to external changes that are communicated through signaling molecules. Thereby, the rate of bone remodeling can be adjusted temporarily to make the system adaptive to situations in which an increased rate of bone remodeling is needed. The demands that a system should be able to maintain a constant rate of bone remodeling in a noisy environment but still be sensitive to changes in the parameters requiring an adaptation are conflicting. We therefore expect that there is a trade-off between dynamical stability and responsiveness. In dynamical systems, the strongest response of steady states is often found close to bifurcations – critical thresholds at which the stability to perturbations is lost. It is thus possible that the physiological state of the bone remodeling system is characterized by parameter values close to a bifurcation point.

These arguments motivate us to investigate the aspect of dynamical stability in

mathematical models of bone remodeling in more detail. To this end, we implement the structural properties of various existing mathematical models into the framework of generalized modeling. The questions that we seek to answer are:

- Is the existence of a stable steady state a prevalent property of mathematical models for bone remodeling or does it depend on strict restrictions on the parameters?
- Can the loss of stability in a bifurcation of the dynamical system explain cases of malfunctions in bone remodeling?

Answers to the first question can lead to a better understanding of the conditions under which mathematical models of bone remodeling can operate from a steady state. Those biological assumptions that are critical to ensure stability can be separated from others and specifically targeted by experiments. Since there exist no earlier comparative studies for mathematical models of bone remodeling, these structural properties are not well understood.

Answers to the second question can also provide cues for experimental studies. If a relation between a disease and a bifurcation is found to be accurate, this allows for new countermeasures aiming to strengthen the stability of the system. For example, the tools of bifurcation theory can be utilized for understanding the causes and consequences of the disease. In particular, existing methods to detect early warning signals for critical transitions in dynamical systems [80] could prove useful in this case.

4.2 A two-variable model of osteoblasts and osteoclasts

Mathematical models capable of describing the dynamics of bone remodeling should include the concentrations of active osteoblasts, B , and of active osteoclasts, C . In this section, we introduce a minimal model having only these two dynamical variables. Because this minimal model potentially oversimplifies the problem by ignoring the different properties of osteoblast precursors, a more detailed model that accounts for osteoblast behavior at different stages of maturation is later introduced in Sec. 4.3.

In the two-variable model, we assign to both state variables gain terms ($F(B, C)$, $H(B, C)$, respectively) describing the recruitment of new cells from a pool of precursor cells, and loss terms ($G(B, C)$, $K(B, C)$), describing the removal of cells due to apoptosis or further differentiation into other cell types such as osteocytes or lining cells that are no longer directly involved in bone remodeling. These assumptions lead to the

basic system of equations

$$\begin{aligned}\frac{d}{dt}B &= F(B, C) - G(B, C) \\ \frac{d}{dt}C &= H(B, C) - K(B, C).\end{aligned}\tag{4.1}$$

In the following, it is assumed that the functions $F(B, C)$, $G(B, C)$, $H(B, C)$ and $K(B, C)$ are positive and continuously differentiable but not restricted to specific functional forms. The state variables B and C are also assumed to be positive.

Assuming the existence of a steady state, we denote the steady-state concentrations of osteoblasts and osteoclasts with B^* and C^* , respectively. We then define normalized variables

$$b = \frac{B}{B^*}, \quad c = \frac{C}{C^*}.\tag{4.2}$$

Similarly, we define a set of normalized functions

$$\begin{aligned}f(b, c) &= \frac{F(B, C)}{F(B^*, C^*)}, & g(b, c) &= \frac{G(B, C)}{G(B^*, C^*)}, \\ h(b, c) &= \frac{H(B, C)}{H(B^*, C^*)}, & k(b, c) &= \frac{K(B, C)}{K(B^*, C^*)}.\end{aligned}\tag{4.3}$$

Using these definitions, the system can be written as

$$\begin{aligned}\frac{d}{dt}b &= \alpha_1 (f(b, c) - g(b, c)) \\ \frac{d}{dt}c &= \alpha_2 (h(b, c) - k(b, c)).\end{aligned}\tag{4.4}$$

where

$$\alpha_1 = \frac{F(B^*, C^*)}{B^*} = \frac{G(B^*, C^*)}{B^*}\tag{4.5}$$

and

$$\alpha_2 = \frac{H(B^*, C^*)}{C^*} = \frac{K(B^*, C^*)}{C^*}.\tag{4.6}$$

The second identities in Eq. (4.5) and Eq. (4.6) hold because the gain and loss terms for each variable cancel each other in a steady state by definition.

The normalization guarantees that in the new coordinates, the formerly unknown steady state is located at $(b, c) = (1, 1)$. The Jacobian of the normalized model can be written as

$$\mathbf{J} = \begin{pmatrix} \alpha_1 & 0 \\ 0 & \alpha_2 \end{pmatrix} \begin{pmatrix} f_b - g_b & f_c - g_c \\ h_b - k_b & h_c - k_c \end{pmatrix}.\tag{4.7}$$

Here we use Roman subscripts to indicate the partial derivatives of the functions, i.e., the elasticities that were introduced in Sec. 2.2.1. For instance, f_b is defined as

$$f_b = \left. \frac{\partial f}{\partial b} \right|_{b=1, c=1} = \left. \frac{B^*}{F(B^*, C^*)} \frac{\partial F}{\partial B} \right|_{B=B^*, C=C^*} = \left. \frac{\partial (\ln F)}{\partial (\ln B)} \right|_{B=B^*, C=C^*}.\tag{4.8}$$

So far, the Jacobian matrices corresponding to all positive steady states in a large class of models have been constructed. We emphasize that it is not necessary to assume that for a given set of conventional parameters there exists only a single steady state. In the general case, where multiple steady states exist, the formal derivation of the Jacobian applies to all steady states in all models within the class considered here. However, the general parameters appearing in the Jacobian matrix generally differ between steady states belonging to the same conventional model because they depend on the steady-state values of the variables.

Although the quantities appearing in the Jacobian, such as f_b , are in general unknown, they do not depend on the dynamical variables and can therefore be treated as parameters with the same right as the parameters that are introduced in conventional models. Like conventional parameters, the generalized parameters have a well-defined interpretation in the context of the model. In the following, we discuss the interpretation for each parameter and confine it to a range of feasible values. The final structure of the two-variable model is summarized in Fig. 4.2.

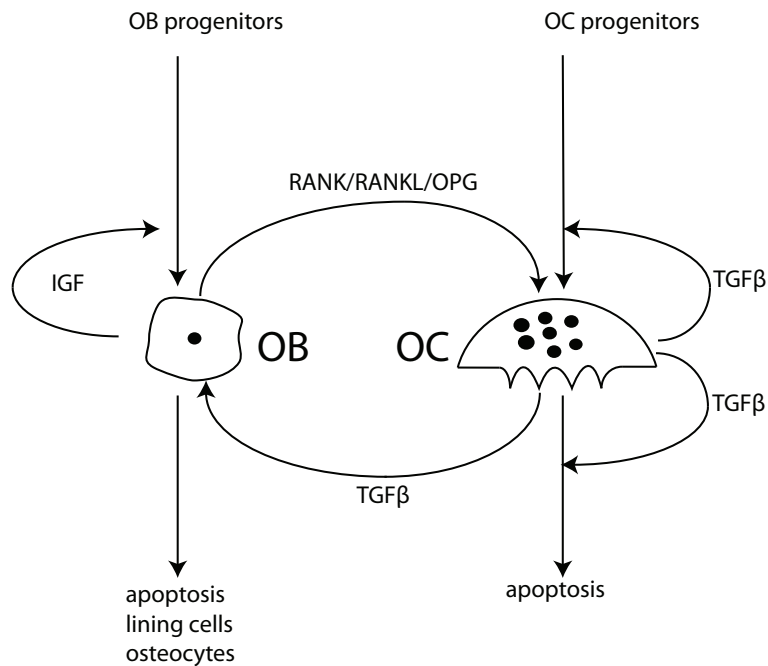


Figure 4.2: Schematic sketch of the two-variable model. Osteoblasts (OB) influence osteoclasts (OC) via the RANKL/RANK/OPG pathway, while the TGF- β pathway exerts a positive feedback from osteoclasts to both osteoclasts and osteoblasts.

The parameters α_1 and α_2 are defined as ratios between a flux and a concentration and thus have the dimension of an inverse time. They represent the respective time scales of the two coupled differential equations and can be interpreted as the inverse lifetime of the respective cell types. Since the average life span of osteoblasts (≈ 3

months) exceeds the life span of osteoclasts (≈ 2 weeks) by a factor close to 6 [64], it is reasonable to assume that $\alpha_1/\alpha_2 \approx 1/6$. Because the scale by which time is measured is arbitrary and does not affect the stability analysis, we are free to fix $\alpha_1 = 1$, leading to $\alpha_2 = 6$.

The remaining parameters in the Jacobian of Eq. (4.7) are elasticities which describe the local derivatives of the gain and loss terms. We note that in the model proposed in Ref. [74], all functional forms were chosen to be power-laws. In this case, the elasticities correspond to the power-law exponents, so that the Jacobian of Eq. (4.7) is similar to the Jacobian derived in Ref. [74]. Nevertheless, Eq. (4.7) describes the local behavior of steady states in a larger class of models, in which the processes can be modeled by arbitrary positive functions.

We assume that the typical life span of the osteoblasts is not affected by regulatory mechanisms. Therefore, the decay term of osteoblasts is linear in the concentration of osteoblasts b and independent of osteoclasts c . It follows that $g_c = 0$ and $g_b = 1$. Likewise, the decay term of osteoclasts is assumed to be independent of osteoblasts, corresponding to $k_b = 0$. The parameter f_b describes the autocrine regulation in the differentiation of osteoblast progenitors into active osteoblasts. Osteoblasts express *Insulin-like growth factors* (IGF), that are known to promote osteoblastogenesis [81,82]. Therefore, it is assumed that $f_b > 0$.

The parameters f_c , h_c and k_c describe the influence of the feedback exerted by the growth factor TGF β [67]. When osteoclasts resorb bone tissue, TGF β is released into the bone matrix, where it can subsequently facilitate the differentiation of osteoblast progenitors to active osteoblasts. This paracrine interaction between osteoblasts and osteoclasts leads to $f_c > 0$. In the bifurcation analysis below, it is shown that more specific assumptions about this elasticity are not required.

The autocrine roles of TGF β , described by the parameters h_c and k_c , are less clear: *In vitro* experiments [83–85] have led to contradictory results on the influence of TGF β on the differentiation of precursors to active osteoclasts, finding both activation and repression [67]. The observed type of feedback depends strongly on the experimental setup of these studies, such as TGF β concentration or whether isolated cultures of osteoclasts or co-cultures with osteoblasts were used. The current belief [67] is that in co-cultures with osteoblasts, TGF β acts indirectly in a repressing way by interacting with the OPG/RANKL/RANK pathway. In contrast, TGF β activates and sustains osteoclasts in isolated cultures. In order to cover both possibilities, we investigate the possible dynamics for both positive and negative values of the corresponding elasticity h_c .

In the absence of additional feedback mechanisms, one would assume the decay term of osteoclasts to be linear, $k_c = 1$. However, the apoptosis of osteoclasts has been

reported to be both promoted [86–88] and suppressed [89,90] by TGF β , corresponding to $k_c > 1$ and $k_c < 1$, respectively. Based on these conflicting experimental results, we assume that k_c is positive but again do not assume a specific value. In the Jacobian, Eq. (4.7), the parameters h_c and k_c appear in the form of the difference $h_c - k_c$. Therefore, the effects of autocrine regulation in the production and decay terms of osteoclasts can be covered by a single parameter $m_c \equiv h_c - k_c$ that takes the autocrine feedback of the production and the decay term simultaneously into account. The “default value” of m_c , describing a situation without autocrine feedback, is $m_c = -1$.

Finally, the effects of the RANKL/RANK/OPG pathway are described by the parameter h_b . This parameter can assume negative or positive values, depending on whether the repressing effects of OPG or the activating effects of RANKL dominate.

The assumptions made above lead to the simplified Jacobian

$$\mathbf{J} = \begin{pmatrix} 1 & 0 \\ 0 & 6 \end{pmatrix} \begin{pmatrix} f_b - 1 & f_c \\ h_b & m_c \end{pmatrix}. \quad (4.9)$$

with four remaining parameters.

4.2.1 Bifurcation analysis of the two-variable model

Having derived the Jacobian and conditions on the parameters, we can now establish the conditions for saddle-node bifurcations and Hopf bifurcations in the two-variable model. In any system of ODEs, a necessary condition for a saddle-node bifurcation is $\det \mathbf{J} = 0$, which is equivalent to the existence of a zero eigenvalue. For the Jacobian of Eq. (4.9), it follows that

$$m_c(f_b - 1) - f_c h_b = 0 \quad (4.10)$$

is satisfied at saddle-node bifurcations.

In a Hopf bifurcation, the spectrum of the Jacobian is characterized by two complex conjugate eigenvalues with zero real part. For a two-dimensional system, this means that the sum of the two eigenvalues, i.e., the trace of the Jacobian, vanishes ($\text{Tr} \mathbf{J} = 0$). It follows that

$$\frac{\alpha_1}{\alpha_2}(f_b - 1) + m_c = 0. \quad (4.11)$$

is a necessary condition for a Hopf bifurcation. Additionally, the inequality $\det \mathbf{J} > 0$ must be fulfilled in order to exclude the case of two real eigenvalues $\lambda_1 = -\lambda_2$ (pseudo-Hopf bifurcation).

Because the ratio of timescales α_1/α_2 has been fixed, the bifurcation conditions that are determined by Eq. (4.10) and Eq. (4.11) depend on the parameters, f_b , m_c and $f_c h_b$. The parameters f_c and h_b appear only as a product in the bifurcation conditions.

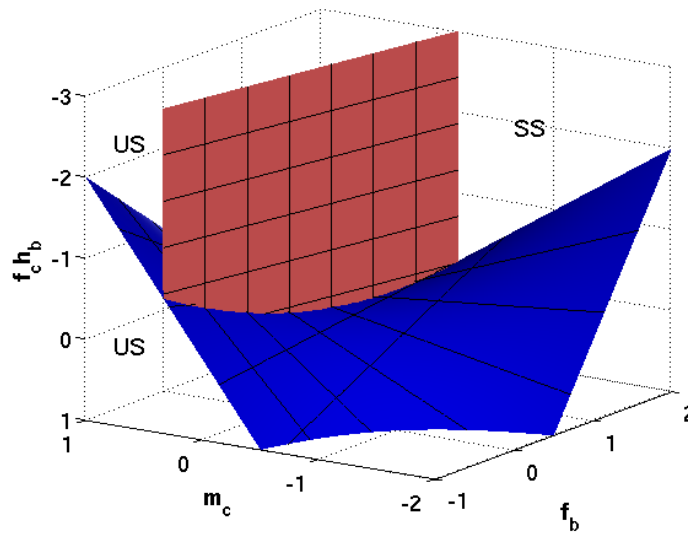


Figure 4.3: Bifurcation diagram for the 2-variable model, depending on f_b , m_c and $f_c h_b$. A Hopf bifurcation (red) and a SN bifurcation (blue) separate regimes of stable steady states (SS) from regimes of unstable steady states (US).

The stability of all steady states in the whole class of models can thus be visualized in a three-parameter bifurcation diagram, which is displayed in Fig. 4.3.

Each combination of the parameters in the three-dimensional volume corresponds to the steady state in a particular model. A Hopf bifurcation and a saddle-node bifurcation divide regions in which the steady state is stable from regions in which it is unstable. We note that the bifurcation diagram in Fig. 4.3 differs from Fig. 4a in Ref. [74], in which the saddle-node bifurcation surface seems to be independent from f_b (called g_{22} there), which is incompatible with the form of Eq. (4.10).

Figure 4.3 shows that for $f_b > 1$, stable steady states exist only for negative values of $f_c h_b$ (upper region), whereas smaller values of f_b allow stability also for small positive values of $f_c h_b$. Since the parameter f_b describes the positive feedback of IGF on the growth term of osteoblasts, it is reasonable to assume $f_b > 0$. In Ref. [74], conventional models were analyzed in which f_b was zero, or, in some cases, positive but small. For $f_b = 0$ and $m_c = -1$ (no autocrine feedback), it is required for stability that $f_c h_b < 1$. Larger values of f_b impose stronger restrictions on the remaining parameters for the stability of steady states.

Because f_c is assumed to be positive, the crucial parameter in the term $f_c h_b$ that determines its sign is h_b . A positive value of h_b , corresponding to the case where activation by RANKL dominates over repression by OPG, leads to a positive value of $f_c h_b$. Therefore, resulting steady states are located close to the unstable region that is separated by a saddle-node bifurcation from the stable regime (lower region of Fig. 4.3).

In contrast, a negative value of h_b places the system in the stable region. In the model, stability is therefore promoted when the inhibitory effect of OPG dominates over the promoting effect RANKL and the effective action of the RANKL signaling pathway is inhibitory. This condition is not necessarily fulfilled *in vivo* and the choice to assume a negative value of h_b has not been justified by biological reasoning in earlier studies such as Ref. [74]. We conclude that under the reasonable assumptions that the effective feedback of the RANKL pathway is activating and the autocrine feedback of osteoblasts is stronger than linear, there are no stable steady states in the two-variable model.

The loss of stability in a Hopf bifurcation appears mostly as an effect of changing the parameter m_c , which describes the autocrine feedback of osteoclasts. Instability requires that $m_c \approx 0$ or larger. In the case of no autocrine feedback of osteoclasts, it would be expected that $m_c = -1$ because in that case, the decay term of osteoblasts is linear in C . Therefore, Hopf bifurcations occur when the effective autocrine feedback on osteoclasts is activating. These relations between the autocrine feedback of osteoclasts and Hopf bifurcations have already been observed in Ref. [74].

In the numerical simulations of Ref. [74], only escalating or damped oscillations were observed in the vicinity of the Hopf bifurcation. Since the complete absence of sustained oscillations close to a Hopf bifurcation is slightly unusual, we analyze the type of Hopf bifurcations in more detail. Without making further assumptions on the higher derivatives as in Chapter 3, we cannot determine in the general model whether the Hopf bifurcation is subcritical or supercritical. We therefore consider the conventional model proposed in [74] as an example of the more general class of models considered here. In our notation, this model can be written as

$$\begin{aligned}\frac{d}{dt}B &= A_b B^{f_b} C^{f_c} - D_b B \\ \frac{d}{dt}C &= A_c B^{h_b} C^{h_c} - D_c C,\end{aligned}\tag{4.12}$$

where A_b, D_b, A_c and D_c are rate constants. This model is a subclass of the general model considered above in which two specifications were made: First, the functions were modeled by power laws, so that the elasticities of the general model describe power-law exponents in this context. Second, the autocrine feedback of osteoblasts and osteoclasts was assumed to affect only the respective gain terms, leading to linear decay terms.

The condition for a Hopf bifurcation in this model is

$$\frac{D_c}{D_b}(h_c - 1) + (f_b - 1) = 0.\tag{4.13}$$

Using the bifurcation software MATCONT [41], we find that the first Lyapunov coefficient is equal to zero for Hopf bifurcations in this model, irrespective of the parameter values. This leads us to the hypothesis that a special symmetry in the particular

conventional model causes the system of Eq. (4.12) to be Hamiltonian at the Hopf bifurcation.

We confirm this hypothesis by showing analytically that under the condition Eq. (4.13), the flow is Hamiltonian. In Hamiltonian systems, a function of the dynamic variables exists which is conserved on all trajectories. Using the elementary technique of an integrating factor (which is $R = B^{-f_b}C^{-h_c}$), we determined this function to be

$$H(B, C) = -\frac{D_c}{f_b - 1}B^{1-f_b}C^{1-h_c} - \frac{A_c}{h_b - f_b + 1}B^{h_b-f_b+1} + \frac{A_b}{f_c - h_c + 1}C^{f_c-h_c+1} \quad (4.14)$$

It can easily be verified that for this function, $\frac{d}{dt}H(B, C) = 0$ is satisfied under the condition Eq. (4.13). The actual Hamilton equations are fulfilled after the coordinate transformation to canonical variables $p(B) = \frac{1}{1-f_b}B^{1-f_b}$ and $q(C) = \frac{1}{1-h_c}C^{1-h_c}$.

It follows that irrespective of parameter values, no limit cycles are created in Hopf bifurcations of this specific model. The steady state exactly at the bifurcation manifold is a center. The Hopf bifurcation is thus neither subcritical nor supercritical, but is just at the brink between the two alternatives. Sustained oscillations can occur only if the parameters are tuned exactly to the bifurcation point, but with an amplitude that depends on the initial conditions. Fig. 4.4 shows the oscillations directly at a Hopf bifurcation for different initial conditions.

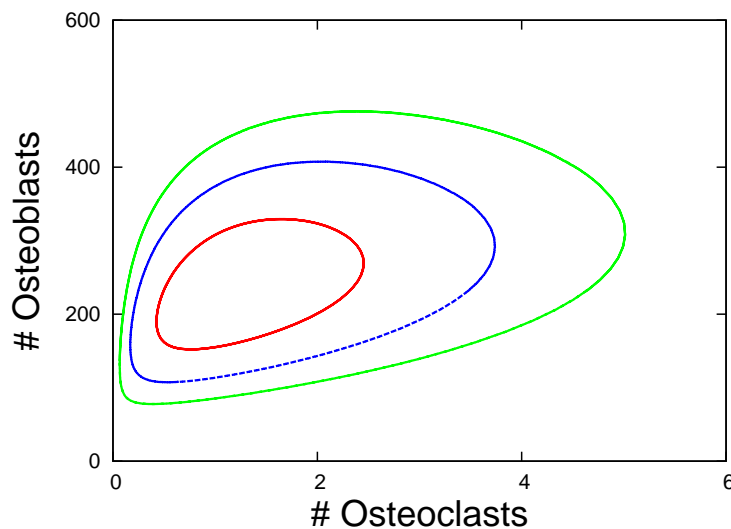


Figure 4.4: Dynamics of the conventional model of Eq. 4.12 at the Hopf bifurcation point for different initial conditions. The amplitude of the oscillations depends on the initial conditions.

The structural instability which effects this degenerate behavior of the model is caused by a symmetry in the special system of ODEs. A biologically feasible mechanism that breaks this symmetry is to assume the existence of feedback in the autocrine

regulation in the loss term of osteoclasts ($k_c \neq 1$). Above, we have mentioned experimental evidence for this feedback. Moreover, feedback in the decay term of osteoclasts has been implemented in other models of bone remodeling such as Ref. [77]. Even for very weak feedback, the system is no longer Hamiltonian at the bifurcation point, so that a subcritical or supercritical Hopf bifurcation can occur. We checked numerically that for $k_c \neq 1$, there exist supercritical Hopf bifurcations, and stable limit cycles with a well-defined amplitude exist in the surrounding parameter regime. Therefore, the result of Ref. [74] that oscillations are either escalating or damped is not robust with respect to small changes in the model structure and is thus only valid in the rather unrealistic situation in which there is no autocrine feedback in the decay terms of osteoclasts.

In summary, our bifurcation analysis reveals problems of the two-dimensional model. For stable steady states to occur, models of this class need to make rather strong assumptions on the parameters. If the autocrine feedback of osteoblasts is positive, the feedback of osteoblasts on osteoclasts must be effectively inhibiting, implying that the repressing effects of OPG should dominate over the activating effects of RANKL. Otherwise, all steady states in the model would be unstable, so that the model could not describe physiologically meaningful situations. Furthermore, we showed that the Hopf bifurcation in the model implies damped or escalating oscillations only for the specific assumption that the decay terms of both osteoclasts and osteoblasts are linear. If the autocrine feedback of osteoblasts or osteoclasts also effects apoptosis and further differentiation, sustained oscillations can occur because the degeneracy of the Hopf bifurcation is removed. In this case, a shift in the parameters that drives the system over the Hopf bifurcation can lead to stable sustained oscillations of osteoclast and osteoblast concentrations.

4.3 A three-variable model with responding osteoblasts

The two-variable model proposed above may be oversimplified because it does not take the dynamics of precursor populations into account. If the involved cell types are regulated differently at different stages of maturation, the structure of the model can change in a way that cannot be covered by the two-variable models considered above. A model with a different structure has been proposed in Ref. [77] and was subsequently extended in Refs. [78, 79]. In this model, cells of osteoblastic lineage are represented by two dynamic variables, responding osteoblasts (ROBs, variable R) and active osteoblasts (AOBs, variable B). ROBs are cells that are committed to the osteoblastic lineage and interact with osteoclasts but are not yet functional osteoblasts.

There are two reasons for distinguishing AOBs and ROBs: First, there is experimental evidence that cells of osteoblastic lineage express RANKL and OPG in a different proportion at different stages of maturation. It has been found that at later stages, the ratio of RANKL to OPG decreases [91, 92], so that the inhibiting effects of OPG become increasingly stronger during the lifetime of the cell.

Second, $\text{TGF}\beta$ promotes osteoblasts particularly at an early stage of maturation. $\text{TGF}\beta$ activates osteoblast differentiation from ROB progenitors, but it inhibits their further differentiation into active osteoblasts [67]. We note that the clear-cut distinction between AOBs and ROBs is an approximation since the term “responding osteoblast” is not describing a well-defined cell type but a collection of cells at different stages of maturation. In reality, changes such as the decline of the OPG to RANKL ratio are expected to be gradual.

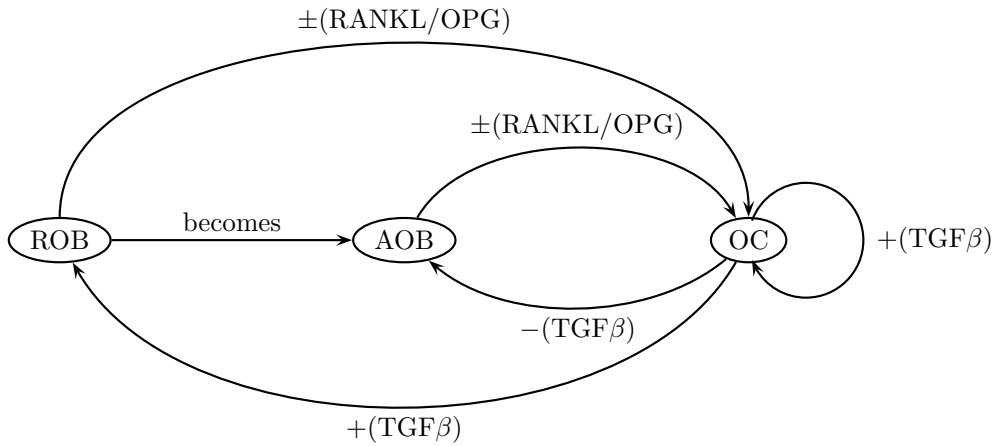


Figure 4.5: Schematic overview of the three-variable model, in which the dynamics of responding osteoblasts (ROB), active osteoblasts (AOB) and osteoclasts (OC) is described. The feedback mechanisms, mediated by the RANK/RANKL/OPG-pathway and by $\text{TGF}\beta$, are inscribed in the diagram in the form of arcs with arrows. The straight arrow from ROB to AOB indicates a flow of biomass due to differentiation of ROBs.

The structure of the three-dimensional model, summarized in Fig. 4.5, translates to the system of ODEs

$$\begin{aligned}\frac{d}{dt}R &= S(C) - T(R, C) \\ \frac{d}{dt}B &= T(R, C) - U(B) \\ \frac{d}{dt}C &= V(B, R) - W(C),\end{aligned}\tag{4.15}$$

where the two terms in each equation correspond again to the gains and losses of the population of the respective cell type. We have already inscribed the functional dependencies in these equations. They are motivated by the biological processes that

are included in the model. We explain these processes in more detail after formally constructing the Jacobian.

Performing the normalization procedure leads to the set of normalized equations

$$\begin{aligned}\frac{d}{dt}r &= \alpha_1 (s(c) - t(r, c)) \\ \frac{d}{dt}b &= \alpha_2 (t(r, c) - u(b)) \\ \frac{d}{dt}c &= \alpha_3 (v(b, r) - w(c))\end{aligned}\tag{4.16}$$

where, in analogy to our treatment of the two-variable model, the lower-case variables and functions denote the normalized quantities and $\alpha_1, \alpha_2, \alpha_3$ are the characteristic timescales of ROB, AOB, and OC turnover.

In analogy to Eq. (4.7), the Jacobian for the three-variable model can be written as

$$\mathbf{J} = \begin{pmatrix} \alpha_1 & 0 & 0 \\ 0 & \alpha_2 & 0 \\ 0 & 0 & \alpha_3 \end{pmatrix} \begin{pmatrix} -t_r & 0 & s_c - t_c \\ t_r & -u_b & t_c \\ v_r & v_b & -w_c \end{pmatrix}.\tag{4.17}$$

A summary of the elasticities occurring in the Jacobian and the ranges that are assigned to them is given in Table 4.1.

Parameter	Interpretation	Range
s_c	activation of ROB production	$[0, 1]$
t_r	ROB decay, linear in r	1
t_c	repression of ROB decay	$[-1, 0]$
u_b	AOB decay, linear in b	1
v_r	action of ROBs on OC	$[-1, 1]$
v_b	action of AOBs on OC	$[-1, 1]$
w_c	activation of OC decay	$[0.5, 1.5]$

Table 4.1: Parameters in the three-variable model

The elasticities s_c , t_c and w_c describe the nonlinearities that are caused by the feedback exerted by the TGF β pathway. This pathway stabilizes the reservoir of ROBs both by promoting the differentiation of osteoblast progenitors to ROBs, leading to $s_c > 0$ and by inhibiting the further differentiation of ROBs to AOBs, leading to $t_c < 0$. In the following, s_c will be restricted to the interval $[0, 1]$ and t_c to $[-1, 0]$. These ranges includes for example the choice of Hill functions with exponents equal to 1 (Michaelis-Menten kinetics) that were used in earlier models [79]. The nature of autocrine regulation of osteoclasts has not been ultimately clarified. Therefore we restrict w_c to the interval $[0.5, 1.5]$. This range is centered around $w_c = 1$, because

without any additional feedback, a linear decay term would be expected. The parameter w_c is smaller (larger) than one if the additional feedback is negative (positive). We note that the functional forms that were assumed in Refs. [77, 78] lead to superlinear decay ($w_c > 1$).

The regulation of osteoclasts by cells of osteoblastic lineage is mediated by the RANKL/RANK/OPG pathway. Depending on the ratio between RANKL and its decoy receptor OPG, the corresponding elasticities v_r and v_b can be either positive or negative. We note the difference to the two-variable model, in which the actions of the RANKL system were described by a single parameter. Different combinations of v_r and v_b describe all possible combinations of RANKL and OPG expression at responding osteoblasts and active osteoblasts. In particular, two important scenarios, which are discussed as models M1 and M2 in Ref. [78], are characterized in the general model by

1. $v_r < 0$, $v_b > 0$. OPG is expressed by responding osteoblasts, RANKL is expressed by active osteoblasts.
2. $v_r > 0$, $v_b < 0$. RANKL is expressed by responding osteoblasts, OPG is expressed by active osteoblasts.

Intermediate situations, in which there is a differential expression of OPG and RANKL that does not lead to different algebraic signs for the elasticities are also covered by our description (e.g. $v_r > v_b > 0$).

4.3.1 Bifurcation analysis of the three-variable model

In the three-variable model, the number of free parameters is larger than in the two-variable model. It is no longer possible to group all parameters having an impact on stability such that they can be visualized in a single bifurcation diagram. In order to gain an overview of the effects that the various parameters have on stability, we instead use a statistical method based on the sampling of random steady states [9]. The idea of this method is to analyze the influence of selected parameters on stability while averaging over the effect of the remaining parameters. This analysis is subsequently combined with a bifurcation analysis of three-dimensional subsets of the larger parameter space, where the remaining parameters are fixed.

In the random sampling analysis, $N = 10^7$ random parameter sets are created. In each set, we assign to all parameters random values that are drawn from uniform distributions in the intervals defined in Tab. 4.1. We then determine the stability of the steady states defined by the individual parameter sets by numerical computation of the eigenvalues of the respective Jacobians. Using the whole ensemble of random parameter sets, we then calculate the percentage of unstable steady states depending on

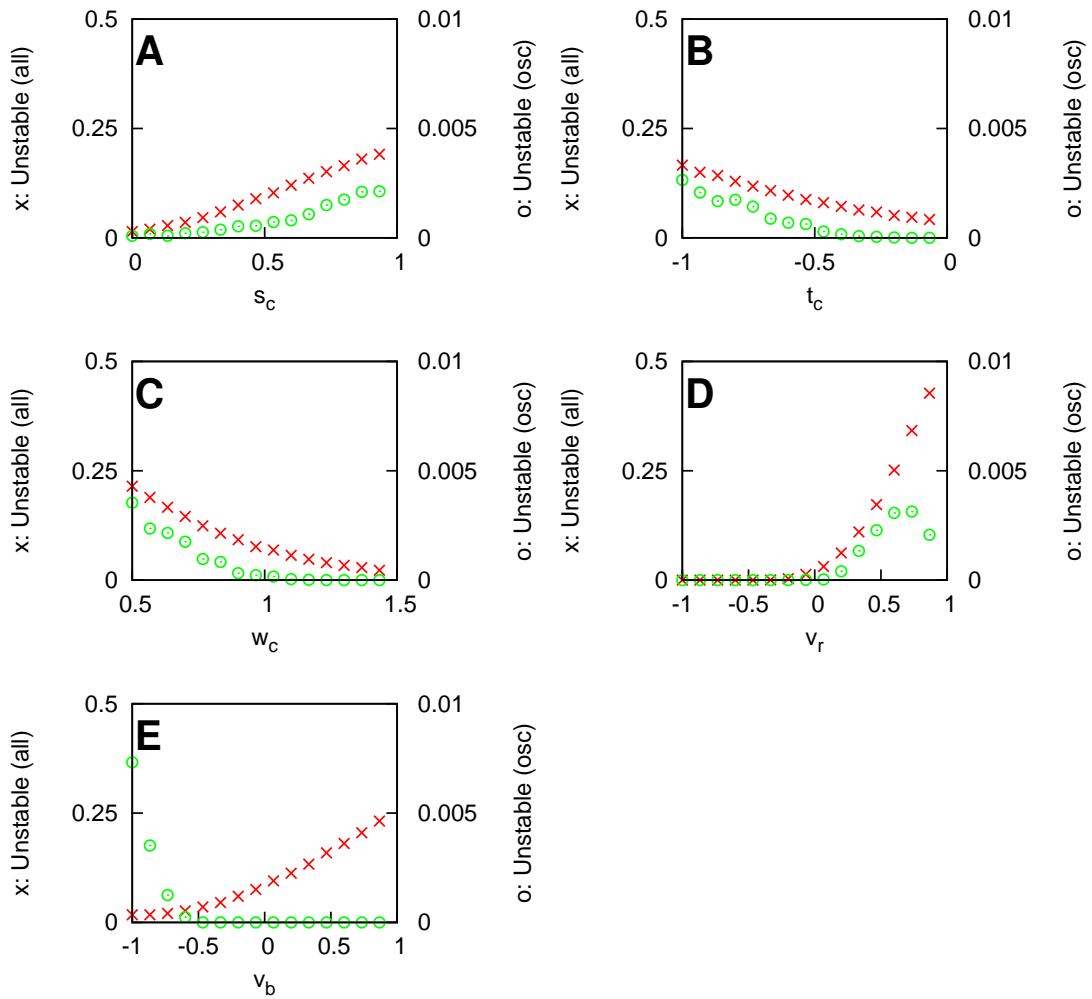


Figure 4.6: Effect of parameters on local dynamics. The histograms show the fraction of randomly drawn steady states that are unstable (red crosses) and the fraction of unstable states with leading complex eigenvalues, indicating oscillatory instabilities (green circles). Each panel shows the effect of one elasticity, while averaging over the other parameters.

the values of single parameters, at the same averaging over the remaining parameters. For the elasticities occurring in the model, the results of the random sampling analysis are shown in the histograms of Fig. 4.6.

Panel A and B of Fig. 4.6 show that strongly nonlinear paracrine feedback exerted by $\text{TGF}\beta$ ($s_c \gg 0$ and $t_c \ll 0$) has a destabilizing effect on the steady state. The parameter w_c , describing the autocrine feedback by $\text{TGF}\beta$, has an opposite effect (Fig. 4.6C): Strong positive feedback of osteoclasts on osteoclast removal stabilizes the steady state.

It follows that the paracrine effects of $\text{TGF}\beta$ on osteoblasts that are described by s_c and t_c destabilize the steady state, whereas the apoptosis-inducing autocrine effects of $\text{TGF}\beta$, described by w_c , stabilize it.

For $v_r < 0$, few unstable states are detected (Fig. 4.6D), showing that models in which OPG is preferentially expressed on ROBs (as opposed to AOBs) usually operate from a stable steady state that cannot be destabilized easily. The second parameter that is related to RANKL signaling, v_b , also acts destabilizingly at large positive values (Fig. 4.6E). As noted above, there is experimental evidence that OPG is expressed stronger by active osteoblasts, while RANKL is expressed stronger on ROBs [91,92]. This implies that the parameter regime that is most likely realized in nature is characterized by $v_r > v_b$, which is also the regime in which instabilities occur most frequently in models.

In order to investigate the nature of the bifurcations leading to the instabilities in more detail, we repeat the sampling analysis, but this time distinguishing between unstable steady states in which the leading eigenvalue, i.e., the eigenvalue with the largest real part, is a real number and those in which it is part of a complex conjugate pair. The significance of the leading eigenvalue lies in its effect on the departure of the system from the unstable state. Specifically, when departing from a state in which the eigenvalue with the largest real part is has a non-zero imaginary part, the system launches into oscillations.

Figure 4.6 shows that for most parameters, the curve for unstable states with a leading pair of complex conjugate eigenvalues has a similar shape as the curve for of all unstable states. However, an exception is the parameter v_b (Fig. 4.6E) for which a very different behavior is observed: Whereas the fraction of unstable states with a real positive eigenvalue increases with increasing v_b , the fraction of unstable states with a leading pair of complex conjugate eigenvalues decreases with an increasing v_b . This behavior suggests that the main route to instability for v_b is to cross a saddle-node bifurcation for large parameter values, whereas the probability of encountering a Hopf bifurcation increases for small values of v_b . We also note that while all other curves are monotonous, a maximum in the fraction of oscillatory unstable steady states is observed for the parameter v_b .

After having identified the overall impact of the parameters on stability on the basis of a statistical ensemble of steady states, we proceed by investigating selected parameters in bifurcation diagrams. Here, we chose to concentrate on the parameters v_b and v_r for which the random-sampling analysis showed the most interesting results, as well as the parameter w_c , which captures the different possibilities of feedback in the decay term of osteoclast. Here, the bifurcation manifolds are shown for a wider range of parameter values than biologically reasonable. The three-dimensional cut of

the parameter space that was investigated in the random sampling analysis is shown in the form of a gray box.

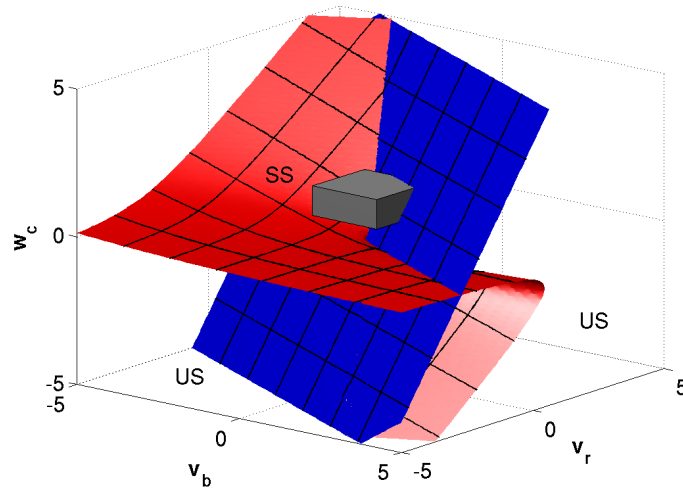


Figure 4.7: Bifurcation diagram of the three-variable model, depending on the effects of RANKL/OPG (v_b , v_r) and the autocrine effects of osteoblast decay (w_c). The parameter regime of stable steady states (SS), which is located in the upper front part of the diagram, can be left via a Hopf bifurcation (red) or a saddle-node bifurcation (blue). The gray cube marks the part of parameter space most likely corresponding to reality, in which the sampling analysis of Fig. 4.6 was performed. Other parameters: $\alpha_1 = 1$, $\alpha_2 = 1$, $\alpha_3 = 6$, $s_c = 0.8$, $t_c = -0.8$.

The bifurcation diagram in Fig. 4.7 shows that parameter sets corresponding to stable steady states are characterized by large values of w_c and small values of v_r (upper front of the figure). The section in parameter space that is most likely realized in nature based on experimental results is characterized by $w_c \approx 1$, which can be close to a Hopf bifurcation depending on the values of v_r and v_b that describe whether OPG and RANK are expressed preferentially on osteoblast precursors or active osteoblasts. Moreover, Fig. 4.7 confirms the findings from the random-sampling analysis that both large values of v_r and small values of w_c are associated with unstable steady states.

For the parameter v_b , the situation is more complicated: For large values of v_b , the steady state loses its stability in a saddle-node bifurcation, whereas stability can be lost in a Hopf bifurcation for small values. This explains the qualitative different stability curves for the parameter v_b in Fig. 4.6D, depending on whether all unstable states or only those with an oscillatory instability were taken into account. Unstable steady states with a leading pair of complex conjugate eigenvalues are found in the space between the Hopf bifurcation and the saddle-node bifurcation, which explains

the maximum observed for instability v_r in Fig. 4.6D.

The bifurcation diagram in Fig. 4.7 also contains bifurcations of higher codimension. The Hopf-bifurcation surface ends in a Takens-Bogdanov bifurcation of codimension two as it connects to the saddle-node bifurcation surface. For low values of w_c , the Hopf-bifurcation intersects with the saddle-node bifurcation in a Gavrilov-Guckenheimer bifurcation. In the center of the Figure, the Takens-Bogdanov bifurcation and the Gavrilov-Guckenheimer bifurcation intersect in a triple-point bifurcation of codimension 3. The presence of codimension-2 bifurcations can be of relevance for applications because they can imply the existence of non-local properties such as homoclinic bifurcations or chaos [11]. However, since it is unlikely that these kinds of dynamics play a role in the system of bone remodeling, a detailed discussion of the dynamics close to the codimension-2 bifurcations is beyond the scope of this present investigation.

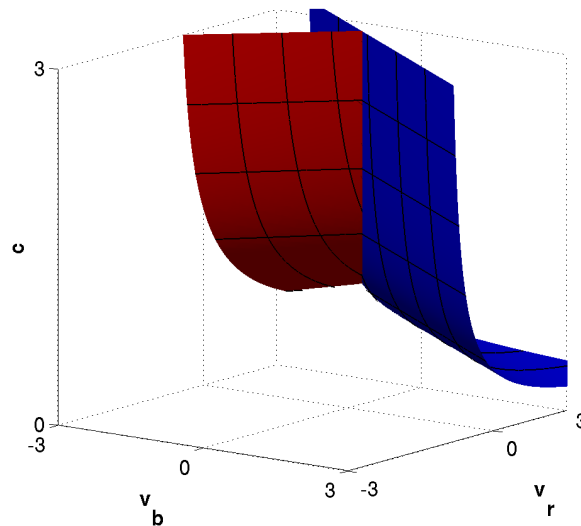


Figure 4.8: Bifurcation diagram in which all processes controlled by TGF β exhibit the same degree of nonlinearity. The strength of this nonlinearity is described by the parameter $c = s_c = -t_c = w_c - 1$. The other bifurcation parameters, v_r and v_b , describe the effect of the RANKL pathway. In the diagram, the red surface describes a Hopf bifurcation, whereas the blue surface describes a saddle-node bifurcation. In the front region of the diagram, steady states are stable.

A different section of the parameter space was considered in Ref. [77], where a single Hill function with one K_m value was chosen for all processes controlled by TGF β . In the case of inhibiting interaction, a sigmoidal inhibition function with the same K_m was used. Translated into the framework of generalized modeling, this means that $s_c = -t_c = w_c - 1 =: c$, leading to a reduction of free parameters. The new parameter c changes simultaneously the local nonlinearity of all functions describing the TGF β

pathway. Figure 4.8 shows that an increase in the nonlinearity of the feedback by $TGF\beta$ can act destabilizingly, which was not observed in Fig. 4.7 where only the parameter w_c was varied. The bifurcation properties with respect to the other parameters, v_r and v_b , are consistent between Fig. 4.8 and Fig. 4.7.

4.4 Bifurcations and diseases of bone

The bifurcation analysis of the three-parameter model suggests that both saddle-node bifurcations and Hopf bifurcations exist close to the operation point of the dynamical system of bone remodeling. This proximity can have beneficial consequences, but it also creates risks to the organism that may lead to diseases.

The main benefit of operating close to a region of instability is that in general, a stronger adaptive response to external changes of the model parameters is possible. In the vicinity of a SN bifurcation where the leading eigenvalue of the Jacobian is only slightly negative, the response to changes in the parameters is stronger, as it is implied by the quadratic normal form of the bifurcation [11]. Generalized models are not designed to study these responses directly. However, in Ref. [78], numerical simulations of the response of the system to parameter changes were performed in a conventional model that belongs to the class of three-variable models analyzed above. These simulations showed that a model structure in which RANKL is exclusively expressed by ROBs, whereas OPG is exclusively expressed by RANKL, leads to a stronger response to changes in the osteoclast differentiation rate than other combinations. The authors conclude that this model structure is “optimal“ because it offers the most effective functional control of bone remodeling [78]. In the general model, we have shown that this structure, described by $v_r > 0$ and $v_b < 0$, leads to steady states close to bifurcations.

Despite these benefits, operating close to a boundary of a bifurcation also poses risks to the system. A larger change in the parameters, invoked by an external process, can shift the system over the bifurcation, so that the stable steady state becomes unstable or ceases to exist. In this case, the balance of bone remodeling can no longer be maintained. Moreover, stability is lost in an abrupt and discontinuous way in many bifurcations. If this is the case, the system can jump to a distant region in phase space, and even a later reversal of the parameter change does not restore the former equilibrium of functional bone remodeling. It is thus a crucial question for the type of analysis we have performed whether certain diseases of bone can be connected to the loss of stability in bifurcations.

Several diseases of bone are related to dysfunctions in the regulation of bone remodeling. Prominent examples include postmenopausal osteoporosis, osteopetrosis, osteopenia or Paget’s disease. Here, we focus on Paget’s disease, a bone disorder of elderly

patients that affects 2% – 3% of the population over the age of 60 [68]. The disease is strongly localized and leads to the enlargement and deformation of single or multiple bones. In patients with Paget’s disease, there are repeated phases of increased bone resorption, which are followed by phases of abundant formation of new bone. This pattern, which can occur in an escalating way, could be caused by oscillations in the numbers of osteoclasts and osteoblasts. Periodic activity of osteoclasts is a phenomenon that has also been observed in cell cultures of osteoclasts and monocytes [93] and is also known to occur in tooth eruption in the development of rats [94].

The transition from the healthy state in which cell numbers remain constant to a disease state with periodic changes in cell numbers could thus be associated with the loss of stability of a steady state in a Hopf bifurcation. To investigate this possibility, we compare whether the model parameter changes leading to loss of stability in a Hopf bifurcation can be identified with known causes of Paget’s disease.

In the two-dimensional model, Hopf bifurcations are caused by an increase of the autocrine feedback of osteoclasts mediated by $TGF\beta$, (parameter m_c in Fig. 4.2). However, $TGF\beta$ was found to be not related to Paget’s disease of bone [95], so that the two-dimensional model does not support a link between Hopf bifurcations and Paget’s disease. In the three-dimensional model, stability can also be lost in Hopf bifurcations by changing RANKL/OPG ratio, i.e. by enlarging v_b and reducing v_r . This is in agreement with findings that the RANKL pathway is involved in Paget’s disease. In particular, OPG deficiency was reported to be related to juvenile Paget’s disease [69], which is consistent with the bifurcation properties of the three-parameter model.

While much work remains to establish a link between diseases of bone and bifurcations, our analysis takes the first step in showing that Hopf- and saddle-node bifurcations exist close to the physiological steady state in current models of bone remodeling. Since a bifurcation occurring *in vivo* should lead to a pathological condition, the proximity to bifurcations in the mathematical model needs an explanation. One possibility is that current mathematical models do not describe the dynamics of bone remodeling adequately, either because crucial parts of the biology are missing or because the parameter estimates are incorrect. In that case, the mathematical models need to be improved, for example by including additional regulatory pathways. However, it is also possible that connections between bifurcations and pathological states such as Paget’s disease exist in reality. If this is indeed confirmed, it would imply that the powerful tools of bifurcation theory can be applied to explore the dynamics of the disease.

4.5 Discussion

In this chapter, we have used the approach of generalized modeling to investigate the stability of steady states in a large class of models for bone remodeling.

In an analysis of the bifurcation behavior of models based on two dynamic variables, describing osteoclasts and osteoblasts, it was shown that both saddle-node bifurcations and Hopf bifurcations can occur. In the two-dimensional model, the stability of steady states requires that either the autocrine feedback of osteoblasts is sufficiently small or that the inhibitory effect of OPG dominates over the activating effect of RANKL. If these conditions are not fulfilled, the two-dimensional model cannot give an adequate description of the process of bone remodeling. We further showed that the possibility of autocrine feedback in the decay term of osteoclasts should be taken into account in the two-variable model because the assumption of a linear removal rate can lead to structurally unstable models. In such models, an arbitrarily small deviation from the model assumptions results in qualitatively different dynamical behavior. Because the generalized model proposed here does not need to assume any specific functional form, it avoids such degeneracies that often are caused by an unfortunate choice of functional forms in conventional models.

In the analysis of an alternative model with three variables, we have combined a random sampling approach with a bifurcation analysis for specific parameters. The bifurcation analysis shows that stability of steady states is possible under less restrictive conditions than in the two-variable model. In the parameter range most likely realized in nature, these conditions place the system into an area of the bifurcation diagram that is close to both saddle-node and Hopf bifurcations. It can be suspected that the proximity to bifurcations helps the system to respond more strongly to external changes. At the same time, the system is exposed to the danger of crossing a bifurcation, which can possibly be connected to diseases of bone. In particular, the bifurcation analysis of the three-variable model supports a link between Hopf bifurcations and Paget's disease of bone, whereas the two-variable model does not. This suggests that responding osteoblasts should be included as a separate variable in future models.

Chapter 5

Bifurcations and chaos in the MAPK signaling cascade

In the last part of this thesis, we study the mitogen-activated protein kinase (MAPK) cascade. The MAPK cascade is an important signaling pathway regulating many fundamental processes of eukaryotic cells. The basic biochemistry of the pathway that defines the structure of mathematical models is well-established today. Moreover, the system has been studied in many computational models since 1996 [96–102]. The MAPK cascade is not only investigated in models with the aim of improving the understanding of the actual biology but is also used as an example to test new computational methods [103, 104].

Despite these advancements, there are still many open questions for computational studies of the MAPK pathway. Detailed mechanistic models include many unknown parameters for which experimental data is scarce, whereas less detailed models that reduce the number of parameters by approximations can potentially miss important dynamical effects.

As a method that can efficiently analyze the steady-state behavior of models in a large parameter space, generalized modeling is a promising tool for models with these characteristics. By a systematic analysis of the stability and bifurcations of a detailed and mechanistic model of the MAPK cascade we confirm, extend and generalize previous results obtained in conventional models. We further show how the analysis of bifurcation can reveal regions in parameter space with unusual dynamics such as irregular oscillations and weak forms of chaos, that were previously not known to exist in models of the MAPK cascade.

After giving an introduction to the biology of the MAPK pathway in Sec. 5.1, we describe our implementation of the method of generalized modeling for the pathway in Sec. 5.2. We then show results for the MAPK pathway and for subsystems forming a

cascade-like composition of phosphorylation-dephosphorylation cycles in Sec. 5.3 and Sec. 5.4. The results presented in this chapter have been published in Ref. [105].

5.1 Biology of the MAPK pathway

The MAPK cascade is a highly conserved signaling pathway in eukaryotic cells. It is involved in the regulation of numerous functions of the cell, among them proliferation, apoptosis, differentiation and cell motility [106–108]. Aberrant activation of the MAPK pathway is related to several diseases, from which cancer is the most prominent example [109]. The oncogene Ras, which is part of the MAPK cascade, is found in a structurally altered form in approximately 25% of human tumors, leading to an activation of the MAPK pathway that is independent from external growth signals [110]. Even though it is not completely understood to what extent changes in MAPK signaling cause the disease and to what extent they are merely consequences of upstream events, some of the proteins involved in the MAPK cascade are targeted by cancer drugs already today [111]. Therefore, a heightened understanding of the dynamics of the pathway can potentially lead to the discovery of better drug targets for cancer treatment [112–114].

There are many homologous MAPK cascades across different cell types and species. However, the basic topological motif shown in Fig. 5.1 is conserved in MAPK pathways throughout all eukaryotic cells [106]. In the figure, we show a prominent example of a MAPK cascade, the growth-factor induced Ras-Raf-MEK-ERK cascade that is involved in many types of human cancer. When a cell is exposed to extracellular stimuli such as growth factors, receptors on the cell membrane are activated that trigger a series of intermediate reactions. These reactions ultimately lead to the activation of the enzyme Ras, which phosphorylates Raf, a protein also called MAPKKK (MAP-Kinase-Kinase-Kinase). In its activated state, Raf activates the protein MEK (MAPKK) by phosphorylating it at two different sites. The double-phosphorylated MEK can then facilitate the double phosphorylation of ERK (MAPK), which, in its phosphorylated state, activates several transcription factors and downstream kinases. Each phosphorylation step in the MAPK cascade can be reversed by a phosphatase.

An earlier study in which Metabolic Control Analysis (MCA) was applied to the cascade suggests that the reactions downstream from Ras are of central importance for the dynamics [115]. We therefore concentrate our investigation on the parts of the pathway that are responsible for the term *cascade* and do not include the processes upstream from Ras in the model.

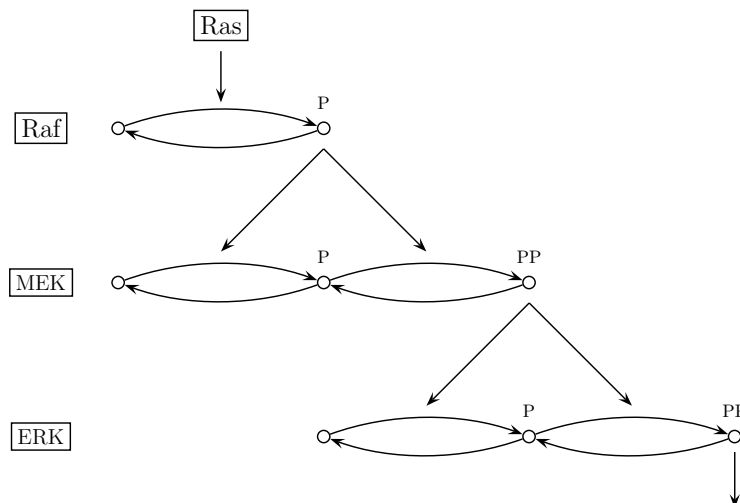


Figure 5.1: Diagrammatic representation of the MAPK signaling cascade. The pathway consists of three layers, a single phosphorylation loop in the top layer and two double-phosphorylation loops in the other two layers. Phosphorylated forms are indicated by P's in the figure. The fully phosphorylated product in each level acts as a kinase for the phosphorylation step of the level below.

5.1.1 History of modeling in the MAPK pathway

The history of mathematical modeling the MAPK pathway begins in 1996 with a model proposed by Huang and Ferrell [96]. In this study, it was shown that the three-level cascade allows the system an *ultrasensitive* response to a stimulus. This term, coined by Goldbeter and Koshland [116], describes a stimulus-response curve that is steeper than that of a Michaelis-Menten enzyme, leading to the existence of a regime in which there is approximately an all-or-none response to changes in the stimulus. While the concept of ultrasensitivity is based on stable steady-state dynamics, it was later found that there are also cases in which nonstationary types of dynamics play a role in the MAPK cascade. Kholodenko showed in 2000 that with the introduction of a negative feedback loop, sustained oscillations are possible [97]. Later, it was shown that even without explicit feedback, the combination of double phosphorylation and enzyme sequestration can result in an implicit feedback that leads to bistability [99, 117] and oscillations [100].

It has been argued before that the complicated structure of a three-layered double-phosphorylation cascade could have evolved as a result of an optimization of the response strength [96] or the response time to signals [101]. However, there may also be adaptive advantages of the evolved topological structure that are based on other dynamical properties of the underlying models.

The experimental data (enzyme concentrations and rate constants) on which the

majority of the previous studies oriented their choice of parameter values, have their origin in experiments on *Xenopus* oocyte extracts conducted in Ref. [96]. However, little is known about the possible parameter ranges in which eukaryotic cells can operate in different species and at different developmental stages.

5.2 Mathematical model of the MAPK cascade

In this section we describe our approach to modeling the MAPK cascade. We first explain the slightly different formulation of generalized modeling that we use in this project, before discussing in detail how we model phosphorylation-dephosphorylation cycles, the basic motifs of the pathway.

5.2.1 Generalized modeling for metabolic networks and signaling networks

For the MAPK cascade, it is useful to formulate the approach of GM in a slightly different way than in the earlier chapters. Here, we follow an approach that was applied to metabolic networks in Ref. [9]. The main advantage of the new formulation is that it allows an automated way of performing the normalization, which was performed “by hand” in the earlier models. Thereby, the alternative formulation provides a more succinct description in models with many dynamic variables.

We consider a network of biochemical interactions regulating a vector of protein concentrations. If the concentrations are sufficiently high to neglect stochastic effects, the dynamics of the system can be captured by the mass balance equation, a system of differential equations of the form

$$\frac{d}{dt}\mathbf{S}(t) = \mathbf{N}\mathbf{f}(\mathbf{S}), \quad (5.1)$$

where \mathbf{S} is a vector of protein concentrations and \mathbf{N} is the stoichiometric matrix and \mathbf{f} is a vector of fluxes depending on the concentrations S_i . \mathbf{N} is a linear map that relates the fluxes to the concentrations and thus describes the topology of the system, which is well-established in the case of the MAPK cascade.

Like in the earlier models discussed in this thesis, we assume that a positive but not necessarily stable steady state \mathbf{S}^* exists and normalize Eq. (5.1) with respect to the steady state concentrations, leading to

$$\frac{d}{dt}\mathbf{x} = \mathbf{\Lambda}\boldsymbol{\mu}(\mathbf{x}) \quad (5.2)$$

with $x_i = S_i/S_i^*$, $\Lambda_{ij} = N_{ij}f_j(\mathbf{S}^*)/\mathbf{S}_i^*$ and $\mu_i(\mathbf{x}) = f_i(\mathbf{S})/f_i(\mathbf{S}^*)$. The Jacobian at the steady state is defined as

$$J_{ij} = \left. \frac{\partial S_i(t)}{\partial S_j} \right|_{\mathbf{S}^*}. \quad (5.3)$$

Since Λ does not depend on \mathbf{x} , the Jacobian of the system can be written as

$$\mathbf{J} = \Lambda \boldsymbol{\theta}_{\mathbf{x}}^{\mu} \quad (5.4)$$

with

$$\boldsymbol{\theta}_{x_i}^{\mu_j} = \left. \frac{\partial \mu_j(\mathbf{x})}{\partial x_i} \right|_{\mathbf{S}^*}. \quad (5.5)$$

The entries of the matrices Λ and $\boldsymbol{\theta}_{\mathbf{x}}^{\mu}$ constitute a complete parametrization for the entire range of possible Jacobians that are consistent with the underlying topology of biochemical interactions. The matrix $\boldsymbol{\theta}_{\mathbf{x}}^{\mu}$ includes the elasticities, as introduced in Sec. 2.2.1.

The entries of Λ have the dimension of an inverse time and represent characteristic time scales of the model. In the steady state under consideration all fluxes in the model have to balance ($\mathbf{Nf}(\mathbf{S}^*) = \mathbf{0}$), which constitutes additional constraints for the permissible values of scale parameters, thus reducing the number of independent parameters. These constraints can be found by computing the *flux modes* [118], which is facilitated by the regular structure of the MAPK cascade.

5.2.2 Implementation of three subsystems

Figure 5.2 gives a detailed overview on the structure of the MAPK cascade and introduces the naming conventions for this chapter. The symbols S_j^i denote the concentrations of proteins and protein complexes which appear as substrates in the model. The superscript index i indicates the layer of the cascade in which the specific protein is involved, while the subscript index j enumerates the different forms in which the substrate appears in the respective layer. Note that although we avoid the use of asterisks for notational convenience, in the following all symbols S_j^i denote concentrations in the steady state. The free concentrations of the kinases and phosphatases that are not bound to a substrate in a complex are labeled K_R^i and P_R^i , respectively. The total concentrations of the substrate, kinase and phosphatase in each layer are denoted S_T^i , K_T^i and P_T^i . These concentrations are assumed to be conserved quantities in the model and thus constitute constant external parameters. The reason for this assumption is that even though the total concentration can be subject to change in a cell due to changes in the rate of protein synthesis and degradation, these processes are assumed to occur on a slower timescale than the signaling that we want to model.

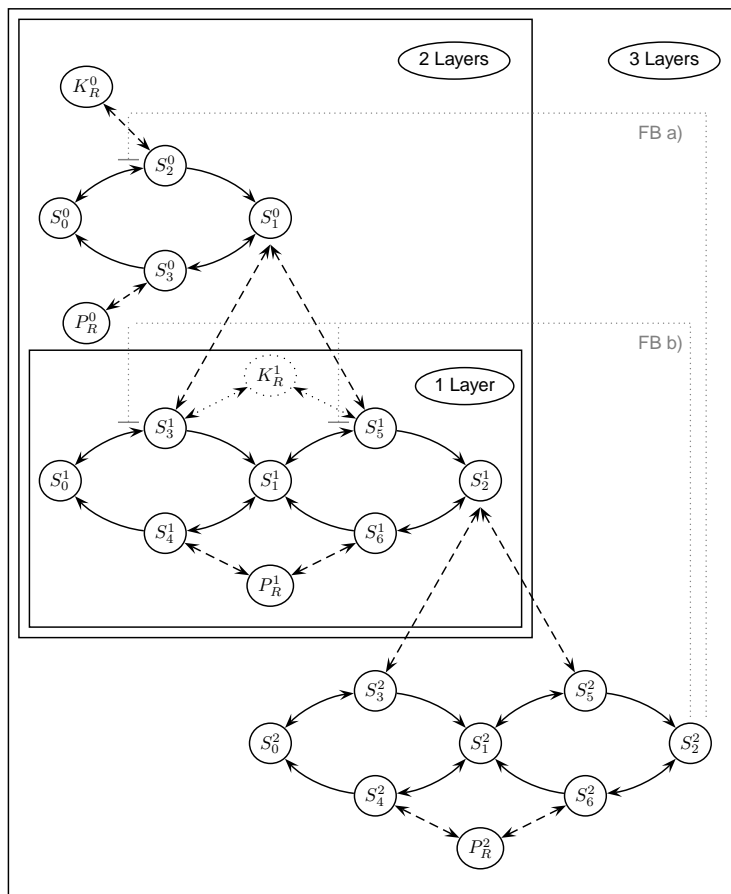


Figure 5.2: Schematic overview and naming conventions of the MAPK cascade. The three different subsystems that are analyzed separately are indicated by boxes. The solid arrows correspond to biochemical reactions while the dashed arrows denote the binding of an enzyme in the formation of an substrate-enzyme complex. In the two-layer and three-layer model, the dotted kinase K_R^1 (1-layer model) is replaced by the activated substrate S_1^0 . The gray dotted lines represent two types of feedback, which represent an extension to the model that is introduced and analyzed in Sec. 5.5.

In the following, we investigate the dynamics in three distinct models with increasing size. The first model contains a single reversible double phosphorylation step with one substrate in isolation, as it occurs in the middle and bottom layer of the cascade. The second model combines the first and second layer of the cascade but does not include the third layer. Finally, the third model contains all three layers. The three models are highlighted by boxes in Fig. 5.2. A technical detail is that the kinase that catalyzes the phosphorylation steps in the second layer is called K_R^1 in the first model in order to indicate that, in the scope of this model, it is constant and does not act as a substrate. In the two larger models, K_R^1 is replaced by S_1^0 , the activated substrate of the top layer.

Having outlined the large-scale structure of the models under consideration, we now explain the detailed structure of the single phosphorylation steps from which all these models are composed. This is shown explicitly for the phosphorylation in the top layer of the cascade,



The first step represents the reversible binding of the kinase K to the unphosphorylated substrate S_0^0 , leading to the formation of the complex S_2^0 . The second step describes the actual phosphorylation step catalyzed by the kinase, resulting in the release of the phosphorylated substrate S_1^0 .

There are different possibilities to model the elementary step of a covalent phosphorylation catalyzed by a kinase. The most widespread approach is to use Michaelis-Menten kinetics. Michaelis-Menten theory relies on the quasi-steady-state approximation that the concentrations of the substrate-enzyme complexes do not change in time. This approximation, which is justified by a separation of timescales, has been found to be not appropriate in many signal transduction networks [119]. Michaelis-Menten kinetics is not a good approximation if sequestration effects of the enzyme play an important role, as it is suspected for the MAPK cascade [120, 117, 100]. Sequestration can affect the dynamics because an enzyme that is bound to a substrate cannot at the same time participate in other reactions, including its own dephosphorylation. In the absence of external feedback, sequestration effects can thereby cause an indirect type of feedback, as will be shown below. Approximation schemes that do not explicitly adopt the complexes as variables, such as Michaelis-Menten kinetics, miss sequestration effects. Although a sequestration-based approximation scheme has been proposed recently [121], we do not make use of this approximation since the efficiency of GM does not strongly rely on the number of reactions or variables being small. For this reason, we represent the complexes explicitly by dynamic variables, following Ref. [100], and break each phosphorylation step into two separate processes.

Assuming that the copy numbers of proteins are sufficiently high for a description with a continuous variable, we capture the dynamics of the cascade by a system of coupled ODEs. For the phosphorylation step in the first layer of the cascade this leads to

$$\begin{aligned} \frac{d}{dt} S_0^0 &= -f_1(S_0^0, K_R^0) + f_2(S_2^0) \\ \frac{d}{dt} S_2^0 &= f_1(S_0^0, K_R^0) - f_2(S_2^0) \\ \frac{d}{dt} S_1^0 &= f_3(S_2^0) \end{aligned} \quad (5.7)$$

where f_1 , f_2 , and f_3 are general functions, which are not yet restricted to specific functional forms.

In an analogous way, the system of ODEs for the complete one-layer model can be constructed. The corresponding system of ODEs is

$$\begin{aligned}
\frac{d}{dt}S_1^1 &= f_9(S_3^1) - f_{10}(S_1^1, P_R^1) + f_{11}(S_4^1) \\
&\quad - f_{13}(S_1^1, K_R^1) + f_{14}(S_5^1) + f_{18}(S_6^1) \\
\frac{d}{dt}S_2^1 &= f_{15}(S_5^1) - f_{16}(S_2^1, P_R^1) + f_{17}(S_6^1) \\
\frac{d}{dt}S_3^1 &= f_7(S_0^1, K_R^1) - f_8(S_3^1) - f_9(S_3^1) \\
\frac{d}{dt}S_4^1 &= f_{10}(S_1^1, P_R^1) - f_{11}(S_4^1) - f_{12}(S_4^1) \\
\frac{d}{dt}S_5^1 &= f_{13}(S_1^1, K_R^1) - f_{14}(S_5^1) - f_{15}(S_5^1) \\
\frac{d}{dt}S_6^1 &= f_{16}(S_2^1, P_R^1) - f_{17}(S_6^1) - f_{18}(S_6^1)
\end{aligned} \tag{5.8}$$

From these equations, the stoichiometric matrix \mathbf{N} is derived according to the rule that $N_{i,j} = 1$ if f_{j+6} appears in the equation for S_i^1 with a positive sign, $N_{i,j} = -1$ if f_{j+6} appears in the equation with a negative sign and $N_{i,j} = 0$ otherwise. Since the top layer of the MAPK cascade is not included in the one-layer model, the enumeration of the fluxes starts with f_7 here.

In the next step, $\Lambda_{ij} = N_{ij}f_{j+6}/S_i^1$ is constructed from the stoichiometric matrix. Since the model explicitly describes the complexes formed by enzymes with their substrates, it is reasonable to assume that the remaining processes are governed by mass action kinetics, thus assuming that all functions depend in a linear way on all of their arguments. In this study, we thus use the ability of GM to deal with general nonlinear functions only at a later stage when we consider the effect of external feedback loops, while the ability to explore a large part of the parameter space efficiently is used throughout the whole study. With this choice, our model corresponds to the conventional models considered in [96, 100].

Note that even after it is assumed that all functional dependencies are linear, the system of equations is still nonlinear as it includes bilinear terms. Because of mass conservation, one of the variables including the substrate can be expressed as a function of the remaining variables and the total substrate concentration, changing some of the bilinear terms into quadratic terms as shown below. Assuming mass action, the matrix

of derivatives is given by

$$\boldsymbol{\theta} = \begin{pmatrix} -\frac{S_1^1}{S_0^1} & -\frac{S_2^1}{S_0^1} & -\frac{S_3^1}{S_0^1} - \frac{S_3^1}{K_R^1} & -\frac{S_4^1}{S_0^1} & -\frac{S_5^1}{S_0^1} - \frac{S_5^1}{K_R^1} & -\frac{S_6^1}{S_0^1} \\ 0 & 0 & 1 & 0 & 0 & 0 \\ 0 & 0 & 1 & 0 & 0 & 0 \\ 1 & 0 & 0 & -\frac{S_4^1}{P_R^1} & 0 & -\frac{S_6^1}{P_R^1} \\ 0 & 0 & 0 & 1 & 0 & 0 \\ 0 & 0 & 0 & 1 & 0 & 0 \\ 1 & 0 & -\frac{S_3^1}{K_R^1} & 0 & -\frac{S_5^1}{K_R^1} & 0 \\ 0 & 0 & 0 & 0 & 1 & 0 \\ 0 & 0 & 0 & 0 & 1 & 0 \\ 0 & 1 & 0 & -\frac{S_4^1}{P_R^1} & 0 & -\frac{S_6^1}{P_R^1} \\ 0 & 0 & 0 & 0 & 0 & 1 \\ 0 & 0 & 0 & 0 & 0 & 1 \end{pmatrix}$$

The entries of $\boldsymbol{\theta}$ that are equal to 1 indicate linear dependencies. The remaining nonzero entries arise due to indirect effects of mass conservation. Since their expressions are derived in a very similar way, we only show the calculation for

$$\theta_{x_1}^{\mu_1} = \left. \frac{\partial \mu_1}{\partial x_1} \right|_{\mathbf{s}=\mathbf{s}^*} \quad (5.9)$$

in which we explicitly use asterisks to denote steady-state concentrations.

Assuming mass action kinetics, $f_7(S_0^1, K_R^1) = \alpha_7 S_0^1 K_R^1$ with a rate constant α_7 . It follows that

$$\mu_1 = \frac{f_7}{f_7^*} = \frac{S_0^1 K_R^1}{S_0^{1,*} K_R^{1,*}} \quad (5.10)$$

Because of mass conservation of the substrate and the kinase, $S_0^1 = S_T^1 - S_1^1 - S_2^1 - S_3^1 - S_4^1 - S_5^1 - S_6^1$ and $K_R^1 = K_T^1 - S_3^1 - S_5^1$. Therefore, taking the derivative with respect to $x_1 = S_1^1/S_1^{1,*}$ yields

$$\theta_{x_1}^{\mu_1} = \left. \frac{\partial \mu_1}{\partial x_1} \right|_{\mathbf{s}=\mathbf{s}^*} = \frac{S_1^{1,*}}{S_0^{1,*} K_R^{1,*}} \left. \frac{\partial}{\partial S_1^1} K_R^1 S_0^1 \right|_{\mathbf{s}=\mathbf{s}^*} = -\frac{S_1^{1,*}}{S_0^{1,*}}. \quad (5.11)$$

The Jacobian $\mathbf{J} = \mathbf{\Lambda}\boldsymbol{\theta}_x^\mu$ is obtained by matrix multiplication. The result can be written as a product of the two matrices:

$$\mathbf{J} = \begin{pmatrix} \frac{1}{S_1^1} & 0 & 0 & 0 & 0 & 0 \\ 0 & \frac{1}{S_2^1} & 0 & 0 & 0 & 0 \\ 0 & 0 & \frac{1}{S_3^1} & 0 & 0 & 0 \\ 0 & 0 & 0 & \frac{1}{S_4^1} & 0 & 0 \\ 0 & 0 & 0 & 0 & \frac{1}{S_5^1} & 0 \\ 0 & 0 & 0 & 0 & 0 & \frac{1}{S_6^1} \end{pmatrix} \cdot \begin{pmatrix} -f_{10}-f_{13} & 0 & f_9+\frac{f_{13}S_3^1}{K_R^1} & \frac{f_{10}S_4^1}{P_R^1}+f_{11} & \frac{f_{13}S_5^1}{K_R^1}+f_{14} & \frac{f_{10}S_6^1}{P_R^1}+f_{18} \\ 0 & -f_{16} & 0 & \frac{f_{16}S_4^1}{P_R^1} & f_{15} & \frac{f_{16}S_6^1}{P_R^1}+f_{17} \\ -\frac{f_7S_1^1}{S_0^1} & -\frac{f_7S_2^1}{S_0^1} & -\frac{f_7S_3^1}{S_0^1}-\frac{f_7S_4^1}{K_R^1}-f_8-f_9 & -\frac{f_7S_4^1}{S_0^1} & -\frac{f_7S_5^1}{S_0^1}-\frac{f_7S_5^1}{K_R^1} & -\frac{f_7S_6^1}{S_0^1} \\ f_{10} & 0 & 0 & -\frac{f_{10}S_4^1}{P_R^1}-f_{11}-f_{12} & 0 & -\frac{f_{10}S_6^1}{P_R^1} \\ f_{13} & 0 & -\frac{f_{13}S_3^1}{K_R^1} & 0 & -\frac{f_{13}S_5^1}{K_R^1}-f_{14}-f_{15} & 0 \\ 0 & f_{16} & 0 & -\frac{f_{16}S_4^1}{P_R^1} & 0 & -\frac{f_{16}S_6^1}{P_R^1}-f_{17}-f_{18} \end{pmatrix}$$

For the two-layer model and the three-layer model, the derivation of the Jacobian works in an analogous way. Since the two-layer model consists of 9 and the three-layer model of 15 dynamic variables, we do not show the large terms here. The system of ODEs for the three-layered cascade can be found in Appendix A.

5.2.3 Parameter ranges

In the two-layer and three-layer models, biologically reasonable estimates of the ranges of the general parameters are used that are based on experiments on *Xenopus* oocyte extracts [96]. The parameters representing total concentrations are summarized in Tab. 5.1. They are varied by a factor of 5 in the random sampling analysis in Sec. 5.4.

Parameter	Value
S_T^0	$2nM$
S_T^1	$1.2\mu M$
S_T^2	$1.2\mu M$
K_T^0	$0.3nM$
P_T^0	$0.3nM$
P_T^1	$0.3nM$
P_T^2	$120nM$

Table 5.1: Total concentrations in the model of the MAPK cascade

Since we are not aware of direct experimental data for typical steady-state fluxes \mathbf{f} , we inferred ranges for these quantities using existing data on rate constants. For

each steady-state flux f_i , there is a rate constant α_i of the conventional model. From Ref. [100] we adopt ranges of $30 - 750\text{min}^{-1}$ for α_{3n+2} and α_{3n} with $n = 1 \dots 10$. Combining this with the steady-state concentrations, most of the steady-state fluxes are estimated. The remaining fluxes are determined by the flux modes. For this reason, and also because continuation of the generalized parameters in the bifurcation analysis alters also the parameters of the conventional models, we cannot guarantee that all α_i of conventional models remain restricted to these ranges. The α_i of the conventional models for which numerical simulations are shown are listed in Appendix B.

5.3 Dynamics of the one-layer model

We begin our investigation of the MAPK cascade with a model of a single layer of the cascade in isolation. This comparably simple system is still analytically tractable and has been investigated in earlier studies [99, 122]. In contrast, our approach to the one-layer system is numerical, based on a statistical analysis of a large ensemble of randomly generated samples, each corresponding to the steady state of a model realization.

5.3.1 Generation of random samples

In comparison with other general models discussed in this thesis, the construction of random parameter sets is more complicated for the MAPK cascade because multiple conservation laws impose additional constraints that must be satisfied. The algorithm that was applied to generate random samples of steady states can be described as follows for the one-layer system.

We first draw random values for the steady-state concentrations which contain the kinase, S_3^1 , S_5^1 and K_R^1 , from a uniform distribution. These concentrations are then normalized such that the total concentration of the kinase is $K_T = 1$. Subsequently, we also assign random values to the variables containing phosphatase, S_4^1 , S_6^1 and P_R^1 , and normalize them such that they add up to $P_T = 1$. To ensure that sequestration effects can play a role in a significant fraction of the samples, the total concentration S_T^1 of the substrate is set to 10, resulting in a significantly higher concentration of the substrate than that of the kinase and the phosphatase. At this point, a fraction of the substrate is already bound in the complexes S_3^1 , S_5^1 , S_4^1 , and S_6^1 . The remaining substrate $r = S_T^1 - S_3^1 - S_5^1 - S_4^1 - S_6^1$ is distributed by drawing random concentrations for S_0^1 , S_1^1 , and S_2^1 and normalizing so that $S_0^1 + S_1^1 + S_2^1 = r$. Finally, the strength of all flux modes in the model is drawn randomly from a uniform distribution.

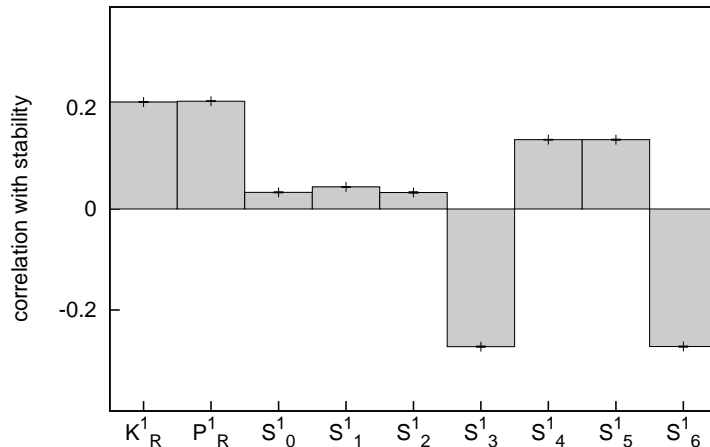


Figure 5.3: Correlations of parameters with stability in the one-layer model, based on a sample of $N = 10^6$ samples. On the vertical axis, the Pearson correlation coefficient of the binary stability values and the parameter values is shown for each parameter. All error bars are below the size of the line width.

5.3.2 Stability analysis of the single-layer model

In order to assess the impact of the individual parameters on stability we determine the stability of steady states in a large ensemble of $N = 10^6$ randomly drawn samples. Stable steady states are assigned the stability value $s_i = 1$, whereas unstable states are assigned the stability value $s_i = 0$. For each parameter k , we then compute the Pearson correlation coefficient

$$c = \sum_{i=1}^N \frac{(s_i - \bar{s})(k_i - \bar{k})}{N\sigma_s\sigma_k} \quad (5.12)$$

of the focal parameter with the stability value across the whole ensemble of N samples (σ_s, σ_k are standard deviations and \bar{s}, \bar{k} the sample means).

The correlation coefficients for the single-layer model are shown in Fig. 5.3. The concentrations of the unbound kinase K_R^1 and phosphatase P_R^1 show a correlation coefficient of 0.21 with stability. Consequently, steady states are likely to be stable if these concentrations are high and likely to be unstable if they are low. This shows that instability occurs most likely if a large fraction of the kinase and phosphatase is sequestered in complexes. The complexes S_3^1 and S_6^1 , which are involved in the production of the single-phosphorylated S_1^1 , are negatively correlated with stability, showing that a high concentration of these complexes has a strong destabilizing effect. By contrast, the complexes S_4^1 and S_5^1 , which appear in reactions decreasing S_1^1 , are positively correlated with stability.

More detailed insights in the effect of the parameters on stability can be gained from showing two-parameter plots of the fraction p of randomly drawn steady states

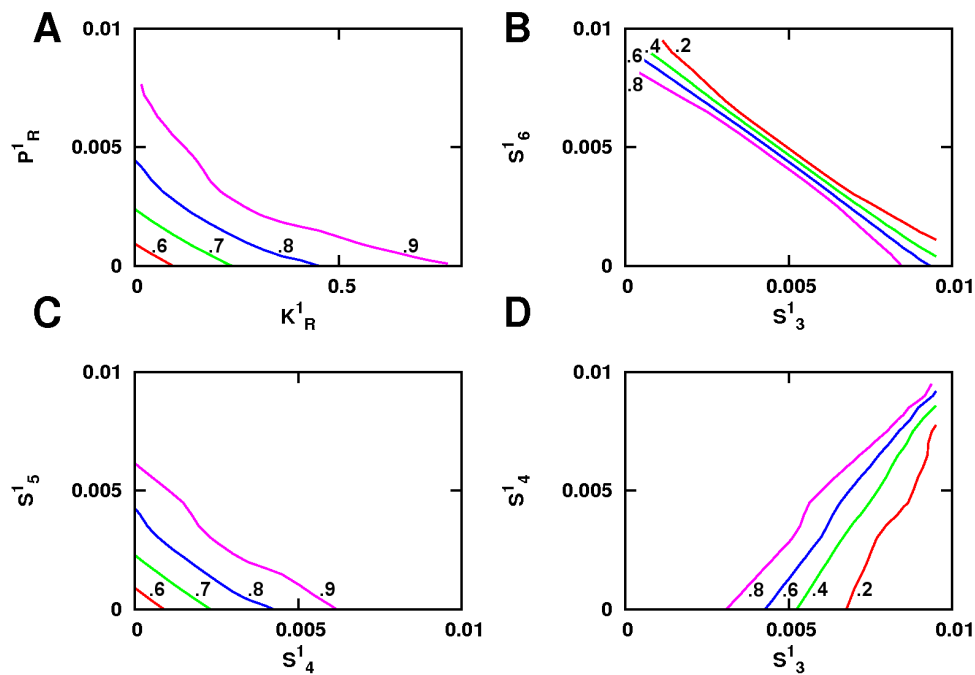


Figure 5.4: Connection between steady-state concentrations and stability. Contour lines computed from 10^7 random parameter sets show the fraction of stable steady states depending on two concentrations, thus showing correlations between parameters that cannot be seen in Fig. 5.3. The top left panel shows that instability is promoted by low concentrations of free kinase and phosphatase, highlighting the importance of sequestration effects. The model parameters with the strongest impact on stability are the concentrations of substrates S^1_3 and S^1_6 (top right).

that are stable. For this purpose, we generate another ensemble of 10^7 parameter sets with the algorithm described above. Figure 5.4 shows p as a function of selected combinations of two parameters. In Fig. 5.4A, p is shown as a function of the free enzyme concentrations K_R^1 and P_R^1 . The figure reveals that low concentrations of the free kinase and phosphatase K_R^1 and P_R^1 promote instability. This confirms that sequestration of the kinase and phosphatase plays a role in the destabilization of steady states. The dependence of p on the parameters S_3^1 and S_6^1 , which were found to have a strongly destabilizing impact in the correlation analysis, is plotted in Fig. 5.4B. The figure shows that the fraction of stable states changes sharply from 0 to 1 as the threshold is crossed. In contrast, even if the stabilizing parameters S_4^1 and S_5^1 are very low p only drops to 0.5 (Fig. 5.4C). This comparison confirms the lesser impact of the two stabilizing parameters, already seen in the correlation analysis. This conclusion is further supported by the direct comparison of the destabilizing parameter S_3^1 with the stabilizing parameter S_4^1 (Fig. 5.4D). In summary we conclude that the main source of instability in the single-layer system lies in high concentrations of the complexes S_3^1 and S_6^1 .

5.3.3 Mechanisms of instability

To understand the mechanism leading to instability in more detail we extend our analysis to the eigenvectors of the Jacobian. In an unstable steady state, the eigenvector corresponding to the eigenvalue with the largest real part represents the direction in which the system departs most rapidly from the steady state. We compute the typical direction of escape from unstable steady states by averaging over the eigenvectors corresponding to the largest eigenvalue in 10^6 unstable, but otherwise random parameter sets. Each eigenvector has been normalized such that $S_5^1 = 1$ before averaging.

The components of this averaged direction of escape are shown symbolically in Fig. 5.5. The figure illustrates qualitatively that perturbations from the unstable steady state cause the substrate to shift its mass into either one of the phosphorylation cycles, while depleting the other. This leads to the hypothesis that the system approaches one of two stable steady states in which the bulk of the substrate is concentrated in either of the two phosphorylation cycles, respectively.

The instability of steady states in the case of sequestration can be understood further by the following argument: In a situation with a large concentration of S_3^1 and with a correspondingly low value of free kinase K_1^R , the kinase is not available for the formation of the complex S_5^1 . This implies that the primary reaction involving S_1^1 as a substrate is the formation of the complex S_4^1 . This leads to a further accumulation in the left phosphorylation loop and consequently increases S_3^1 further. Therefore, there exists an indirect positive feedback caused by sequestration effects.

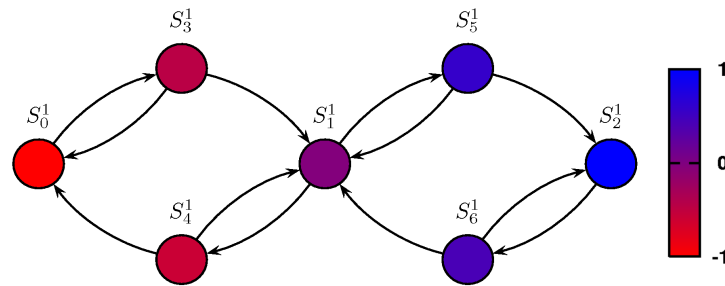


Figure 5.5: Instability in a single layer of the cascade. The components of the eigenvector corresponding to the leading eigenvalue of the Jacobian are analyzed. For each dynamic variable, the color indicates the averaged value of the corresponding entry of the eigenvector. All eigenvectors are normalized so that $S_5^1 = 1$ before averaging over 10^6 samples. The diagram shows that the system leaves the region of a typical unstable state by accumulating mass in either one of the two phosphorylation cycles, while depleting the other.

5.3.4 Relation to bistability

Unstable steady states are often located on a separatrix that divides the basins of attraction of different attractors. Moreover, previous works in the MAPK cascade have shown that a single layer of the cascade can support bistable dynamics [99, 117, 100], in which the system can reside in either one of two stable steady states. To confirm that the unstable steady states observed in the generalized model mark the separatrix between two stable steady states, we perform simulations in corresponding conventional models [100], using a stiff numerical integrator based on the modified extended backward differentiation formula (MEBDF) [123]. We randomly select 100 starting points corresponding to unstable states computed in the generalized model and slightly perturb the vector of steady-state concentration in different directions. For all of these samples it is found that trajectories starting close to the unstable steady state eventually converge to one of two different steady states, depending on the direction of the perturbation. An example for a time series with bistability is shown in Fig. 5.6. This result suggests that, in a class of reasonable conventional models of a single layer of the MAPK cascade, the long-term dynamics is bistable whenever we find an unstable steady state in the generalized model.

The origin of bistable parameter regimes can also be identified via cusp bifurcations, as it was explained in Chapter 3. We apply this procedure to the MAPK cascade in order to identify whether the origin of the bistable parameter is indeed in a cusp bifurcation. Because of the assumption of mass action kinetics, the higher derivatives needed for the calculation of the normal form parameters can be calculated and do not have to be represented by parameters as in Chapter 3.

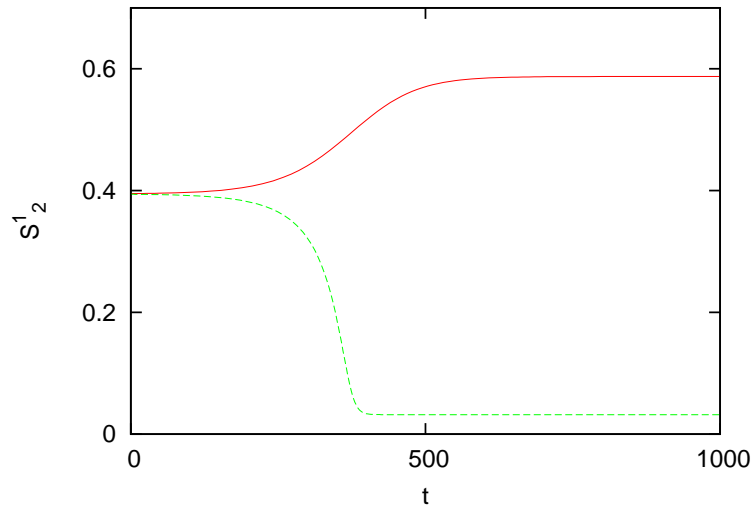


Figure 5.6: Example for bistability in the one-layer model. An unstable steady state that was found in the generalized model is mapped to a corresponding conventional model. We then perturb the system slightly by adding (red curve) and subtracting (green curve) a small amount of concentration from S_2^1 and integrate the system of ODEs numerically. As a result, the system approaches two different stable steady states.

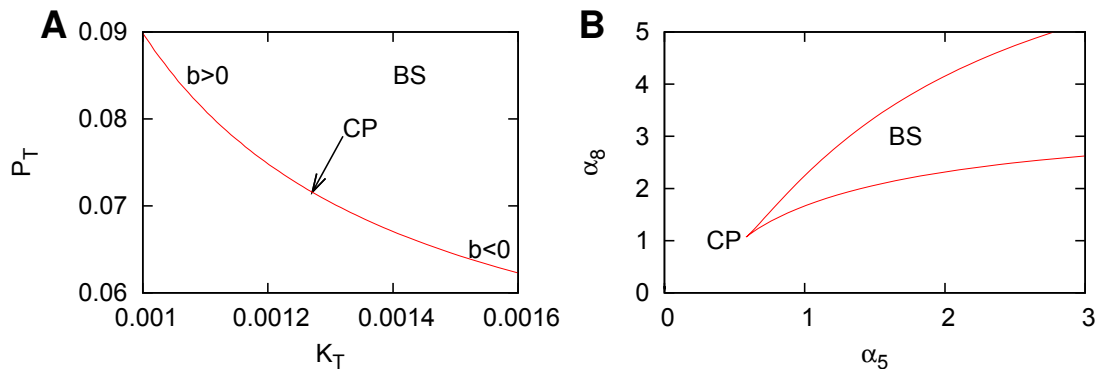


Figure 5.7: Cusp bifurcation in the general and conventional one-layer model. Panel A: Continuation of a saddle-node bifurcation in the general model. At the cusp point (CP), the normal form parameter b vanishes. Panel B: Bifurcation diagram depending on two rate constants after the transformation to a conventional model. Inside the cusp, bistability (BS) is detected.

The technical problem of detecting cusp bifurcations in a high-dimensional parameter space is solved by the following procedure: As an initial point of the search, a parameter set of the general model is chosen, which is characterized by a proximity to a bifurcation but otherwise random. Subsequently, the system is optimized towards a nearby saddle-node bifurcation using a Newton method and the bifurcation manifold

is continued by changing the general parameters in the direction that lets the normal form parameter b approach zero. In Fig. 5.7A, a bifurcation diagram depending on two parameters of the general model is shown. In order to verify that the cusp point indeed signifies the onset of a bistable region in parameter space, the general model is transformed back to a special model exactly at the cusp bifurcation point. The bifurcation diagram for the conventional model is shown in Fig. 5.7B, displaying the typical cusp shape. We verify that the system is indeed bistable inside the “pocket” of the cusp by computing time series with initial conditions close to the steady state under consideration. Different perturbations of the initial concentrations at $t = 0$ lead to trajectories approaching different steady states, so that it is confirmed that the bistability in the one-layer model has its origin in cusp bifurcations.

5.4 Dynamics of the two-layer and three-layer models

As a next step, we extend the investigation of stability and bifurcations to the two larger subsystems of the MAPK cascade. We proceed analogously to the investigation of the single-layer model by first generating a large ensemble of randomly drawn parameter sets and then correlating the stability of the corresponding steady states with the parameter values. Subsequently, we explore the bifurcation landscape of the larger models.

5.4.1 Correlations of parameters with stability

In the two-layer system and the three-layer system, the random sampling of steady states is performed in an analogous way to the one-layer system. In particular, the algorithm to construct random samples is based on the same pattern as in the one-layer system. Beginning with the top layer and proceeding to the bottom layer, the randomly sampled steady states are constructed in a stepwise manner, at each step taking into account the remaining fraction of substrate and enzyme which has not been used in earlier steps. In the investigation of the larger models, describing two and three layers of the cascade, we chose parameter values based on experimental data from Ref. [96]. As explained in Sec. 5.2.3, this affects the total concentrations and the steady-state fluxes.

The results of the correlation analysis for all three models are shown in Fig. 5.8. For comparison, Figure 5.8A displays again the stability correlations of the one-layer model that were discussed in the previous section. Figure 5.8B shows the stability correlations in the second model, which consists of the first and second layer of the cascade. The

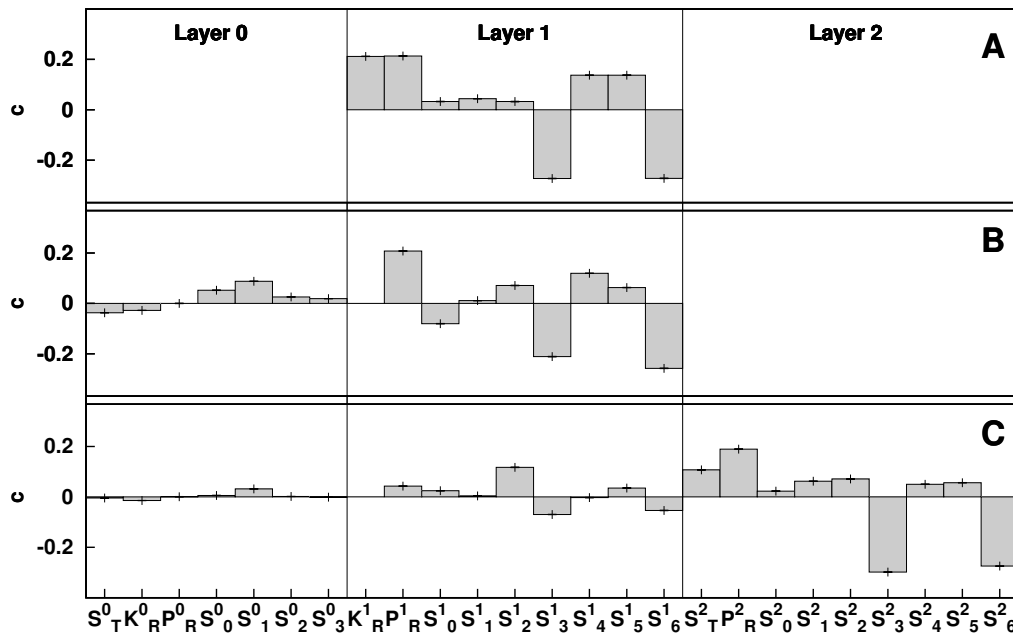


Figure 5.8: Correlations of parameters with stability. We consider three different subsystems of the cascade, a single layer (A), two connected layers (B) and three layers (C). The bars show the correlation of a given parameter with the stability of the steady states in an ensemble of $N = 10^6$ randomly generated parameter sets. The statistical errors, which are determined by bootstrap resampling, are on the order of the line width. The plots show a conserved pattern of correlations and indicate the parameters that are important for stability.

additional parameters, describing the top layer of the cascade, have a weaker impact on the stability of steady states, as evidenced by the low values of the corresponding correlation coefficients. Note furthermore that the pattern of correlation coefficients in the second model is very similar to that found in the first model. In particular, there is a repeated motif of strong positive correlations in P_R^1 , S_4^1 , and S_5^1 .

In the third model, consisting of all three layers of the cascade, the pattern of correlations observed above reappears twice. As shown in Fig. 5.8C, the correlation coefficients corresponding to both the first and second layer of the cascade are now smaller, indicating a reduced impact on the dynamics. Nevertheless, the pattern of correlations is still visible in the second layer. More importantly, the pattern reappears in a stronger form in the third layer.

These results suggest that the respective bottom layer has the strongest impact on the stability of steady states. Moreover, the basic mechanism of instability, i.e., the implicit positive feedback induced by sequestration of substrates into the complexes S_3^i and S_6^i , remains the same in all three models.

5.4.2 Bifurcation structure of the larger models

Next, we focus on the dynamics that can be observed after the stability of a steady state is lost. For this purpose, we search for bifurcations, marking a change in the stability of steady states. We start by generating an ensemble of 10^7 randomly sampled unstable steady states, discarding all samples in which the steady state is stable. In Table 5.2, we show the statistics of the number of real positive eigenvalues and complex conjugate pairs of eigenvalues with a positive real part in this ensemble. The eigenvalue patterns indicate the possible types of bifurcations close to which unstable steady states with the respective pattern of eigenvalues can be found.

Real	Complex	1 layer	2 layers	3 layers
1	0	100%	96.5%	36.7%
2	0	-	2.5%	29.4%
3	0	-	-	0.1%
0	2	-	1.0%	33.5%
1	2	-	-	0.3%
0	4	-	-	0.001%

Table 5.2: Statistics of positive eigenvalues among a sample of 10^7 randomly drawn unstable steady states for the subsystems of the MAPK cascade. The fraction of steady states with different number of real positive eigenvalues and complex eigenvalues with a positive real part are listed.

Since the probability that a random sample is located exactly at a bifurcation is of measure zero, bifurcations cannot be detected directly by random sampling. However, the signature of the eigenvalues can point towards bifurcations in the vicinity. We verify the existence of the bifurcations by a continuation of the steady state towards a nearby bifurcation with the help of a Newton method [56]. In all cases with at least one real positive eigenvalue, saddle-node bifurcations were found in the nearby parameter regime, while a complex pair with a positive real part in all cases implied the existence of a Hopf bifurcation in the vicinity. The results from the random sampling method in combination with the optimization method can be summarized as follows:

In the one-layer model, no unstable steady states with complex leading eigenvalues were found, showing the absence of oscillatory dynamics in the vicinity of Hopf bifurcations. Only bifurcation points of saddle-node type were found, which mark the transition from a parameter regime with a stable steady state to a regime of bistability.

By contrast, leading complex eigenvalues exist in unstable steady states of the two-layer system and, with a larger frequency, in the three-layer system. This suggests that in addition to bistability, oscillatory dynamics are also possible in these models and appear in a comparatively larger part of the parameter space in the three-layer cascade.

Finally, there are also regions in parameter space with multiple positive eigenvalues that point to the existence of bifurcations with a higher codimension. For example, a parameter set with 4 positive eigenvalues with non-vanishing imaginary part suggests that the general parameters can be varied in a way that a double Hopf bifurcation is crossed. The dynamics in the vicinity of bifurcations of higher codimension are investigated in the subsequent section.

5.4.3 Codimension-2 bifurcations and complex nonlocal dynamics

In the previous section we showed that Hopf bifurcations do not exist in the one-layer system, but appear when a second layer is added and, in a larger part of the parameter space, in the complete three-layer model. Next, we investigate whether the three-layer system can exhibit additional types of dynamic behavior that cannot occur in the two-layer model. Possible candidates for this would be quasiperiodic or chaotic dynamics. Generalized modeling, being essentially based on a local analysis, cannot detect such nonlocal properties of the system directly. However, generalized models can be used to search for local bifurcations of higher codimension that can then point to parameter regions in which conventional models show the respective type of dynamics.

In order to detect a bifurcation of codimension two, two parameters of the sys-

tem must be adjusted simultaneously to their exact bifurcation values. We locate codimension-2 bifurcations starting from potential candidates among the ensemble of random samples with a characteristic signature in the eigenvalues (for example, two pairs of complex conjugate eigenvalues for a double Hopf bifurcation). Subsequently, the surrounding area is scanned for bifurcations by a variation of selected general parameters. Explicit numerical simulation in the conventional model is then used to explore the dynamics close to codimension-2 bifurcation points. Thereby, the higher efficiency of generalized models is combined with the higher predictive power of conventional models.

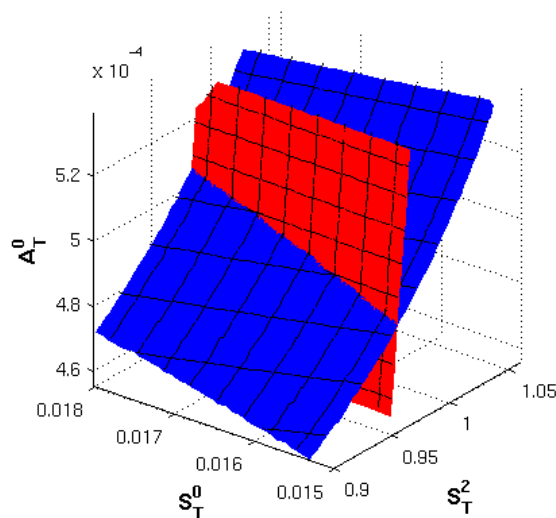


Figure 5.9: Three-parameter bifurcation diagram of a codimension-2 Gavrilov-Guckenheimer bifurcation. The codimension-2 bifurcation is formed at the intersection line of a Hopf bifurcation (red) with a saddle-node bifurcation (blue). Bifurcations of higher codimension such as Gavrilov-Guckenheimer and double Hopf bifurcations can serve as proxies that indicate parameter regions in which complex dynamics can potentially be observed. See Appendix B for additional parameters.

An example of a codimension-2 bifurcation in the three-layer model is shown in Fig. 5.9 in a three-parameter bifurcation diagram, which is created by a triangulation algorithm described in Ref. [124]. The fixed parameters are listed in Appendix B. In the three-dimensional parameter space, a surface of Hopf bifurcation points (red surface) and a surface of saddle-node bifurcation points (blue surface) intersect. On the intersection line of the bifurcations, the Jacobian has both a single zero eigenvalue and a purely imaginary eigenvalue pair, marking the points on the intersection line as codimension-2 Gavrilov-Guckenheimer bifurcation points. It is well known from normal form analysis that close to this type of bifurcation quasiperiodic dynamics

should generally occur [11](p. 345).

Another example of a codimension-2 bifurcation is the double-Hopf bifurcation, which is characterized by the presence of two purely imaginary eigenvalue pairs. This bifurcation generically involves the creation of chaotic and quasiperiodic regions [11](p. 369).

Although the existence of Gavrilov-Guckenheimer or double Hopf bifurcations cannot strictly guarantee non-transient complex dynamics, the bifurcations serve as proxies indicating parameter regions in which such complex dynamics is detected in many cases. We therefore perform at selected steady states in the vicinity of codimension-2 bifurcations a transformation to a conventional model that is identical to the models analyzed in Ref. [96, 100]. We then perturb the variables of the conventional model slightly and retrieve a time series by numerical integration.

In the three-layer model of the MAPK cascade, this procedure does not reveal unusual types of dynamics close to Gavrilov-Guckenheimer bifurcations such as in Fig. 5.9. Depending on the choice of parameters, the system shows either stationary behavior, bistability (thus approaching different stable steady states for different kinds of perturbations) or sustained oscillations with a regular, sinusoidal form.

More interesting dynamics can be found close to double-Hopf bifurcations, which appear exclusively in the three-layer system. A two-parameter bifurcation diagram of a double-Hopf bifurcation and two example time series from different regions are shown in Fig. 5.10. The corresponding parameters are listed in Table B.3 and Table B.3 in Appendix B. Both time series show evidence for complex mixed-mode oscillations. Moreover, the spike-like time-series shown in Fig. 5.10C exhibits an irregularity that is indicative of Šilnikov chaos. Similar dynamics were also observed at multiple points in the neighborhood (not shown). We are therefore confident that the system shows chaotic long-term behavior in a finite parameter region. However, to confirm the chaotic nature of the dynamics and to determine the parameter ranges in which they occur will require more extensive numerical investigations, including the computation of Lyapunov exponents, which exceeds the scope of this investigation.

5.5 Explicit Feedback

In addition to the implicit negative feedback that is caused by sequestration effects in the double-phosphorylation cycles of the cascade, we also consider the implications of additional explicit forms of feedback on the stability of steady states. While the structure of the MAPK cascade is widely conserved throughout eukaryotic cells, this is not necessarily the case for the types of feedback that may depend on species and tissue [125]. Here, we implement two types of negative feedback mechanisms that have

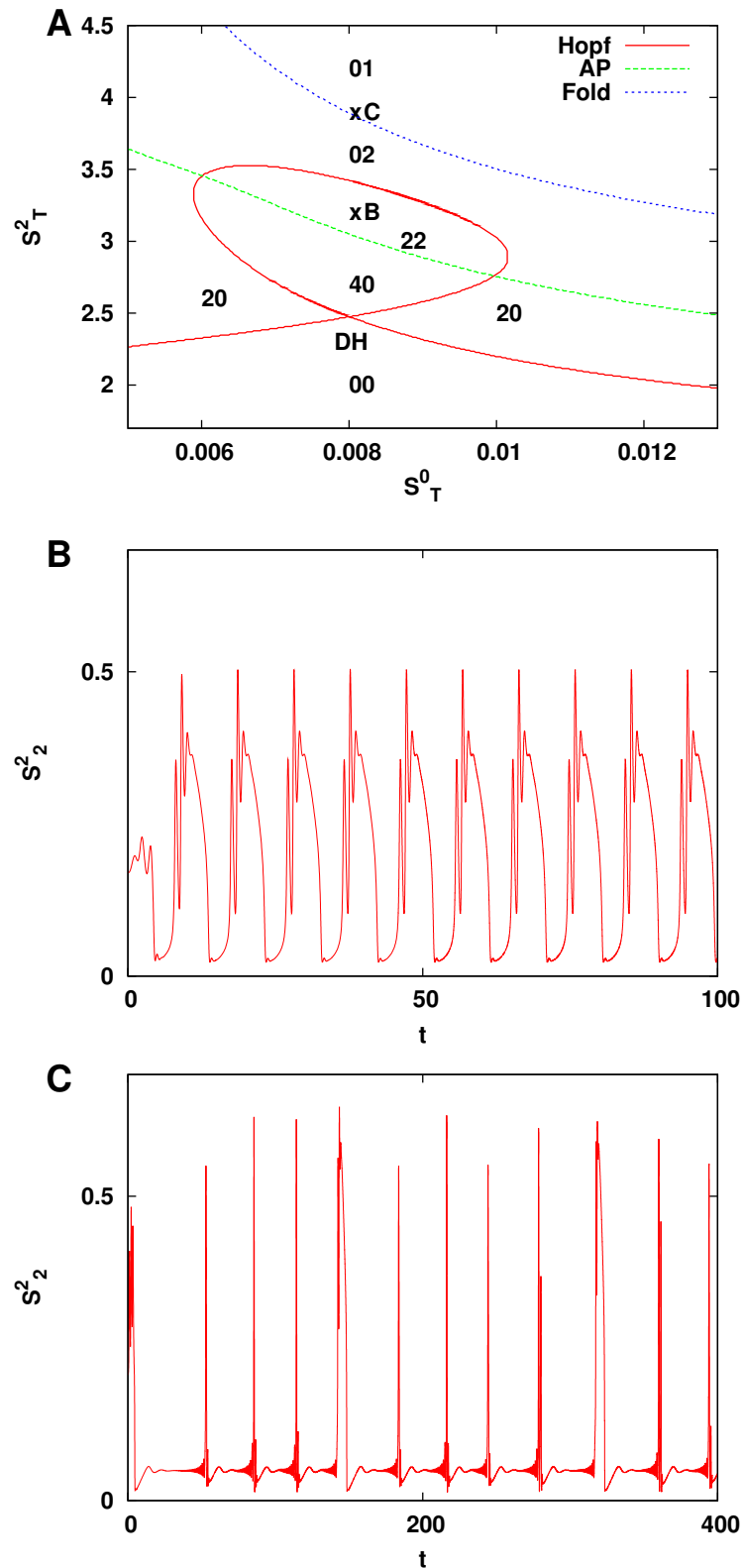


Figure 5.10: Complex dynamics close to a double-Hopf bifurcation. **A**: Two-dimensional bifurcation diagram with a double Hopf bifurcation. Parameters are S_T^0 and S_T^2 . Hopf bifurcations are drawn in red, saddle-node bifurcations in blue. At the green line (AP), a Hopf pair loses its imaginary part, leading to two distinct real eigenvalues. The numbers denote the number of complex and real eigenvalues with a positive real part, in this order. The stable region corresponds therefore to the label 00. The points B and C at which we show numerical integration results are drawn in. **B** and **C**: Complex oscillations and chaos close to the double-Hopf bifurcation.

been identified in the literature:

a) In fibroblasts, SOS, a protein upstream from Ras (K_R^0 in our notation), can undergo inhibitory phosphorylation by ERK (S_2^2). Even though SOS is not included in our model, the feedback effectively propagates downstream to Ras, inhibiting the formation of the Ras-Raf complex (S_2^0) [126, 97]. The resulting feedback loop extends from the output of the cascade in the third layer back to the first layer.

b) In COS1-cells, activated ERK (S_2^2) feeds back to MEK (S_0^1) during cell adhesion by phosphorylating it at the site T292, which inhibits phosphorylation by PAK at the adjacent site S298. The suppressed phosphorylation facilitates the formation of ERK-Raf complexes (S_3^1, S_5^1) [127], resulting in a negative feedback exerted by S_2^2 on S_0^1 . Therefore, the second type of feedback extends from the third layer back to the second layer.

Because it is widely believed that the MAPK cascade is utilized mainly as an ultrasensitive switch, it is conceivable that the function of the feedback loops is to suppress non-stationary dynamics such as oscillations. We therefore investigate whether the oscillatory parameter regime is reduced by introducing feedback in the system. To study this question in conventional models is not trivial for two reasons: First, in a conventional model the effect of the feedback has to be restricted to a specific functional form, which can be difficult to derive. Second, and perhaps more importantly, it is hard to study the effect of feedback in isolation in conventional models. If feedback parameters in conventional models are changed, one generally observes the combined effect of the altered feedback strength and the corresponding shift in the steady state, so that it cannot be directly investigated how the stability of a given steady state observed in nature depends on the nonlinearity of the feedback. Both of these difficulties are avoided in generalized models, that are designed to deal with unknown functions and parametrize the position of the steady state independently from the nonlinearities in the system.

We study the effect of the feedback of type a) and b) by adding an inhibitory link from the final product of the cascade, S_2^2 , back to the phosphorylation steps in the first (a) and second (b) layer, respectively. The feedback loops are also inscribed in Fig. 5.2. Because the feedback is inhibitory in both cases, the corresponding elasticities are negative. The effect of the feedback can therefore be modeled by introducing elasticities $\theta_f = \theta_{S_2^2}^{\mu_1} < 0$ (feedback a) and $\theta_f = \theta_{S_2^2}^{\mu_7} = \theta_{S_2^2}^{\mu_{13}} < 0$ (feedback b). In the case of no feedback, both parameters are zero. In order to determine the effect of the feedback we generate an ensemble consisting of 10^7 parameter sets for each of the two feedback mechanisms. The parameter sets are drawn randomly with the algorithm explained in the previous sections, except for the additional feedback parameter θ_f , which is drawn randomly from a uniform distribution in the interval $[-2, 0]$. This range is consistent

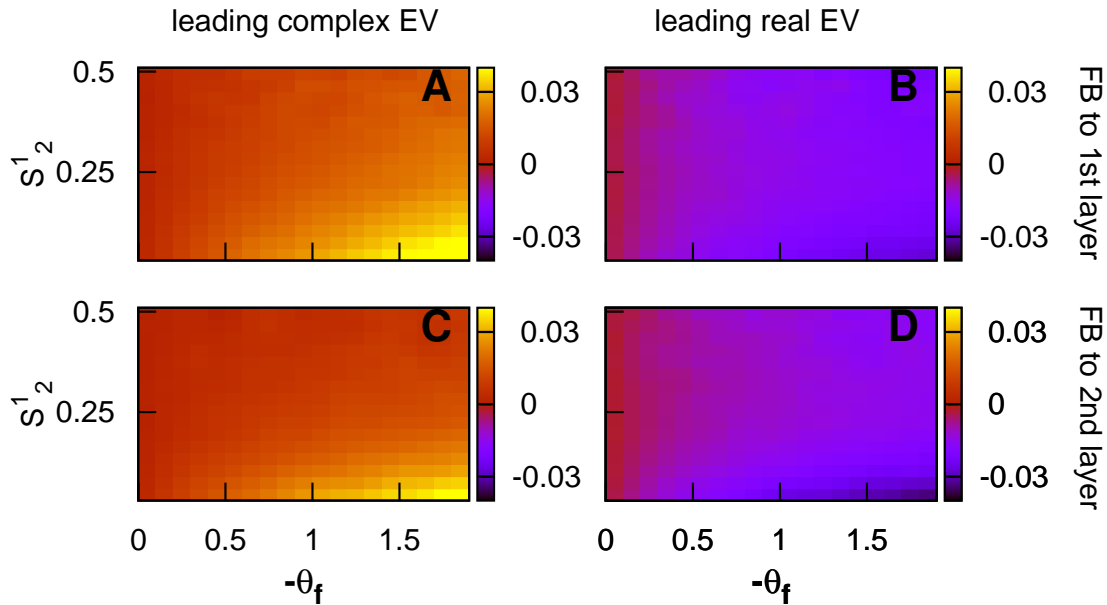


Figure 5.11: The effect of external feedback. Color-coded is the change in relative abundance of unstable stationary states as feedback is switched on. This change is shown separately for unstable states with leading complex eigenvalues (left) and leading real eigenvalues (right). The top row corresponds to feedback to the first layer (type a) while the bottom row corresponds to feedback to the second layer (type b). In both cases stronger feedback (large values of θ) means that more unstable steady states with a complex and less states with a real leading eigenvalue occur. This suggests that the feedbacks promote rather than inhibit oscillatory dynamics.

with inhibition modeled by a Hill function with exponent two, allowing for some degree of cooperativity. For each parameter set, we then compute the spectrum of the Jacobian with and without feedback.

As a first result, we find that the stability of a significant number of steady states changes when the feedback is switched on. However, the net effect on the percentage of stable steady states over the whole ensemble is very small because stable samples becoming unstable as a result of the feedback cancel with unstable samples becoming stable. Therefore, overall stability does not capture the relative abundance of Hopf bifurcations as a source of instability.

The effect of the feedback is better understood if the signature of the eigenvalue is investigated more closely, analyzing whether instability is characterized by a positive, real eigenvalue or by a complex conjugate pair with positive real part. Figure 5.11 shows how the number of unstable states changes as a result of feedback, separately for unstable states in which leading eigenvalue of the Jacobian is complex or real, respectively. For both types feedback, it is observed that as the feedback strength increases,

the number of unstable steady states with complex leading eigenvalues increases, while the number of unstable steady states with real leading eigenvalues decreases. Although the observation of an unstable steady state with complex leading eigenvalues does not strictly imply that the long-term dynamics of the system is oscillatory, the increase of such states over a wide parameter range strongly suggests that also oscillatory long-term dynamics is promoted by the two feedback loops under consideration, whereas bistability is suppressed.

5.6 Discussion

In this chapter, we have used generalized modeling to analyze the dynamics of a class of enzymatic models describing the MAPK cascade. Starting out with a correlation analysis, building on tens of millions of parameter sets, we first determined the impact of the individual model parameters on the stability of the steady states. This analysis confirmed that sequestration of enzymes has a strong impact on the dynamics of the cascade. In particular, we showed that instability is likely if large portions of the kinase and phosphatase acting on the lowest level of the cascade are sequestered into complexes (S_3^2 and S_6^2 in our notation). In this case a positive feedback loop is formed that destabilizes stationary states.

In a second step we used bifurcation analysis, spectral analysis of unstable states, and explicit simulation to investigate the dynamics subsequent to the loss of stability. In a subsystem consisting of only one layer of the cascade, bifurcation analysis of the generalized model revealed that steady states lose their stability only in saddle-node bifurcations. By contrast, in the two- and three-layer subsystems Hopf bifurcations as well as saddle-node bifurcations occur. In the present model it was confirmed by numerical simulations that the saddle-node bifurcations mark the onset of bistability, while the Hopf bifurcations mark the onset of oscillations. Our results are therefore in agreement with earlier work [100] showing that, without external feedback, at least two layers of the cascade are required to observe oscillatory dynamics, while bistability already occurs in a single layer of the cascade.

Using a combination of generalized and conventional modeling we then identified a parameter region in which complex and potentially chaotic mixed-mode oscillations occur. To determine the exact nature of these oscillations and the parameter ranges in which they can be observed is a promising question for future studies, but will probably require more extensive numerical simulations and the computation of Lyapunov exponents.

Finally, we have investigated the impact of two known feedback loops acting on the MAPK cascade. Our analysis indicates that, under general conditions, the effect of

these loops is to reduce bistability and promote oscillatory dynamics in the cascade.

Sustained oscillations in cells can be generated by several different mechanisms [128]. The most prominent cause of oscillations is negative feedback, sometimes in connection with a time delay. Explicit negative feedback led to sustained oscillations in various models of the MAPK cascade [97, 129] and indeed enlarged the oscillatory parameter regime in our model, too. However, negative feedback cannot be the mechanism behind the oscillations in the two-layer and three-layer systems without an explicit feedback loop, which must therefore rely on a different mechanism. It is known that in a system with positive feedback that exhibits bistability, a slow process can cause the system to jump between the two stable states. As a result, relaxation oscillations occur that usually have a pulse-like shape [4]. Indeed, it was found that in the MAPK cascade, the second layer is in the regime of bistability when the whole system oscillates [100]. The bistable double phosphorylation loop is controlled by a slow process in the top level, thus alternating between the two stable states. It is conceivable that a third process in the full cascade could interact with an already oscillating two-layer system and thereby cause chaotic behavior.

An important question is whether oscillatory dynamics in the MAPK cascade play a role *in vivo*. Based on the early modeling results, it is often assumed that the cascade is utilized as an ultrasensitive switch, and other dynamics appear only as nonfunctional byproducts. Our results illustrate that the oscillatory parameter space is quite large and therefore likely to be encountered *in vivo*. This view is supported by the recent experimental observation of MAPK oscillations [130, 129].

Further support for the functional role of oscillations comes from an evolutionary argument. If oscillations were indeed non-functional one could suspect that specific mechanisms suppressing oscillations should have evolved. Yet, the basic topology of the MAPK cascade that can sustain oscillations is conserved through evolution. By contrast, external feedback loops, that could potentially suppress oscillations, differ among organisms and cell types. Moreover, the two examples of feedback loops studied here were found to promote oscillations instead of suppressing them. If the MAPK cascade is indeed used both as a switch and as an oscillator under different physiological conditions, it is intuitive that the system should be very well conserved, as any further mutations are unlikely to maintain both of the cascade's function.

To ascribe a biological function also to the irregular oscillations reported here is highly speculative. Nevertheless, it is conceivable that the observed spike-like dynamics could play a useful role. One could alternatively suspect that the complex oscillations are a byproduct of a mechanism that enhances differences between individual cells.

Such a mechanism may be useful because if in a population of cells, a substantial fraction of the populations changed their behavior at a similar level of an external

stimulus, then the response would become switch-like also on the population level. This could have detrimental consequences because it could seriously decrease the dynamical stability on the population level and produce unnecessarily strong responses. It may therefore be advantageous to sustain a high sensitivity not only to the stimulus but also to enzyme concentrations that may differ between individual cells. Thereby, signals in different cells could be triggered at different levels of the stimulus, so that the response of the population is smooth, while the response of the individual cell stays sharp. Weakly chaotic dynamics could possibly arise as a byproduct of this internal sensitivity.

The question whether the detected forms of dynamics can appear *in vivo* is closely connected to the question how realistic the space of parameters assessed in our study is. The ranges that we assigned to the general parameters were motivated by experimental data. While the total concentrations of the involved enzymes have been measured in one cell type [96], less is known about the remaining parameters. Note, however, that large differences in the fluxes f_i (see Appendix B) are to be expected since also the total concentration listed in Table 5.1 vary strongly between different layers. Therefore the parameter ranges in which oscillations and complex dynamics were observed in this study are not unreasonable. Nevertheless, future experimental work covering further variables and different cell types and developmental stages would be highly desirable to clarify the dynamics and function of the MAPK cascade *in vivo*.

Chapter 6

Discussion and outlook

In this thesis, different dynamical systems from cell biology were analyzed with the method of generalized modeling. In this chapter, we first summarize the results of the different projects. We then proceed to discuss the implications of the results under the broader perspective of how generalized models can contribute to problems from cell biology. We conclude with an outlook for future investigations.

Summary of results

In the first subproject, chapter 3, an extension of the method of generalized modeling was introduced that allows to incorporate the analysis of normal forms of bifurcations. In addition to the information of the Jacobian, also the second and third derivatives of the functions were utilized. The extended method was applied to two different models of gene-regulatory networks, the Goodwin model and a model of a mammalian circadian oscillator. For the Goodwin model, we derived an analytical expression for the first Lyapunov coefficient that describes the conditions under which Hopf bifurcations in the model are supercritical or subcritical. Since only minimal assumptions were made on the nonlinear negative feedback function, the type of the Hopf bifurcation could be determined for a large class of feasible functions. For the widespread choice of a sigmoidal inhibition function, it was shown that the Hopf bifurcation is supercritical, regardless of the value of the Hill coefficient. However, it was also demonstrated that slight deviations from this form can render the bifurcation subcritical.

By an analysis of a model of a circadian oscillator, it was then shown that the normal form analysis can also be applied to larger general models with multiple nonlinear functions. While the higher number of parameters complicates a systematical investigation of the bifurcation properties, statistical methods were used to show conditions under which supercritical and subcritical Hopf bifurcations can occur. As a second application of the extension, we proposed a novel method to locate bistability

in classes of models by detecting cusp bifurcations in the general model. Using abstract gene-regulatory networks based on the model of the circadian oscillator, it was shown that the method can indeed locate regions of bistability.

In the second subproject, chapter 4, the dynamics of bone remodeling was studied. Two basic model structures were investigated, on which the majority of previously proposed models are based. For the two-variable model, which describes the dynamics of osteoblasts and osteoclasts, an analytical bifurcation analysis was performed. It was shown that a symmetry in earlier models renders the system Hamiltonian, thus preventing sustained oscillations. It is biologically reasonable to abandon this symmetry, thereby introducing the possibility of sustained oscillations close to Hopf bifurcations. Further, we argued that restrictive conditions on the parameters are necessary to allow for stable steady states. Although the parameters in earlier studies were chosen to meet these conditions, some of these decisions are supported by little biological evidence. For a three-variable model that divides the population of osteoblasts into two groups based on their stage of maturation, it was shown that weaker assumptions are required for stability. However, also the three-variable model entails the danger of losing stability in bifurcations. We related the loss of stability in a Hopf bifurcation to Paget's disease, in which periodic surges of bone remodeling are observed. While further studies are needed to verify possible connections between bifurcations and diseases, our study demonstrates that the stability of steady states in current models for bone remodeling is a serious problem that has been neglected in the past.

The third subproject, chapter 5, focused on the MAPK cascade, an important signaling pathway that consists of a cascading arrangement of phosphorylation-dephosphorylation cycles. By investigating different subsystems of the MAPK pathway in general models, it was studied how the combination of different cascade layers affects the possible types of dynamics in the system. The stability of steady states was studied by a statistical analysis of correlations between the parameters and stability. It allows to identify parameters that affect the stability of steady states strongly, thus revealing possible targets for experimental studies. Moreover, it was shown that an implicit form of feedback caused by sequestration effects can cause bistability in a single layer of the cascade. The combination of two layers led to additional Hopf bifurcations and oscillatory dynamics. In the three-layer model, codimension-2 bifurcations revealed a parameter region in which irregular oscillations and bursting-type behavior could be observed. Finally, it was shown that an additional negative feedback loop leads to the growth of the oscillatory regime, which is compensated by a decrease of the bistable regime.

Implications for the method of generalized modeling

All of the systems analyzed in this thesis share the common property that they can be described by mathematical models consisting of ordinary differential equations. Beyond that, the systems differ in various important aspects. Among these aspects are the length and time scales on which the processes described by the model occur, the amount of existing knowledge about the biological processes that are modeled, and the size and degree of complexity of the mathematical model itself.

In the majority of earlier studies, generalized modeling has been applied to systems with many unknown properties. For systems of this type, the construction of conventional models involves necessarily a considerable amount of ad-hoc decisions and speculation. Bone remodeling is an example of such a system for which mathematical modeling is still at an early stage. Fewer earlier studies exist than for the other systems analyzed in this thesis, and currently, several alternative models coexist. These models have not been investigated in comparative studies and a paradigmatic model has yet to emerge.

In the chapter on bone remodeling, it was shown that the method of generalized modeling is a useful tool under these circumstances, because it reveals connections between structural properties and the dynamics in large class of potential model candidates. For example, certain classes of models can be identified that do not exhibit stable steady states and are therefore not suitable to describe the dynamics of bone remodeling. Inside the framework of conventional modeling, such connections cannot be easily found, especially when conventional models include several complicated functional forms with multiple parameters. In a specific conventional model of this kind, it is unclear to which extent the observed dynamics are caused by choices of the functional forms and to which extent they are caused by the general topology of the model structure. Generalized modeling is thus a natural way to capture the essential properties of the functional forms. In the study on bone remodeling, practical suggestions are given for future models by showing the assumptions that are necessary for stability and by advocating the inclusion of osteoblast precursors as an explicit dynamical variable.

The most important advantage of conventional modeling is the ability of comparing numerical time series generated from the model with experimental data. However, in situations where the existing knowledge about the system is so limited that this direct comparison is not possible, whether it is due to the lack of quantitative experimental data or due to the lack of quantitative mathematical models, this advantage can not be exploited, so that the alternative framework of GM can be a more efficient approach to a problem.

Based on the reasoning above, generalized modeling was previously only applied to

systems in which the functional forms of at least some processes were unknown. The investigation of the MAPK cascade stands in contrast to these properties and shows that general models can also shed new light on problems with less unknowns. Many earlier studies and the long history of enzyme kinetics have led to a broad agreement regarding the structure and the functional forms of models for the MAPK cascade and the phosphorylation steps it consists of. The most advantageous property of generalized modeling for problems with these characteristics is its ability to investigate the stability properties of steady states in a large parameter space with a high computational efficiency, at the same time avoiding numerical integration of the ODEs. This thesis showed that the tools of bifurcation analysis can be used to detect regions in parameter space in which corresponding conventional models exhibit interesting and previously unknown dynamics such as bursting behavior and chaos.

Another aspect in which the models analyzed in this thesis vary is the size and the complexity of the mathematical model itself. While the earliest mathematical models that are developed to describe a problem are usually simple and provide qualitative results, subsequent models aiming for quantitative agreement with experiments typically become larger and include more dynamic variables and parameters. Therefore, it is important how the method of generalized modeling scales with the system size. From a purely computational point of view, generalized modeling has clear advantages compared to conventional modeling approaches because they rely on the computation of eigenvalues of the Jacobian. Fast algorithms with a complexity that scales polynomially with the system size exist for this problem.

However, the more important problem that arises with larger models is to maintain the interpretability of the generalized model. When there are many unknown parameters, the bifurcation landscape can no longer be visualized easily. Restricting the majority of general parameters to fixed values and then analyzing the bifurcations depending on the remaining parameters is an undesirable solution because it sacrifices one of the main strengths of the method, its generality. In this thesis, different statistical methods to deal with this problem were developed. By an analysis of a large sample of steady states that are randomly drawn from the ensemble of all steady states described by the model, it is possible to gain different types of insights into the properties of a high-dimensional parameter space.

First, the question which types of local bifurcations are *possible* in a given model structure, can be answered with a high degree of certainty. After the existence of a certain bifurcation type has been confirmed, the conditions on the parameters under which the bifurcation occurs can be investigated. Second, by a calculation of correlation coefficients between parameters and stability, it can be identified whether certain parameters have a stabilizing or destabilizing effect on *typical* steady states. While the

correlation coefficients can only give qualitative cues regarding the impact of parameters on stability, the analysis of selected parameters can be extended by investigating correlations between different parameters. These points show that the method of GM is not only suited to analyze small models but can also be applied to larger and more complicated models.

The work presented in this thesis also contributes to the mitigation of existing constraints for generalized modeling. Since the method is local, it cannot directly investigate nonlocal properties, among them oscillations and bistability. The extension of the method to normal-form analysis of bifurcations softens these restrictions. By determining that a Hopf bifurcation is supercritical, the existence of stable limit cycles and sustained oscillations can be shown. Moreover, bistable regimes that arise via codimension-2 cusp bifurcations can be identified. Since oscillations and bistability are important properties of gene-regulatory networks, signaling pathways and other problems from cell biology, the extension expands the scope of generalized modeling for future investigations.

Outlook

In this thesis, it was shown that the method of generalized modeling can contribute to a better understanding of many problems in cell biology. There are various possible directions for future applications of general models to cell-biological problems, either by building upon the results of the specific systems investigated in this thesis, or by new studies of other systems from cell biology.

The extension of generalized modeling to normal-form analysis needs to be applied to more systems to evaluate its practical benefits. In particular, the proposed method of detecting bistability via cusp bifurcations should be applied to models of well-known bistable systems in order to find out how strong the link between bistability and cusp bifurcations is.

A promising direction for further research on the dynamics of bone remodeling is to go beyond stability and analyze also the sensitivity of stable steady-states to changes in the parameters in a general model. An extension of the method of GM in this direction would allow to study connections to various diseases of bone that are not related to bifurcations and to compare results of earlier publications in this direction.

Another point of future research is to improve the method of generalized modeling by developing more sophisticated statistical approaches to large models. While the current procedures, such as the calculation of correlation coefficients between stability and general parameters, provide results of qualitative nature, more quantitative methods are desirable to estimate the size of regions in general parameter space with certain

signatures in the eigenvalues of the Jacobian.

While the focus of this thesis has been placed upon the investigation of general models by mostly avoiding conventional models, a possible field of future investigations is to combine general and conventional models to a higher degree. In particular, a formalized application-oriented implementation of generalized modeling for researchers working on conventional models is desirable. One can envision that in the future, generalized modeling will be integrated in existing software tools, e.g. for the analysis of metabolic pathways. In this context, a generalized version of a newly developed model can serve as a pre-screening tool, giving a first impression on the bifurcation structure and the types of dynamical behavior that can be expected. For a more in-depth analysis, automated methods to switch interactively between the general model and corresponding special models could be developed.

Appendix A

Three-layer model of the MAPK cascade

The dynamics of the three-layer model is governed by the following set of equations.

$$\begin{aligned}\frac{d}{dt}S_1^0 &= f_3(S_2^0) - f_4(S_1^0, P_R^0) + f_5(S_3^0) - f_7(S_0^1, S_1^0) + f_8(S_3^1) + f_9(S_3^1) \\ &\quad - f_{13}(S_1^1, S_1^0) + f_{14}(S_5^1) + f_{15}(S_5^1) \\ \frac{d}{dt}S_1^1 &= f_9(S_3^1) - f_{10}(S_1^1, P_R^1) + f_{11}(S_4^1) - f_{13}(S_1^1, S_1^0) + f_{14}(S_5^1) + f_{18}(S_6^1) \\ \frac{d}{dt}S_2^1 &= f_{15}(S_5^1) - f_{16}(S_2^1, P_R^1) + f_{17}(S_6^1) - f_{19}(S_0^2, S_2^1) + f_{20}(S_3^2) + f_{21}(S_3^2) \\ &\quad - f_{25}(S_1^2, S_2^1) + f_{26}(S_5^2) + f_{27}(S_5^2) \\ \frac{d}{dt}S_1^2 &= f_{21}(S_3^2) - f_{22}(S_1^2, P_R^2) + f_{23}(S_4^2) - f_{25}(S_1^2, S_2^1) + f_{26}(S_5^2) + f_{30}(S_6^2) \\ \frac{d}{dt}S_2^2 &= f_{27}(S_5^2) - f_{28}(S_2^2, P_R^2) + f_{29}(S_6^2) \\ \frac{d}{dt}S_2^0 &= f_1(S_0^0, K_R^0) - f_2(S_2^0) - f_3(S_2^0) \\ \frac{d}{dt}S_3^0 &= f_4(S_1^0, P_R^0) - f_5(S_3^0) - f_6(S_3^0) \\ \frac{d}{dt}S_3^1 &= f_7(S_0^1, S_1^0) - f_8(S_3^1) - f_9(S_3^1) \\ \frac{d}{dt}S_4^1 &= f_{10}(S_1^1, P_R^1) - f_{11}(S_4^1) - f_{12}(S_4^1) \\ \frac{d}{dt}S_5^1 &= f_{13}(S_1^1, S_1^0) - f_{14}(S_5^1) - f_{15}(S_5^1) \\ \frac{d}{dt}S_6^1 &= f_{16}(S_2^1, P_R^1) - f_{17}(S_6^1) - f_{18}(S_6^1)\end{aligned}$$

$$\begin{aligned}\frac{d}{dt}S_3^2 &= f_{19}(S_0^2, S_2^1) - f_{20}(S_3^2) - f_{21}(S_3^2) \\ \frac{d}{dt}S_4^2 &= f_{22}(S_1^2, P_R^2) - f_{23}(S_4^2) - f_{24}(S_4^2) \\ \frac{d}{dt}S_5^2 &= f_{25}(S_1^2, S_2^1) - f_{26}(S_5^2) - f_{27}(S_5^2) \\ \frac{d}{dt}S_6^2 &= f_{28}(S_2^2, P_R^2) - f_{29}(S_6^2) - f_{30}(S_6^2).\end{aligned}$$

The concentrations $S_0^0, S_0^1, S_0^2, K_R^0, K_R^2, P_R^0, P_R^1, P_R^2$ are defined by the conservation relationships

$$\begin{aligned}S_T^0 &= S_0^0 + S_1^0 + S_2^0 + S_3^0 \\ S_T^1 &= S_0^1 + S_1^1 + S_2^1 + S_3^1 + S_4^1 + S_5^1 + S_6^1 \\ S_T^2 &= S_0^2 + S_1^2 + S_2^2 + S_3^2 + S_4^2 + S_5^2 + S_6^2 \\ K_T^0 &= K_R^0 + S_2^0 \\ P_T^0 &= P_R^0 + S_3^0 \\ P_T^1 &= P_R^1 + S_4^1 + S_6^1 \\ P_T^2 &= P_R^2 + S_4^2 + S_6^2.\end{aligned}$$

In the case of mass action, the f_i are products of the arguments and a rate constant, e.g. $f_3(S_2^0) = \alpha_3 S_2^0$ or $f_4(S_1^0, P_R^0) = \alpha_4 S_1^0 P_R^0$. The rate constants α_i can be determined from the set of generalized parameters. They are used for numerical integration in the conventional model at selected points in parameter space.

Appendix B

Parameters for bifurcation diagrams of the three-layered MAPK cascade

In this appendix, we list the general parameters of the bifurcation diagrams in Fig. 5.9 and Fig. 5.10A and the parameters of the corresponding conventional models in which numerical integrations were performed. For the conventional model, the rate constants α_i are linear prefactors of the functions f_i , as it is explained in Appendix A.

Parameter	Value (B1)	Value (B2)	Parameter	Value (B1)	Value (B2)
f_1	2.050463E - 01	3.941433E - 01	f_{16}	2.847627E + 00	2.534890E + 00
f_2	1.665547E - 01	6.896530E - 02	f_{17}	7.331041E - 02	5.148198E - 03
f_3	3.849159E - 02	3.251780E - 01	f_{18}	2.774316E + 00	2.529741E + 00
f_4	3.406789E - 01	4.111991E + 00	f_{19}	1.297541E + 02	7.924804E + 01
f_5	3.021873E - 01	3.786813E + 00	f_{20}	8.498013E + 01	3.908750E + 01
f_6	3.849159E - 02	3.251780E - 01	f_{21}	4.477395E + 01	4.016053E + 01
f_7	1.953008E + 00	5.815648E - 02	f_{22}	4.742998E + 01	4.707532E + 01
f_8	9.370957E - 01	8.308026E - 03	f_{23}	2.656029E + 00	6.914784E + 00
f_9	1.015912E + 00	4.984845E - 02	f_{24}	4.477395E + 01	4.016053E + 01
f_{10}	1.057423E + 00	5.920622E - 02	f_{25}	4.015206E + 01	1.060230E + 01
f_{11}	4.151087E - 02	9.357769E - 03	f_{26}	1.020828E + 01	6.362480E + 00
f_{12}	1.015912E + 00	4.984845E - 02	f_{27}	2.994378E + 01	4.239818E + 00
f_{13}	3.506192E + 00	4.903314E + 00	f_{28}	1.073260E + 02	4.301534E + 01
f_{14}	7.318762E - 01	2.373572E + 00	f_{29}	7.738227E + 01	3.877552E + 01
f_{15}	2.774316E + 00	2.529741E + 00	f_{30}	2.994378E + 01	4.239818E + 00

Table B.1: Parameter values for the bifurcation diagrams shown in Fig. 5.9 (B1) and Fig. 5.10A (B2).

Parameter	Value (B1)	Value (B2)
S_T^0	varied	varied
S_T^1	1.000000E + 00	1.000000E + 00
S_T^2	varied	varied
K_T^0	2.041991E - 02	1.434858E - 01
P_T^0	9.254583E - 02	1.025566E - 01
P_T^1	varied	4.452295E - 04
P_T^2	2.061241E - 01	1.807347E - 01
S_1^0	1.287000E - 02	3.301018E - 02
S_2^0	3.603446E - 02	2.167873E - 01
S_3^0	1.305162E - 01	1.964587E - 01
S_1^1	8.199895E - 02	5.778893E - 01
S_2^1	7.987105E - 02	5.301747E - 02
S_3^1	3.498895E - 04	2.071199E - 03
S_4^1	9.180356E - 04	7.786264E - 03
S_5^1	1.994971E - 03	9.842025E - 05
S_6^1	2.956850E - 04	2.887999E - 05
S_1^2	4.618296E - 03	4.011806E - 03
S_2^2	1.415927E - 04	7.515946E - 06
S_3^2	4.093548E - 01	6.710682E - 02
S_4^2	4.151353E - 03	2.205266E - 02
S_5^2	2.424960E - 01	2.924887E - 02
S_6^2	1.075892E - 01	1.370494E - 01

Table B.2: Continuation of Table B.1

Parameter	Value (P1)	Value (P2)	Parameter	Value (P1)	Value (P2)
α_1	7.858130E + 02	8.634851E + 02	S_T^0	8.000000E - 03	7.666667E - 03
α_2	3.329728E + 01	3.329728E + 01	S_T^1	1.000000E + 00	1.000000E + 00
α_3	1.569999E + 02	1.569999E + 02	S_T^2	3.900000E + 00	3.200000E + 00
α_4	1.643016E + 05	1.714452E + 05	K_T^0	1.147886E - 03	1.100058E - 03
α_5	4.863453E + 02	4.863453E + 02	P_T^0	8.204528E - 04	7.862673E - 04
α_6	4.176303E + 01	4.176303E + 01	P_T^1	4.452295E - 04	4.452295E - 04
α_7	1.064798E + 03	8.378507E + 02	P_T^2	7.048653E - 01	5.783510E - 01
α_8	8.441379E + 01	8.441379E + 01	S_1^0	2.640814E - 04	2.530780E - 04
α_9	5.064857E + 02	5.064857E + 02	S_2^0	2.167873E - 01	2.167873E - 01
α_{10}	6.680161E + 02	6.680161E + 02	S_3^0	1.964587E - 01	1.964587E - 01
α_{11}	3.240226E + 02	3.240226E + 02	S_1^1	2.253768E + 00	1.849246E + 00
α_{12}	1.726055E + 03	1.726055E + 03	S_2^1	2.067681E - 01	1.696559E - 01
α_{13}	8.564815E + 04	8.937198E + 04	S_3^1	1.656959E - 05	1.587919E - 05
α_{14}	5.916468E + 02	5.916468E + 02	S_4^1	6.229011E - 05	5.969469E - 05
α_{15}	6.305741E + 02	6.305741E + 02	S_5^1	9.842025E - 05	9.842025E - 05
α_{16}	3.156031E + 04	3.156031E + 04	S_6^1	2.887999E - 05	2.887999E - 05
α_{17}	6.849701E + 02	6.849701E + 02	S_1^2	4.011806E - 03	4.011806E - 03
α_{18}	3.365832E + 05	3.365832E + 05	S_2^2	7.515946E - 06	7.515946E - 06
α_{19}	3.549795E + 03	3.549795E + 03	S_3^2	2.617166E - 01	2.147418E - 01
α_{20}	5.824669E + 02	5.824669E + 02	S_4^2	8.600537E - 02	7.056851E - 02
α_{21}	5.984568E + 02	5.984568E + 02	S_5^2	1.140706E - 01	9.359638E - 02
α_{22}	9.655494E + 02	1.176763E + 03	S_6^2	5.344927E - 01	4.385581E - 01
α_{23}	3.135578E + 02	3.135578E + 02			
α_{24}	1.821120E + 03	1.821120E + 03			
α_{25}	9.338652E + 01	9.338652E + 01			
α_{26}	2.175291E + 02	2.175291E + 02			
α_{27}	1.449566E + 02	1.449566E + 02			
α_{28}	9.616792E + 03	1.172047E + 04			
α_{29}	2.829310E + 02	2.829310E + 02			
α_{30}	3.093642E + 01	3.093642E + 01			

Table B.3: Parameter values for the conventional models corresponding to the unstable steady states of Fig. 7B and C, close to which irregular dynamics (P1) and complex oscillations (P2) were found.

Appendix C

List of abbreviations

The following abbreviations are repeatedly used in the text or in the figures. Although they are explained at the point of their first occurrence, they are listed here again to give an overview.

AOB	Active Osteoblast
BMU	Basic Multicellular Unit
BS	Bistability
CP	Cusp (bifurcation) Point
DH	Double Hopf (bifurcation)
GG	Gavrilov-Guckenheimer (bifurcation)
GM	Generalized Modeling
HB	Hopf Bifurcation
MAPK	Mitogen-Activated Protein Kinase
OB	Osteoblast
OC	Osteoclast
ROB	Responding Osteoblast
SN	Saddle-Node (bifurcation)
TB	Takens-Bogdanov (bifurcation)

Bibliography

- [1] B. Alberts. The cell as a collection overview of protein machines: Preparing the next generation of molecular biologists. *Cell*, 92:291–294, 1998.
- [2] H. Kitano. Systems biology: a brief overview. *Science*, 295(5560):1662, 2002.
- [3] A.L. Barabási and Z.N. Oltvai. Network biology: understanding the cell’s functional organization. *Nat. Rev. Genet.*, 5(2):101–113, 2004.
- [4] B.N. Kholodenko. Cell signalling dynamics in time and space. *Nat. Rev. Mol. Cell Biol.*, 7(3):165–176, 2006.
- [5] P.W. Anderson. More is different - Broken symmetry and the nature of the hierarchical structure of science. *Science*, 177(4047):393–396, 1972.
- [6] R.B. Laughlin and D. Pines. The theory of everything. *Proc. Natl. Acad. Sci.*, 97(1):28, 2000.
- [7] N. Goldenfeld and L.P. Kadanoff. Simple lessons from complexity. *Science*, 284(5411):87–89, 1999.
- [8] T. Gross and U. Feudel. Generalized models as an universal approach to the analysis of nonlinear dynamical systems. *Phys. Rev. E*, 73:016205–14, 2006.
- [9] R. Steuer, T. Gross, J. Selbig, and B. Blasius. Structural kinetic modeling of metabolic networks. *Proc. Natl. Acad. Sci.*, 103:11868–11874, 2006.
- [10] T. Gross, L. Rudolf, S.A. Levin, and U. Dieckmann. Generalized models reveal stabilizing factors in food webs. *Science*, 325:747–750, 2009.
- [11] Y.A. Kuznetsov. *Elements of Applied Bifurcation Theory*. Springer Verlag, New York, third edition, 1995.
- [12] J. Guckenheimer and P. Holmes. *Nonlinear oscillations, dynamical systems, and bifurcations of vector fields*. Springer, New York, third edition, 1997.

-
- [13] V. Szebehely. Review of concepts of stability. *Celestial Mechanics and Dynamical Astronomy*, 34(1):49–64, 1984.
- [14] S.L. Pimm. The complexity and stability of ecosystems. *Nature*, 307(5949):321–326, 1984.
- [15] A. Novick and M. Weiner. Enzyme induction as an all-or-none phenomenon. *Proc. Natl. Acad. Sci.*, 43(7):553, 1957.
- [16] J.S. Griffith. Mathematics of cellular control processes II. Positive feedback to one gene. *J. Theor. Biol.*, 20(2):209–216, 1968.
- [17] E. Hopf. Abzweigung einer periodischen Lösung von einer stationären Lösung eines Differentialsystems. *Ber. Math.-Phys. Kl Sächs. Akad. Wiss. Leipzig*, 94:1–22, 1942.
- [18] F. Takens. Singularities of vector fields. *Inst. Hautes Études Sci. Publ. Math.*, 43:47–100, 1974.
- [19] R.I. Bogdanov. Versal deformation of a singularity of a vector field on the plane in the case of zero eigenvalues. (English translation). *Selecta Math. Soviet*, 1(4):389–421, 1981.
- [20] N. Gavrilov. On some bifurcations of an equilibrium with one zero and a pair of pure imaginary roots. *Methods of Qualitative Theory of Differential Equations*, pages 33–40, 1978.
- [21] J. Guckenheimer. On a codimension two bifurcation. In D. Rand and L. Young, editors, *Dynamical Systems and Turbulence, Warwick 1980*, pages 99–142. Springer, 1981.
- [22] N. Gavrilov. On some bifurcations of an equilibrium with two pairs of pure imaginary roots. *Methods of Qualitative Theory of Differential Equations*, pages 17–30, 1980.
- [23] N.N. Bautin. Behavior of Dynamic Systems Near the Boundaries of a Stability Domain. *Gostekhizdat, Leningrad-Moscow*, 1949.
- [24] L.P. Shilnikov. *Methods of qualitative theory in nonlinear dynamics. Part II*. World Scientific, 2001.
- [25] V.I. Arnold. *Catastrophe theory*. Springer, 1992.

- [26] T. Gross, W. Ebenhöf, and U. Feudel. Enrichment and foodchain stability: the impact of different forms of predator-prey interaction. *J. Theor. Biol.*, 227(3):349–358, 2004.
- [27] T. Gross, W. Ebenhöf, and U. Feudel. Long food chains are in general chaotic. *Oikos*, 109(1):135–144, 2005.
- [28] G.A.K. Van Voorn, D. Stiefs, T. Gross, B.W. Kooi, U. Feudel, and S.A.L.M. Kooijman. Stabilization due to predator interference: comparison of different analysis approaches. *Math. Biosci. Eng.*, 5:567–583, 2008.
- [29] D. Stiefs, E. Venturino, and U. Feudel. Evidence of chaos in eco-epidemic models. *Math. Biosci. Eng.*, 6:855–871, 2009.
- [30] D. Stiefs, G.A.K. van Voorn, B.W. Kooi, U. Feudel, and T. Gross. Food Quality in Producer-Grazer Models: A Generalized Analysis. *The American Naturalist*, 176(3):367–380, 2010.
- [31] J.D. Yeakel, D. Stiefs, M. Novak, and T. Gross. Generalized modeling of ecological population dynamics. *Theoretical Ecology*, 4(2):179–194, 2011.
- [32] R. Steuer, A.N. Nesi, A.R. Fernie, T. Gross, B. Blasius, and J. Selbig. From structure to dynamics of metabolic pathways: Application to the plant mitochondrial TCA cycle. *Bioinformatics*, 23:1378–1385, 2007.
- [33] E. Reznik and D. Segrè. On the stability of metabolic cycles. *J. Theor. Biol.*, 266:536–549, 2010.
- [34] E. Gehrman and B. Drossel. Boolean versus continuous dynamics on simple two-gene modules. *Physical Review E*, 82(4):046120, 2010.
- [35] C. Kuehn, S. Siegmund, and T. Gross. On the dynamical analysis of evolution equations via generalized models. *arXiv:1012.4340*, 2010.
- [36] U. Alon. *An introduction to systems biology: design principles of biological circuits*, volume 10. CRC Press, 2007.
- [37] B. Alberts, A. Johnson, J. Lewis, M. Raff, K. Roberts, and P. Walter. *Molecular Biology of the Cell*. Garland Science, 2007.
- [38] D.A. Fell. Metabolic control analysis: a survey of its theoretical and experimental development. *Biochem. J.*, 286:313–330, 1992.

- [39] B.C. Goodwin. Oscillatory behavior in enzymatic control processes. *Adv. Enz. Regul.*, 3:425–428, 1965.
- [40] D. Stiefs. *Relating generalized and specific modeling in population dynamical systems*. Dissertation, 2009.
- [41] A. Dhooge, W. Govaerts, and Y.A. Kuznetsov. MATCONT: a MATLAB package for numerical bifurcation analysis of ODEs. *ACM Transactions on Mathematical Software (TOMS)*, 29(2):164, 2003.
- [42] J.C. Dunlap. Molecular Bases for Circadian Clocks Review. *Cell*, 96:271–290, 1999.
- [43] M. Hastings, J.S. O’Neill, and E.S. Maywood. Circadian clocks: regulators of endocrine and metabolic rhythms. *Journal of Endocrinology*, 195(2):187, 2007.
- [44] A. Goldbeter. Computational approaches to cellular rhythms. *Nature*, 420(6912):238–245, 2002.
- [45] O. Pourquie. The segmentation clock: converting embryonic time into spatial pattern. *Science*, 301(5631):328, 2003.
- [46] R.L. Bar-Or, R. Maya, L.A. Segel, U. Alon, A.J. Levine, and M. Oren. Generation of oscillations by the p53-mdm2 feedback loop: A theoretical and experimental study. *Proc. Natl. Acad. Sci.*, 97(21):11250–11255, 2000.
- [47] M.B. Elowitz and S. Leibler. A synthetic oscillatory network of transcriptional regulators. *Nature*, 403(6767):335–338, 2000.
- [48] J. Lewis. Autoinhibition with Transcriptional Delay:: A Simple Mechanism for the Zebrafish Somitogenesis Oscillator. *Curr. Biol.*, 13(16):1398–1408, 2003.
- [49] J.M. Höfener, G.C. Sethia, and T. Gross. Stability and Resonance in Networks of Delay-Coupled Delay Oscillators. *arXiv*, 1012.4340, 2010.
- [50] J.S. Griffith. Mathematics of Cellular Control Processes. I. Negative Feedback to One Gene. *J. Theor. Biol.*, 20:202–208, 1968.
- [51] A. Hunding. Limit-cycles in enzyme-systems with nonlinear negative feedback. *European Biophysics Journal*, 1(1):47–54, 1974.
- [52] F. Boulier, M. Lefranc, F. Lemaire, P.E. Morant, and A. Ürgüplü. On proving the absence of oscillations in models of genetic circuits. *Algebraic Biology*, pages 66–80, 2007.

- [53] T. Gross and U. Feudel. Analytical search for bifurcation surfaces in parameter space. *Physica D*, 195:292–302, 2004.
- [54] S. Becker-Weimann, J. Wolf, H. Herzel, and A. Kramer. Modeling feedback loops of the mammalian circadian oscillator. *Biophys. J.*, 87(5):3023–3034, 2004.
- [55] J.C. Leloup and A. Goldbeter. Toward a detailed computational model for the mammalian circadian clock. *Proc. Natl. Acad. Sci.*, 100(12):7051, 2003.
- [56] C.T. Kelley. *Solving nonlinear equations with Newton's method*. SIAM, Philadelphia, 2003.
- [57] M.J.A. Van Hoek and P. Hogeweg. In silico evolved lac operons exhibit bistability for artificial inducers, but not for lactose. *Biophys. J.*, 91(8):2833–2843, 2006.
- [58] D. Battogtokh and J.J. Tyson. Bifurcation analysis of a model of the budding yeast cell cycle. *Chaos*, 14:653, 2004.
- [59] M. Zumsande, D. Stiefs, S. Siegmund, and T. Gross. General analysis of mathematical models for bone remodeling. *Bone*, 48(4):910–917, 2011.
- [60] D.G. Steele and C.A. Bramblett. *The anatomy and biology of the human skeleton*. TAMU Press, 1988.
- [61] T.D. White and P.A. Folkens. *Human osteology*. Academic Press San Diego (California), 2000.
- [62] A.G. Robling, A.B. Castillo, and C.H. Turner. Biomechanical and molecular regulation of bone remodeling. *Annu. Rev. Biomed. Eng.*, 8:455–498, 2006.
- [63] B.F. Boyce and L. Xing. Functions of RANKL/RANK/OPG in bone modeling and remodeling. *Arch. Biochem. Biophys.*, 473:139–146, 2008.
- [64] S.C. Manolagas. Birth and death of bone cells: basic regulatory mechanisms and implications for the pathogenesis and treatment of osteoporosis. *Endocrine Reviews*, 21(2):115, 2000.
- [65] H.M. Frost. Tetracycline-based histological analysis of bone remodeling. *Calcif. Tissue Int.*, 3(1):211–237, 1969.
- [66] A.P. Anandarajah. Role of RANKL in bone diseases. *Trends Endocrinol. Metab.*, 20(2):88–94, 2009.
- [67] K. Janssens, P. ten Dijke, S. Janssens, and W. Van Hul. Transforming growth factor- β 1 to the bone. *Endocrine Reviews*, 26(6):743–774, 2005.

- [68] S.V. Reddy, N. Kurihara, C. Menea, and G.D. Roodman. Paget's disease of bone: a disease of the osteoclast. *Rev. Endocr. Metab. Disord.*, 2:195–201, 2001.
- [69] M.P. Whyte. Paget's disease of bone and genetic disorders of RANKL/OPG/RANK/NF- κ B signaling. *Ann. N.Y. Acad. Sci.*, 1068:143–164, 2006.
- [70] A.E. Kearns, S. Khosla, and P.J. Kostenuik. Receptor activator of nuclear factor κ B ligand and osteoprotegerin regulation of bone remodeling in health and disease. *Endocrine Reviews*, 29(2):155–192, 2008.
- [71] L.M. McNamara. Perspective on post-menopausal osteoporosis: establishing an interdisciplinary understanding of the sequence of events from the molecular level to whole bone fractures. *J. R. Soc. Interface*, 7(44):353–372, 2010.
- [72] P. Pivonka and S.V. Komarova. Mathematical modeling in bone biology: From intracellular signaling to tissue mechanics. *Bone*, 2010.
- [73] M.D. Ryser, N. Nigam, and S.V. Komarova. Mathematical modeling of spatio-temporal dynamics of a single bone multicellular unit. *J. Bone Miner. Res.*, 24:860–870, 2009.
- [74] S.V. Komarova, R.J. Smith, S.J. Dixon, S.M. Sims, and L.M. Wahl. Mathematical model predicts a critical role for osteoclast autocrine regulation in the control of bone remodeling. *Bone*, 33(2):206–215, 2003.
- [75] S.V. Komarova. Mathematical model of paracrine interactions between osteoclasts and osteoblasts predicts anabolic action of parathyroid hormone on bone. *Endocrinology*, 146(8):3589–3595, 2005.
- [76] B. Ayati, C. Edwards, G. Webb, and J. Wikswo. A mathematical model of bone remodeling dynamics for normal bone cell populations and myeloma bone disease. *Biology Direct*, 5(1):28, 2010.
- [77] V. Lemaire, F.L. Tobin, L.D. Greller, C.R. Cho, and L.J. Suva. Modeling the interactions between osteoblast and osteoclast activities in bone remodeling. *J. Theor. Biol.*, 229(3):293–309, 2004.
- [78] P. Pivonka, J. Zimak, D.W. Smith, B.S. Gardiner, C.R. Dunstan, N.A. Sims, T.J. Martin, and G.R. Mundy. Model structure and control of bone remodeling: a theoretical study. *Bone*, 43(2):249–263, 2008.

- [79] P. Pivonka, J. Zimak, D.W. Smith, B.S. Gardiner, C.R. Dunstan, N.A. Sims, T.J. Martin, and G.R. Mundy. Theoretical investigation of the role of the RANK-RANKL-OPG system in bone remodeling. *J. Theor. Biol.*, 262(2):306–316, 2010.
- [80] M. Scheffer, J. Bascompte, W.A. Brock, V. Brovkin, S.R. Carpenter, V. Dakos, H. Held, E.H. Van Nes, M. Rietkerk, and G. Sugihara. Early-warning signals for critical transitions. *Nature*, 461(7260):53–59, 2009.
- [81] E. Canalis and D. Agnusdei. Insulin-like growth factors and their role in osteoporosis. *Calcif. Tissue Int.*, 58(3):133–134, 1996.
- [82] A. Giustina, G. Mazziotti, and E. Canalis. Growth hormone, insulin-like growth factors, and the skeleton. *Endocrine Reviews*, 29(5):535, 2008.
- [83] H.M. Massey, J. Scopes, M.A. Horton, and A.M. Flanagan. Transforming growth factor- β 1 (tgf- β) stimulates the osteoclast-forming potential of peripheral blood hematopoietic precursors in a lymphocyte-rich microenvironment. *Bone*, 28(6):577–582, 2001.
- [84] M.A. Karsdal, P. Hjorth, K. Henriksen, T. Kirkegaard, K.L. Nielsen, H. Lou, J.M. Delaissé, and N.T. Foged. Transforming growth factor- β controls human osteoclastogenesis through the p38 mapk and regulation of rank expression. *Journal of Biological Chemistry*, 278(45):44975, 2003.
- [85] M. Karst, G. Gorny, R.J.S. Galvin, and M.J. Oursler. Roles of stromal cell RANKL, OPG, and M-CSF expression in biphasic TGF- β regulation of osteoclast differentiation. *Journal of cellular physiology*, 200(1):99–106, 2004.
- [86] D.E. Hughes, A. Dai, J.C. Tiffée, H.H. Li, G.R. Mundy, and B.F. Boyce. Estrogen promotes apoptosis of murine osteoclasts mediated by TGF- β . *Nat. Med.*, 2(10):1132–1136, 1996.
- [87] Transforming growth factor- β 1 increases mRNA levels of osteoclastogenesis inhibitory factor.
- [88] N. Houde, E. Chamoux, M. Bisson, and S. Roux. Transforming growth factor- β 1 (TGF- β 1) induces human osteoclast apoptosis by up-regulating Bim. *J. Biol. Chem.*, 284(35):23397–23404, 2009.
- [89] K. Fuller, JM Lean, KE Bayley, MR Wani, and TJ Chambers. A role for TGF β 1 in osteoclast differentiation and survival. *J. Cell Sci.*, 113(13):2445, 2000.

- [90] M. Ruan, L. Pederson, E.W. Bradley, A.M. Bamberger, and M.J. Oursler. Transforming growth factor- β coordinately induces suppressor of cytokine signaling 3 and leukemia inhibitory factor to suppress osteoclast apoptosis. *Endocrinology*, 151(4):1713–1722, 2010.
- [91] F. Gori, L.C. Hofbauer, C.R. Dunstan, T.C. Spelsberg, S. Khosla, and B.L. Riggs. The expression of osteoprotegerin and RANK ligand and the support of osteoclast formation by stromal-osteoblast lineage cells is developmentally regulated. *Endocrinology*, 141(12):4768–4776, 2000.
- [92] G.P. Thomas, S.U.K. Baker, J.A. Eisman, and E.M. Gardiner. Changing RANKL/OPG mRNA expression in differentiating murine primary osteoblasts. *J. Endocrinology*, 170(2):451, 2001.
- [93] T. Akchurin, T. Aissiou, E. Prosk, N. Nigam, and S.V. Komarova. Complex dynamics of osteoclast formation and death in long-term cultures. *PLoS One*, 3:e2104, 2008.
- [94] S. Yao, F. Pan, and G.E. Wise. Chronological gene expression of parathyroid hormone-related protein (PTHrP) in the stellate reticulum of the rat—Implications for tooth eruption. *Archives of Oral Biology*, 52(3):228–232, 2007.
- [95] S.H. Ralston, S.A. Hoey, S.J. Gallacher, B.B. Adamson, and I.T. Boyle. Cytokine and growth factor expression in Paget’s disease: analysis by reverse-transcription/polymerase chain reaction. *Br. J. Rheumatol.*, 33(7):620, 1994.
- [96] C.Y. Huang and J.E. Ferrell, Jr. Ultrasensitivity in the mitogen-activated protein kinase cascade. *Proc. Natl. Acad. Sci.*, 93:10078–10083, 1996.
- [97] B.N. Kholodenko. Negative feedback and ultrasensitivity can bring about oscillations in the mitogen-activated protein kinase cascades. *Eur. J. Biochem.*, 267:1583–1588, 2000.
- [98] S.Y. Shvartsman, M.P. Hagan, A. Yacoub, P. Dent, H.S. Wiley, and D.A. Luffenburger. Autocrine loops with positive feedback enable context-dependent cell signaling. *Am. J. Physiol. Cell*, 282(3):C545, 2002.
- [99] N.I. Markevich, J.B. Hoek, and B.N. Kholodenko. Signaling switches and bistability arising from multisite phosphorylation in protein kinase cascades. *J. Cell Biol.*, 164:353–359, 2004.

- [100] L. Qiao, R.B. Nachbar, I.G. Kevrekidis, and S.Y. Shvartsman. Bistability and oscillations in the Huang-Ferrell model of MAPK signaling. *PLoS Comput Biol*, 3:1819–1826, 2007.
- [101] S. Frey, T. Millat, S. Hohmann, and O. Wolkenhauer. How quantitative measures unravel design principles in multi-stage phosphorylation cascades. *J. Theor. Biol.*, 254(1):27–36, 2008.
- [102] S. Lapidus, B. Han, and J. Wang. Intrinsic noise, dissipation cost, and robustness of cellular networks: The underlying energy landscape of MAPK signal transduction. *Proc. Natl. Acad. Sci.*, 105(16):6039, 2008.
- [103] B.N. Kholodenko, A. Kiyatkin, F.J. Bruggeman, E. Sontag, and H.V. Westerhoff. Untangling the wires: A strategy to trace functional interactions in signaling and gene networks. *Proc. Natl. Acad. Sci.*, 99:12841–12846, 2002.
- [104] D. Angeli, J.E. Ferrell, and E.D. Sontag. Detection of multistability, bifurcations, and hysteresis in a large class of biological positive-feedback systems. *Proc. Natl. Acad. Sci.*, 101(7):1822, 2004.
- [105] M. Zumsande and T. Gross. Bifurcations and chaos in the MAPK signaling cascade. *J. Theor. Biol.*, 265:481–491, 2010.
- [106] R. Seger and E.G. Krebs. The MAPK signaling cascade. *FASEB J.*, 9(9):726, 1995.
- [107] L. Chang and M. Karin. Mammalian MAP kinase signalling cascades. *Nature*, 410:37–40, 2001.
- [108] G.L. Johnson and R. Lapadat. Mitogen-Activated Protein Kinase Pathways Mediated by ERK, JNK, and p38 Protein Kinases. *Science*, 298:1911–1912, 2002.
- [109] M.C. Lawrence, A. Jivan, C. Shao, L. Duan, D. Goad, E. Zaganjor, J. Osborne, K. McGlynn, S. Stippec, S. Earnest, et al. The roles of MAPKs in disease. *Cell Research*, 18(4):436–442, 2008.
- [110] D. Hanahan and R.A. Weinberg. The hallmarks of cancer. *Cell*, 100(1):57–70, 2000.
- [111] B. Escudier, T. Eisen, W.M. Stadler, C. Szczylik, S. Oudard, M. Siebels, S. Negrier, C. Chevreau, E. Solska, A.A. Desai, et al. Sorafenib in advanced clear-cell renal-cell carcinoma. *New England Journal of Medicine*, 356(2):125, 2007.

-
- [112] J. Downward. Targeting RAS signalling pathways in cancer therapy. *Nat. Rev. Cancer*, 3(1):11–22, 2003.
- [113] P.J. Roberts and C.J. Der. Targeting the Raf-MEK-ERK mitogen-activated protein kinase cascade for the treatment of cancer. *Oncogene*, 26(22):3291–3310, 2007.
- [114] J.S. Sebolt-Leopold. Advances in the development of cancer therapeutics directed against the RAS-mitogen-activated protein kinase pathway. *Clinical cancer research*, 14(12):3651, 2008.
- [115] J.J. Hornberg, B. Binder, F.J. Bruggeman, B. Schoeberl, R. Heinrich, and H.V. Westerhoff. Control of MAPK signalling: from complexity to what really matters. *Oncogene*, 24:5533–5542, 2005.
- [116] A. Goldbeter and D.E. Koshland, Jr. An amplified sensitivity arising from covalent modification in biological systems. *Proc. Natl. Acad. Sci.*, 78:6840.
- [117] S. Legewie, B. Schoeberl, N. Blüthgen, and H. Herzel. Competing docking interactions can bring about bistability in the MAPK cascade. *Biophys. J.*, 93:2279–2288, 2007.
- [118] S. Schuster, T. Dandekar, and D.A. Fell. Detection of elementary flux modes in biochemical networks: a promising tool for pathway analysis and metabolic engineering. *Trends in Biotechnology*, 17(2):53–60, 1999.
- [119] W.W. Chen, M. Niepel, and P.K. Sorger. Classic and contemporary approaches to modeling biochemical reactions. *Genes & development*, 24(17):1861, 2010.
- [120] N. Blüthgen, F.J. Bruggeman, S. Legewie, H. Herzel, H.V. Westerhoff, and B.N. Kholodenko. Effects of sequestration on signal transduction cascades. *FEBS J.*, 273:895–906, 2006.
- [121] A.C. Ventura, J.A. Sepulchre, and S.D. Merajver. A hidden feedback in signaling cascades is revealed. *PLoS. Comput. Biol.*, 4:1–14, 2008.
- [122] F. Ortega, J.L. Garcés, F. Mas, B.N. Kholodenko, and M. Cascante. Bistability from double phosphorylation in signal transduction. Kinetic and structural requirements. *FEBS J.*, 273:3915–3926, 2006.
- [123] E. Hairer and G. Wanner. *Solving ordinary differential equations II: Stiff and differential-algebraic problems*. Springer, Berlin, 1991.

-
- [124] D. Stiefs, T. Gross, R. Steuer, and U. Feudel. Computation and visualization of bifurcation surfaces. *Int. J. Bifurc. Chaos*, 18:2191–2206, 2008.
- [125] W. Kolch, M. Calder, and D. Gilbert. When kinases meet mathematics: the systems biology of MAPK signalling. *FEBS Lett.*, 579:1891–1895, 2005.
- [126] W.J. Langlois, T. Sasaoka, A.R. Saltiel, and J.M. Olefsky. Negative Feedback Regulation and Desensitization of Insulin- and Epidermal Growth Factor-stimulated p21ras Activation. *J. Biol. Chem.*, 270:25320–25323, 1995.
- [127] S.T. Eblen, J.K. Slack-Davis, A. Tarcsafalvi, J.T. Parsons, M.J. Weber, and A.D. Catling. Mitogen-activated protein kinase feedback phosphorylation regulates MEK1 complex formation and activation during cellular adhesion. *Mol. Cell Biol.*, 24:2308–2317, 2004.
- [128] J.J. Tyson, K.C. Chen, and B. Novak. Sniffers, buzzers, toggles and blinkers: dynamics of regulatory and signaling pathways in the cell. *Curr. Opin. Cell Biol.*, 15(2):221–231, 2003.
- [129] H. Shankaran, D.L. Ippolito, W.B. Chrisler, H. Resat, N. Bollinger, L.K. Opresko, and H.S. Wiley. Rapid and sustained nuclear–cytoplasmic ERK oscillations induced by epidermal growth factor. *Mol. Sys. Biol.*, 5(1), 2009.
- [130] Z. Hilioti, W. Sabbagh, Jr, S. Paliwal, A. Bergmann, M.D. Goncalves, L. Bardwell, and A. Levchenko. Oscillatory phosphorylation of yeast Fus3 MAP kinase controls periodic gene expression and morphogenesis. *Curr. Biol.*, 18:1700–1706, 2008.

Acknowledgements

First and foremost, I want to thank Dr. Thilo Gross for guiding my research in the last years. Thilo was always available for discussions related to my work and taught me much about science and scientific writing.

I also want to thank Prof. Dr. Frank Jülicher for supervising and reviewing this thesis, and for giving me the opportunity to be a member of the biological physics group at the MPI for the Physics of Complex Systems.

I am thankful to Prof. Dr. Stefan Siegmund, both for the fruitful collaboration in the project on bone remodeling and for agreeing to be a referee of this thesis.

Furthermore, I am grateful to Prof. Dr. Jörg Weber, Prof. Dr. Roland Ketzmerick and PD Dr. Sergei Flach for being members of my committee.

In the past years I have collaborated with several other people. I especially want to thank Dr. Dirk Stiefs and Dr. Ralf Steuer for their contributions in the projects on bone remodeling and on normal forms.

I wish to thank the members of the group "Dynamics of biological networks" for many discussions, especially Dr. Lars Rudolf, Johannes Hoefener and Dr. Christian Kuehn who also work on generalized models. I am also grateful to Dr. Steven Lade for critically reading parts of the manuscript.

Many thanks go to my room mates Dr. Anne-Ly Do and Dr. Lars Rudolf for creating a great atmosphere to work in. I also want to thank my former room mates Dr. Christian Schreiber and Rick Mukherjee.

Also, I would like to thank Mr. Scherrer and the computer department of the MPI PKS, who were very helpful in case of computer problems.

I am grateful to Prof. Dr. Alexander Hartmann for completing the publication of the results from diploma thesis when I was already working on new topics.

Last but not least, I want to thank my family for their constant support on many levels throughout the last years.

Versicherung

Hiermit versichere ich, dass ich die vorliegende Arbeit ohne unzulässige Hilfe Dritter und ohne Benutzung anderer als der angegebenen Hilfsmittel angefertigt habe; die aus fremden Quellen direkt oder indirekt übernommenen Gedanken sind als solche kenntlich gemacht. Die Arbeit wurde bisher weder im Inland noch im Ausland in gleicher oder ähnlicher Form einer anderen Prüfungsbehörde vorgelegt.

Die Arbeit wurde am Max-Planck-Institut für Physik komplexer Systeme in der Abteilung Biologische Physik (Untergruppe: Dynamics of Biological Networks) angefertigt und von Dr. Thilo Gross sowie Prof. Dr. Frank Jülicher betreut. Ich erkenne die Promotionsordnung der Fakultät Mathematik und Naturwissenschaften der Technischen Universität Dresden an.

Martin Zumsande

